NOTE TO USERS

This reproduction is the best copy available.

UMI®

"What lies behind us and what lies before us are tiny matters compared to what lies within us"

Ralph Waldo Emerson

University of Alberta

ASPHALTENES, MALTENES AND SILICA NANOPARTICLES AT AIR-WATER AND TOLUENE-WATER INTERFACES

by

Robert Lopetinsky ©

A thesis submitted to the Faculty of Graduate Studies and Research in partial
fulfillment of the requirements for the degree of
Master of Science

in

Chemical Engineering

Department of Chemical and Materials Engineering

Edmonton, Alberta
Fall 2005

Library and
Archives Canada

Published Heritage
Branch

395 Wellington Street
Ottawa ON K1A 0N4
Canada

Bibliothèque et
Archives Canada

Direction du
Patrimoine de l'édition

395, rue Wellington
Ottawa ON K1A 0N4
Canada

0-494-09228-9

Your file *Votre référence*
ISBN:
Our file *Notre reference*
ISBN:

NOTICE:
The author has granted a non-exclusive license allowing Library and Archives Canada to reproduce, publish, archive, preserve, conserve, communicate to the public by telecommunication or on the Internet, loan, distribute and sell theses worldwide, for commercial or non-commercial purposes, in microform, paper, electronic and/or any other formats.

AVIS:
L'auteur a accordé une licence non exclusive permettant à la Bibliothèque et Archives Canada de reproduire, publier, archiver, sauvegarder, conserver, transmettre au public par télécommunication ou par l'Internet, prêter, distribuer et vendre des thèses partout dans le monde, à des fins commerciales ou autres, sur support microforme, papier, électronique et/ou autres formats.

The author retains copyright ownership and moral rights in this thesis. Neither the thesis nor substantial extracts from it may be printed or otherwise reproduced without the author's permission.

L'auteur conserve la propriété du droit d'auteur et des droits moraux qui protège cette thèse. Ni la thèse ni des extraits substantiels de celle-ci ne doivent être imprimés ou autrement reproduits sans son autorisation.

In compliance with the Canadian Privacy Act some supporting forms may have been removed from this thesis.

Conformément à la loi canadienne sur la protection de la vie privée, quelques formulaires secondaires ont été enlevés de cette thèse.

While these forms may be included in the document page count, their removal does not represent any loss of content from the thesis.

Bien que ces formulaires aient inclus dans la pagination, il n'y aura aucun contenu manquant.

Canada

For Sierra

-You raise me up-

Abstract

In this thesis, deasphalted bitumen (maltenes) and asphaltenes extracted from Athabasca oil sands bitumen, and fumed silica nanoparticles were studied at air-water and toluene-water interfaces. Interfacial behaviours of individual components and their mixtures were characterized with pressure–area isotherms obtained with a Langmuir trough. Single layer Langmuir-Blodgett films were deposited onto silicon wafers and examined with an atomic force microscope and scanning electron microscope.

At the air-water interface, similarities in the pressure-area isotherms of the asphaltene and silica films were observed. Langmuir films of asphaltenes or silica mixed with maltenes showed similar phase transitions. Silica particles were aggregated into clusters at the interface, and when maltenes and asphaltenes are present with silica the size of the clusters is reduced.

At the toluene-water interface, maltenes form a compressible film and most of the maltenes dissolve into the toluene. Observed interfacial characteristics of asphaltenes and silica support their role as emulsion stabilizers.

Acknowledgements

I would like to gratefully acknowledge the enthusiastic supervision of Dr. Jacob Masliyah and Dr. Zhenghe Xu. I appreciate their guidance, wisdom and friendship throughout this difficult journey.

All my fellow members of the oil sands research program deserve acknowledgement; they are a fantastic group to belong to and most definitely improved my graduate studies experience. I thank Dr. Liyan Zhang for his kind assistance throughout my thesis experiments; his help simplified many tasks, and contributed to my understanding of the subject. This thesis would not be the same without Dr. Zhang's contributions. I thank Tina Barker for performing the SEM imaging. I thank Alejandro Magual for assisting me with ultrasonic size analysis and for his friendship. I thank Mike Paulsen who has been my coach, and the best kind of friend.

Special gratitude is devoted to my friends and family, who can't really be thanked enough.

The NSERC Industrial Research Chair in Oil Sands Engineering and its sponsors provided financial support for this project.

Table of Contents

1 Introduction 1
  1.1 Introduction 1
  1.2 Thesis Overview 2
2 Background Information 3
  2.1 Introduction 3
  2.2 Water-in-Oil Emulsions in Bitumen Processing 3
    2.2.1 Asphaltenes and Their Role in Emulsion Stability 5
    2.2.2 Maltenes and Their Contributions to Emulsion Stability 6
    2.2.3 Properties of Solids from Bitumen 7
  2.3 Thesis Objective 10
  2.4 Langmuir Films 11
    2.4.1 Theory 11
    2.4.2 Asphaltenes on the Langmuir Trough 17
    2.4.3 Solid Particles on the Langmuir Trough 19
  2.5 Langmuir-Blodgett Films 25
    2.5.1 Atomic Force Microscopy 26
    2.5.2 Scanning Electron Microscopy 27
    2.5.3 Review of Langmuir-Blodgett Film Literature 28
  2.6 Chapter Summary 29
  2.7 References 31
  2.8 Figures 37
3 Experimental Materials and Methods 51
  3.1 Introduction 51
  3.2 Materials 51
    3.2.1 Reagents 51
    3.2.2 Asphaltenes and Maltene Preparation 52
    3.2.3 Silica Nanoparticles 54

3.2.4 Solution Preparation 57
3.3 Langmuir Trough Experiments 59
3.3.1 Langmuir Trough Set-up 59
3.3.2 Pressure-Area Isotherm Procedure 61
3.4 Langmuir-Blodgett Film Imaging 64
3.4.1 Substrate Preparation 64
3.4.2 Film Deposition 65
3.4.3 Scanning Electron Microscopy 65
3.4.4 Atomic Force Microscopy 66
3.5 Chapter Summary 66
3.6 References 68
3.7 Figures 69
4 Preliminary Experiments 73
4.1 Introduction 73
4.2 Langmuir Film Experiments 74
4.2.1 Comparison to Published Results 74
4.2.2 Hydrophilic Silica 75
4.2.3 Compression Rate 76
4.2.4 Evaporation Time 77
4.2.5 Aging of Mixtures 77
4.3 Langmuir-Blodgett Deposition Experiments 79
4.3.1 Carbon Coating of LB Films 79
4.4 Conclusions 80
4.5 References 81
4.6 Figures 82
5 Nanoparticles, Deasphalted Bitumen, Asphaltenes and Their Mixtures at Air-Water Interface 88
5.1 Introduction 88
5.2 Isotherms of Silica, Asphaltenes, and Maltenes 89
5.3 Isotherms of Mixed Films 89

5.3.1 Maltene-Silica Mixtures 90
5.3.2 Asphaltene-Silica Mixtures 92
5.3.3 Maltene-Asphaltene Mixtures 93
5.4 Compressibility 96
5.5 Deposited Film Images 96
5.6 Discussions 98
5.6.1 Single Component Films 98
5.6.2 Maltene-Silica Mixtures 99
5.6.3 Asphaltene-Silica Mixtures 102
5.6.4 Maltene–Asphaltene Mixtures 103
5.7 Conclusions 104
5.8 References 105
5.9 Figures 108
6 Nanoparticles, Deasphalted Bitumen, Asphaltenes and Their Mixtures at Toluene-Water Interface 122
6.1 Introduction 122
6.2 Results 123
6.2.1 Pressure-area Isotherms and Compressibility 123
6.2.2 SEM and AFM images of LB films: 128
6.3 Discussion 130
6.3.1 Single Component films 130
6.3.2 Maltene-Silica films 131
6.3.3 Asphaltene-Silica films 132
6.4 Summary and Conclusions 134
6.5 References 135
6.6 Figures 136
7 Conclusions and Recommendations 147
7.1 Summary and Conclusions 147
7.2 Recommendations for Future Work 149
A Appendix A: Additional Trough Experiments 150

A.1 Silica Dispersions in Different Containers 150
A.2 Sequential Spreading 152
B Appendix B: Procedure to Construct Compressibility Curves 154
B.1 Introduction 154
B.2 Procedure 155
B.3 References 157
C Appendix C: Isotherm Averaging Technique 158
C.1 Introduction 158
C.2 Procedure 158
C.3 References 162
D Appendix D: Mixed Langmuir Films and the Additive Rule 163
D.1 Introduction 163
D.2 Maltene-Silica Mixtures 166
D.3 Asphaltene-Silica Mixtures 168
D.4 References 170
E Appendix E: Area per Mass Isotherms of Maltene-Asphaltene Mixtures 171
E.1 Introduction 171
E.2 Results 172
E.3 Discussion 174
E.4 Conclusion 176
F Comparison of Toluene-Water Interface to Air-Water Interface 177
F.1 Introduction 177
F.2 Unmixed Films 178
F.2.1 Silica 178
F.2.2 Maltenes 181
F.2.3 Asphaltenes 181
F.3 Mixtures 183
F.4 Conclusion 189

List of Tables

Table 3.1: Elemental analysis of asphaltenes (Zhang et al., 2003b) and deasphalted bitumen. 53

Table 3.2: Molecular weight and density of asphaltenes and deasphalted bitumen (a- from Zhang et al. (2003b)).......... 53

Table 3.3: Properties of fumed silica nanoparticles used in experiments. Surface treatments are a) Dimethyldichlorosilane, b) Hexamethyldisilazane, and c) Aminosilane 54

Table 3.4: Summary of mixtures of silica, asphaltenes and maltenes used in Langmuir trough experiments.......... 59

Table 3.5: Typical amounts of substances used for pressure-area isotherm experiments 62

Table 3.6: Typical amounts of individual components from mixtures used for pressure-area isotherm experiments 63

Table 5.1: Extrapolated limiting area (A_0), collapse areas, and collapse pressures determined from intercepting lines fit to π-a isotherms of maltene-silica mixtures. 91

Table 5.2: Extrapolated limiting area A_0, collapse areas, and collapse pressures determined from intercepting lines fit to π-A isotherms of asphaltene-silica mixtures.......... 93

Table 5.3: Molecular weights of maltene-asphaltene mixtures 94

Table 5.4: Transition and collapse points of maltene-asphaltene mixtures 95

Table 5.5: Transfer ratios of the Langmuir-Blodgett depositions.......... 97

List of Figures

Figure 2.1: Process flow of a bitumen extraction plant (reproduced from Yan et al., 1999) 37

Figure 2.2: Two possible compositions of the interfacial film formed by asphaltenes a) asphaltene aggregates form a network at the interface (reproduced from Auflem, 2002), and b) asphaltenes behave as surfactants and form an interfacial film (reproduced from Lee, 1999) 38

Figure 2.3: TEM micrograph of fine solid particle obtained from coker feed bitumen (reproduced from Sztukowski and Yarranton, 2004) 39

Figure 2.4: Wilhelmy plate across an air-water interface. 39

Figure 2.5: Surface pressure-area isotherm of arachidic acid at an air-water interface ... 40

Figure 2.6: Sketch of a typical Langmuir trough device 40

Figure 2.7: Surface pressure-area isotherms for different asphaltene fractions extracted from Athabasca bitumen. (reproduced from Zhang et al., 2003a) 41

Figure 2.8:a) Isotherms of various amounts of Cab-O-Sil silica nanoparticles where pressure is plotted against trough area (reproduced from Maté et al., 1998), and b) Isotherm of silanized glass spheres (d~3μm). The trough area has been normalized by the number of particles spread on the water surface (reproduced from Hórvölgyi et al., 1996) 42

Figure 2.9: Microscopic images of the collapse of a polystyrene particulate film: a) some monolayer is folding soon after collapse is seen in the π-a isotherm, and b) upon further compression the folds expand and deepen. White scale bars are 50μm wide. (reproduced from Aveyard et al., 2000b) 43

Figure 2.10: Brewster angle microscope images showing clusters of hydrophobic silica particles at an air-water interface. Hydrophobicity decreases from a) to c). Image width is 550 μm. (Reproduced from Tolnai et al., 2001) 44

Figure 2.11: Microscopic images showing complex pattern formation in monolayers of 3μm latex particles. Approximate image dimensions are as shown. (reproduced from Ghezzi et al., 1999) 45

Figure 2.12: Langmuir-Blodgett deposition of a Langmuir film onto a solid substrate ... 46

Figure 2.13: Major components of an atomic force microscope and details of its operation 47

Figure 2.14: Major components of a scanning electron microscope. (reproduced from Bindle et al., 1992) 48

Figure 2.15: AFM images of Athabasca asphaltenes deposited from an air-water interface. Π= 30mN/m (reproduced from Zhang et al., 2003b) 49

Figure 2.16 AFM images of Athabasca asphaltenes deposited from a toluene-water interface. Π= 20mN/m (reproduced from Zhang et al., 2005b) 50

Figure 3.1: Measurement of contact angle from the shape of a sessile drop on a solid surface. Shown is the air-water contact angle of hydrophilic and hydrophobic solids 69

Figure 3.2: Transmission Electron Micrograph (TEM) of fumed silica nanoparticles (modified from Degussa Corporation website) 69

Figure 3.3: Density particle size distribution on weight basis of R974 hydrophobic silica in toluene (1.05 wt%) measured with acoustic spectrometer device. 70

Figure 3.4: Mean diameter of silica in toluene measured with acoustic spectrometer at various concentrations of silica in toluene. 70

Figure 3.5: Variation of mean diameter of silica in toluene with an increase in the age of the suspension. Values from before time zero correspond to the values from the dilution graph in Figure 3.4. Measurements made after time zero are at a concentration of 0.29 wt%. 71

Figure 3.6: KSV mini-trough system. 71

Figure 3.7: Cross section of the two Langmuir trough designs. Sketch shows the position of the barriers in the trough and the basic design of each trough. 72

Figure 3.8: Image of silicon wafer loaded into the dipping mechanism prior to Langmuir-Blodgett deposition. 72

Figure 4.1: Surface pressure-area isotherms of arachidic acid at air-water interface. Comparison of experimental data with published results. 82

Figure 4.2: Surface pressure-area isotherms of maltenes and maltenes mixed with hydrophilic silica. Films formed at air-water interface. 83

Figure 4.3: Surface pressure-area isotherms of R504 hydrophobic silica obtained with various film compression rates. Films formed at air-water interface 83

Figure 4.4: Surface pressure-area isotherms of maltenes for films that had different evaporation times (time between film spreading and initial compression). Films formed at air-water interface 84

Figure 4.5: Surface pressure-area isotherms of mixtures of hydrophobic silica (θ_{aw}=117°) and maltenes. Each isotherm represents a film formed at a different time measured from the initial combination of the 2 substances. 84

Figure 4.6: Variation in surface pressure and film area for maltene-silica mixtures of different ages 85

Figure 4.7: Surface pressure-area isotherms of mixtures of hydrophobic silica (θ_{aw}=117°) and asphaltenes. Each isotherm represents a film formed at a different time measured from the initial combination of the 2 substances. 85

Figure 4.8: Variation in surface pressure and film area for asphaltene-silica mixtures of different ages 86

Figure 4.9: AFM images of a 50 wt % asphaltene – 50 wt% silica mixture deposited from an air-water interface a) uncoated film and b) carbon coated film. 86

Figure 4.10: AFM images of an (a) uncoated and (b) carbon coated silicon wafer. 87

Figure 4.11: AFM images of a 50 wt % maltene – 50 wt% asphaltene mixture deposited from an air-water interface a) uncoated film and b) carbon coated film. 87

Figure 5.1: Density particle size distribution, on weight basis, of R974 hydrophobic silica nanoparticles in toluene (1.05 wt%) measured with an acoustic spectrometer device. 108

Figure 5.2: Surface pressure-area isotherms of silica nanoparticles, maltenes and asphaltenes. 108

Figure 5.3: Surface pressure-area isotherms of films from maltene and silica mixtures of varying ratios of maltenes:silica. Isotherms are normalized by the mass of silica at the interface 109

Figure 5.4: Surface pressure-area isotherms of films from maltene and silica mixtures of varying ratios of maltenes:silica. Isotherms are normalized by the mass of maltenes at the interface 109

Figure 5.5: Area shift from the isotherm of a silica film for maltene-silica mixtures. At various surface pressures plotted against the ratio of silica:maltenes 110

Figure 5.6: Area shift from the isotherm of a maltene film for maltene-silica mixtures. At various surface pressures plotted against the ratio of maltenes:silica 110

Figure 5.7: Surface pressure-area isotherms of films from asphaltenes and silica mixtures of varying ratios of asphaltenes:silica. Isotherms are normalized by the mass of asphaltenes at the interface. 111

Figure 5.8: Surface pressure-area isotherms of films from asphaltenes and silica mixtures of varying ratios of asphaltenes:silica. Isotherms are normalized by the mass of silica at the interface. Collapse points are enlarged. 111

Figure 5.9: Area shift from the isotherm of a silica film for asphaltene and silica mixtures. At various surface pressures plotted against the ratio of asphaltenes:silica. 112

Figure 5.10: Area shift from the isotherm of an asphaltene film for asphaltene and silica mixtures. At various surface pressures plotted against the ratio of silica:asphaltenes. 112

Figure 5.11: Surface pressure-area isotherms of films from asphaltenes and maltenes mixtures of varying ratios of asphaltenes:maltenes. Isotherms are normalized by the number of molecules at the interface. 113

Figure 5.12: Surface pressure-area isotherms of films from asphaltenes and maltenes mixtures at lower area per molecule range than Figure 5.11. Estimated transition and collapse points are highlighted. 113

Figure 5.13: Area per molecule of maltene-asphaltene mixtures at 5, 10 and 15 mN/m surface pressures plotted as a function of mole fraction of maltene. 114

Figure 5.14: Compressibility of films formed from maltene-silica mixtures. 114

Figure 5.15: Compressibility of films formed from asphaltene-silica mixtures. 115

Figure 5.16: AFM images of single layer LB films deposited on to silicon wafers from air-water interface. Surface pressure at deposit, $\pi_{deposit}$ = 10 mN/m. a) Silica only TR=0.51, b) 50 wt % maltene – 50 wt% silica mixture TR = 1.39 c) 50 wt % asphaltene – 50 wt% silica mixture TR = 2.46 d) Asphaltene only TR =0.57 116

Figure 5.17: AFM images of single layer LB films deposited on to silicon wafers from air-water interface. Images are of areas with a relatively low height compared to the rest of the film. a) 50 wt % maltene – 50 wt% silica mixture TR = 1.39 b) 50 wt % asphaltene – 50 wt% silica mixture TR = 2.46 117

Figure 5.18: SEM images of single layer LB film of silica deposited onto silicon wafers from air-water interface. Inset image shows same film at higher magnification. Surface pressure at deposit, $\pi_{deposit}$ = 10 mN/m. Film was coated with carbon to enable SEM imaging. 118

Figure 5.19: SEM images of single layer LB film of 50 wt% silica –50 wt% maltene deposited onto silicon wafers from air-water interface. Inset image shows same film at higher magnification. Surface pressure at deposit, $\pi_{deposit}$ = 10 mN/m. Film was coated with carbon to enable SEM imaging. 119

Figure 5.20: SEM images of single layer LB film of 50 wt% silica –50 wt% asphaltene deposited onto silicon wafers from air-water interface. Inset image shows same film at higher magnification. Surface pressure at deposit, $\pi_{deposit}$ = 10 mN/m. Film was coated with carbon to enable SEM imaging. 120

Figure 5.21: Height along cross section of an AFM image for a silica cluster. Inset AFM image from LB film of 50 wt% silica –50 wt% asphaltene mixture. 121

Figure 6.1: Interfacial pressure-area isotherms of silica nanoparticles, maltenes and asphaltenes. 136

Figure 6.2: Interfacial pressure-area isotherms of films from maltene and silica mixtures of varying maltenes:silica ratios. Isotherms are normalized by the mass of silica at the interface........ 136

Figure 6.3: Area shift from the isotherm of a silica film for maltene-silica mixtures. At various interfacial pressures plotted against the ratio of maltenes:silica. 137

Figure 6.4: Interfacial pressure-area isotherms of films from maltene and silica mixtures of varying maltenes:silica ratios. Isotherms are normalized by the mass of maltenes at the interface........ 137

Figure 6.5: Area shift from the isotherm of a maltene film for maltene-silica mixtures. At various interfacial pressures plotted against the ratio of silica:maltenes. 138

Figure 6.6: Compressibility of films formed from maltene-silica mixtures at toluene-water interface........ 138

Figure 6.7: Interfacial pressure-area isotherms of films from asphaltenes and silica mixtures of varying ratios of asphaltenes:silica. Isotherms are normalized by the mass of asphaltenes at the interface. 139

Figure 6.8: Area shift from the isotherm of an asphaltene film for asphaltene-silica mixtures. At various interfacial pressures plotted against the ratio of silica:asphaltenes........ 139

Figure 6.9: Interfacial pressure-area isotherms of films from asphaltenes and silica mixtures of varying ratios of asphaltenes:silica. Isotherms are normalized by the mass of silica at the interface. 140

Figure 6.10: Area shift from the isotherm of a silica film for asphaltene -silica mixtures. At various interfacial pressures plotted against the ratio of asphaltenes:silica....... 140

Figure 6.11: Compressibility of films formed from asphaltene-silica mixtures at toluene-water interface.. 141

Figure 6.12: Interfacial pressure-area isotherms of films from asphaltenes and maltenes mixtures of varying ratios of asphaltenes:maltenes. Isotherms are normalized by the mass of asphaltenes at the interface... 141

Figure 6.13: SEM images of single layer LB film of silica deposited onto silicon wafers from toluene-water interface. Inset image shows same film at higher magnification. Interfacial pressure at deposit, $\pi_{deposit}$ = 10 mN/m. Film coated with carbon to enable SEM imaging.. 142

Figure 6.14: SEM images of single layer LB film of 50wt% silica –50 wt% maltene deposited onto silicon wafers from toluene-water interface. Inset image shows same film at higher magnification. Interfacial pressure at deposit, $\pi_{deposit}$ = 10 mN/m. Film coated with carbon to enable SEM imaging.. 143

Figure 6.15: SEM images of single layer LB film of 50wt% silica –50 wt% asphaltene deposited onto silicon wafers from toluene-water interface. Inset image shows same film at higher magnification. Interfacial pressure at deposit, $\pi_{deposit}$ = 10 mN/m. Film coated with carbon to enable SEM imaging.. 144

Figure 6.16: AFM height images of single layer LB films deposited on to silicon wafers from toluene-water interface. Interfacial pressure at deposit, $\pi_{deposit}$ = 10 mN/m. a) Silica only TR=0.21, b) 50 wt % maltene – 50 wt% silica mixture TR = 0.90 c) 50 wt % asphaltene – 50 wt% silica mixture TR = 1.89 d) 50 wt % maltene – 50 wt% asphaltene TR =1.70 145

Figure 6.17: AFM height image of single layer LB films deposited on to silicon wafers from toluene-water interface. Image is of areas with a relatively low profile compared to the rest of the film. 50 wt % asphaltene – 50 wt% silica mixture TR =1.89 146

Figure A.1: Surface pressure-area isotherms of hydrophobic silica (118°) where silica in toluene dispersion was stored in different container materials............................. 152

Figure A.2: Surface pressure-area isotherms of mixtures of hydrophobic silica (118°) and maltenes. Isotherms shown include silica only, maltene only, mixture formed with classic spreading technique and mixture formed with sequential spreading.......... 153

Figure B.1: Comparison of smooth data with measured data for asphaltene isotherm.. 156

Figure B.2: Comparison of compressibility calculations using a forward difference method (Excel) and a macro from SigmaPlot 157

Figure C.1: Maximum and minimum determined 159

Figure C.2: Standard areas applied 160

Figure C.3: Interpolation of pressures at standard area values 160

Figure C.4: Average surface pressure values are calculated 161

Figure C.5: Comparison of average isotherm to two measured isotherms 162

Figure D.1: Area occupied by a mixture of maltenes and silica at an air-water interface. Area per mass plotted as a function of weight fraction of silica 166

Figure D.2: Area occupied by a mixture of maltenes and silica at a toluene-water interface. Area per mass plotted as a function of weight fraction of silica 167

Figure D.3: Schematic showing a possible cause of the negative excess areas reported by mixed films. 167

Figure D.4: Area occupied by a mixture of asphaltenes and silica at an air-water interface. Area per mass plotted as a function of weight fraction of silica 168

Figure D.5: Area occupied by a mixture of asphaltenes and silica at a toluene-water interface. Area per mass plotted as a function of weight fraction of silica 169

Figure E.1: Surface pressure-area isotherms of films from maltene-asphaltene mixtures. Isotherms are normalized by the mass of maltenes at the interface 172

Figure E.2: Area shift from the isotherm of a maltene film for maltene-asphaltene mixtures. At various interfacial pressures plotted against the ratio of asphaltenes:maltenes. 173

Figure E.3: Surface pressure-area isotherms of films from maltene-asphaltene mixtures. Isotherms are normalized by the mass of maltenes at the interface 173

Figure E.4: Area shift from the isotherm of an asphaltene film for maltene-asphaltene mixtures. At various interfacial pressures plotted against the ratio of maltenes:asphaltenes. 174

Figure F.1: Pressure-area isotherms of R974 hydrophobic silica nanoparticles at air-water and toluene-water interfaces. 178

Figure F.2: Pressure-area isotherms from silica films with pressure normalized by the interfacial tension (γ_{tw}=36 mN/m, γ_{aw}=72.8 mN/m) 179

Figure F.3: SEM images of silica films from (a) air-water interface and (b) toluene-water interface........ 180

Figure F.4: Comparison of normalized pressure-area isotherms of maltene films from air-water and toluene-water interfaces. 180

Figure F.5: Comparison of normalized pressure-area isotherms of asphaltene films from air-water and toluene-water interfaces........ 182

Figure F.6: Pressure-area isotherms of maltene and asphaltene films at air-water and toluene-water interfaces. 183

Figure F.7: Pressure-area isotherms of maltene-silica mixtures and asphaltene-silica mixtures at air-water and toluene-water interfaces. 184

Figure F.8 Pressure-area isotherms of 25 wt% maltene – 75 wt % silica mixture from films at air-water and toluene-water interfaces........ 185

Figure F.9: Normalized pressure-area isotherms of 25 wt% maltene – 75 wt % silica mixture from films at air-water and toluene-water interfaces. 185

Figure F.10: SEM images of 50 wt% maltenes – 50 wt% silica films from (a) air-water interface and (b) toluene-water interface 186

Figure F.11: Pressure-area isotherms of 25 wt% asphaltene – 75 wt % silica mixture from films at air-water and toluene-water interfaces........ 187

Figure F.12: Pressure-area isotherms of 25 wt% asphaltene – 75 wt % silica mixture from films at air-water and toluene-water interfaces........ 187

Figure F.13: SEM images of 50 wt% asphaltenes – 50 wt% silica films from (a) air-water interface and (b) toluene-water interface 189

List of Symbols

π, Π	Surface or interfacial pressure (m)
π_c, Π_c	Interfacial pressure at film collapse (N/m)
π_t, Π_t	Interfacial pressure at phase transition (N/m)
γ_o	Interfacial tension of a "pure" interface (N/m)
γ	Interfacial tension in presence of an interfacial film (N/m)
θ	Contact angle (°)
γ_{ow}	Oil-water interfacial tension (N/m)
ρ_{tol}	Measured density of toluene (kg/m^3)
ρ_{sample}	Calculated density of sample (kg/m^3)
ρ_{mix}	Measured density of solution (kg/m^3)
F	Force on Wilhelmy plate measured by electrobalance (N)
A_t	Langmuir trough area (m^2)
t	Wilhelmy plate thickness (m)
w	Wilhelmy plate width (m)
A_o	Initial molecular area or limiting area of a Langmuir film (m^2/molecule)
C_s	Film compressibility (m/N)
A_c	Interfacial area at film collapse (m^2)
A_t	Interfacial area at phase transition (m^2)
TR	Transfer ratio of film deposition
$N_{initial}$	Number of particles on droplet surface
ΔA	Change in interfacial area (m) OR Area shift of isotherm (m)
x_{sample}	Mass fraction of sample in the solution.
Xa, Xm	Mass Fraction of asphaltenes, maltenes
MW, MW_a, MW_m	Molecular weight (g/mol)

"Relax. What is mind? No matter. What is matter? Never mind!"

-Homer Simpson

1

Introduction

1.1 Introduction

There are many technical challenges during the processing of oil sands ore to produce usable petroleum products. One of these challenges is the existence of stable water droplets in diluted bitumen produced from froth treatment. The presence of an interfacial film on the droplet surface results in the formation of a stable water droplet and prevents complete phase separation of oil and water. In order to overcome this challenge and remove all of the water and solids from diluted bitumen during froth treatment, an understanding of the interfacial films responsible for the stability of the droplets is needed. Methods of investigating interfacial films vary widely. Two such methods are to create and study Langmuir and Langmuir-Blodgett films. Langmuir films are monolayers of a substance spread at an interface. Depositing a Langmuir film onto a solid substrate creates a Langmuir-Blodgett film.

This thesis encompasses work investigating Langmuir and Langmuir-Blodgett films of asphaltenes, deasphalted bitumen and fumed silica particles. Fumed silica was used to represent the fine solids that are present naturally in bitumen. This study was undertaken in order to investigate the behaviour of asphaltenes and maltenes when present in interfacial films with fine solids.

1.2 Thesis Overview

A literature review that focuses on research related to the oil sands industry is provided in Chapter 2. This includes an introduction into oil-sands ore and associated components such as asphaltenes, maltenes and fine solids. The role of these components in emulsion stability is discussed. Previous research conducted using Langmuir and Langmuir films of these various components is reviewed. As well, background information describing the principles behind the important equipment used in experiments is given.

Detailed experimental procedures and descriptions of the materials used are provided in Chapter 3. In addition, results of some preliminary experiments conducted to establish different experimental parameters are presented and discussed in Chapter 4.

Chapter 5 focuses on experimental results from an air-water interface. Experiments involve the measurement of pressure-area isotherms of various mixtures of asphaltenes, maltenes and fumed silica with a Langmuir trough. Mixtures were made from various ratios of components in order to study the results of varying the composition of the film. Langmuir-Blodgett films were created and images of the films were obtained with atomic force microscopy and scanning electron microscopy.

Experimental results obtained from a toluene-water interface are presented and discussed in Chapter 6. As with Chapter 5, many films of various compositions were investigated with a Langmuir trough and the imaging techniques.

Chapter 7 states the major conclusions of the thesis and provides some recommendations for areas of further study.

"Every time I learn something new, it pushes some old stuff out of my brain. Remember when I took that home winemaking course, and I forgot how to drive?"
-Homer Simpson

2

Background Information

2.1 Introduction

The current chapter presents a review of background information pertinent to this thesis. In order to provide an industrial context the literature review incorporates an introduction into oil sands extraction, and the role of various bitumen components in emulsion stabilization. In addition, information necessary for the introduction of the tools used in the thesis is obtained from literature. Studies that utilize similar tools, applicable to the current work, are reviewed.

2.2 Water-in-Oil Emulsions in Bitumen Processing

Emulsions are important in many industries. The industrial process that has the most relevance to this thesis is the froth treatment process used during the development of the Athabasca Oil Sands deposit in Northern Alberta. Oil sands are an unconsolidated mixture of coarse sand, water, bitumen and fine solids. The exact composition of oil sands ore varies substantially with the source location. In general, oil sands ore is composed of about 85% solids, 5% water and 10% bitumen (Camp, 1976; Yan, Elliott and Masliyah, 1999). The particle size distribution of the solids also varies quite substantially, but the percentage of fines (<44μm) is inversely related to the bitumen content (Camp, 1976; Masliyah and Gray, 2004). To give a general number, fines account for approximately 25% of the total solids in ores with 10% bitumen, for a recent sampling of oil sands ore (Masliyah and Gray, 2004).

The basic steps in the production of marketable synthetic crude oil from oil sands are: mining of the oil sands, bitumen extraction via flotation, chemical and physical treatments of the bitumen froth, and upgrading of the froth-treated bitumen. Several sources are available for greater detail about this complex industrial process (Camp F.W., 1976; Masliyah and Gray, 2004). Figure 2.1 presents a simplified flow diagram of a bitumen extraction plant. After the extraction process, bitumen froth consisting of approximately 10% solids, 30% water and 60% bitumen is created (Yan et al., 1999). A froth treatment process is then used to remove water and solids from the aerated bitumen froth. During froth treatment the bitumen froth is diluted in order to reduce the bitumen viscosity and improve the density differences between the petroleum component and the solids and water. The diluted bitumen is then subjected to various physical processes, including centrifugation and inclined plate settling, to remove water and solids. Unfortunately, not all of the water and solids are removed during froth treatment. When naphtha is used as a diluent, the treated bitumen contains approximately 2-3% water and 0.5% solids (Chen et al., 1999; Yan et al., 1999)

Residual water and solids in the treated bitumen continue downstream to the bitumen upgrading process. Salts contained in the emulsified water are corrosive to downstream equipment, and the salts and fines cause fouling of downstream equipment such as catalyst surfaces and packed bed hydrotreaters (Kotlyar et al., 1999). Problems associated with the fines and water in froth treated bitumen provide ample reason to investigate water-in-oil emulsions. Emulsion stability is usually attributed to the presence of fine solids and asphaltenes. Fine solids and asphaltenes present in bitumen possess the ability to stabilize water-in-diluted bitumen emulsions (Yan et al., 1999). Furthermore, other water-soluble surfactants in bitumen do not stabilize water-in-toluene emulsions, emphasizing the role of asphaltenes (Gu et al., 2002). "It is suggested by many researchers that asphaltenes and/or solids form a steric sheath that covers the water droplets and offers stabilization against water droplet coalescence" (Chen et al., 1999, p. 329).

2.2.1 Asphaltenes and Their Role in Emulsion Stability

Asphaltene properties have been studied extensively to investigate the role of asphaltenes in emulsion stability. Asphaltenes also play an important role in upgrading and crude oil properties. Therefore, information about their behaviour and structure is important to many facets of the petroleum industry. Part of asphaltene research is directed to determining the chemistry and behaviour of asphaltenes that allow them to make such a strong contribution to emulsion stability.

Asphaltenes are generally defined as a solubility class of petroleum liquids, such as bitumen. They are soluble in toluene but not in *n*-pentane or *n*-heptane. Once asphaltenes are extracted, the remainder of the petroleum are named "maltenes", which are composed of saturated hydrocarbons, aromatics and resins (McLean et al., 1998). Asphaltenes are a group of molecular species composed of the highest molecular weight and most polar species in petroleum. Measured molecular weights of asphaltenes range from 1000-10000 g/mol (Yarranton et al., 2000). Structure, composition and chemical properties of asphaltenes are highly dependent on the source of the asphaltenes and the solvent used to extract them (McLean et al., 1998). Although the specific details of asphaltene structure are widely varied, some common features do exist. Asphaltenes are polyaromatic with heteroatom functional groups and contain hydrophilic and hydrophobic structures (Yarranton et al., 2000).

Due to the attraction of water to polar head groups the asphaltenes adsorb to water-oil interfaces. This allows asphaltenes to form interfacial films that are responsible for water-in-oil emulsion stability. The way that asphaltenes adsorb on the interface, the mode of film formation and the organization of the asphaltenes at the interface have not been fully established. The most widely accepted concept for emulsion stability by asphaltenes is the formation of a networked film of aggregates by crosslinking (McLean et al., 1998). This concept is demonstrated in Figure 2.2a showing an emulsion drop interface protected by a layer of networked aggregates. The interfacial film provides a mechanical barrier to droplet coalescence. McLean et al. (1998) reviewed work supporting this mechanism. However, other mechanisms may be possible. Asphaltenes have been shown to adsorb at water-oil interfaces as molecular surfactants when present in low concentrations in the oil phase (Yarranton et al., 2000). When this occurs, the interfacial film would be composed of molecules with the polar component in the water phase and the hydrophobic ends remaining in the oil phase, as shown in Figure 2.2b. The interfacial film provides a steric barrier to droplet coalescence. The steric repulsion forms because the hydrophobic components in the oil phase favour interaction with the solvent, creating an energy barrier preventing the molecules from being close or overlapping (Masliyah and Gray, 2004; McLean et al., 1998).

Many studies indicate the existence of an interfacial skin at oil-water interface when asphaltenes are present (McLean et al., 1998). The Langmuir trough is a useful method for studying the properties of interfacial films. Several investigations on asphaltene films have been conducted. Experiments using a Langmuir trough can provide information about the film compressibility (rigidity) and attributes of film structure can be determined from Langmuir-Blodgett deposition. Details of Langmuir trough studies with asphaltenes are outlined in section 2.4.2. One important result from Langmuir trough research indicates that both asphaltene molecules and precipitated aggregates adsorb from heptol (a mixture of *n*-heptane and toluene) to the heptol-water interface and both form films rigid enough to stabilize emulsions (Zhang et al., 2005a). This finding provides support to both the molecular surfactant and aggregate network concepts of asphaltene-stabilized emulsions.

2.2.2 Maltenes and Their Contributions to Emulsion Stability

Deasphalted bitumen (maltenes) is the fraction of bitumen that is soluble in *n*-alkanes (for example, *n*-heptane). Maltenes are composed of saturated hydrocarbons, aromatics and resins. The emulsion stabilizing power of maltenes is much less than other bitumen components as water-in-diluted maltenes emulsions are very unstable (Yan et al., 1999). There is also evidence that maltenes reduce the emulsion stabilizing capacity of asphaltenes and solids from bitumen (Yan et al., 1999). Although the entire maltenes fraction was shown to be unable to stabilize emulsions, components of the maltenes may contribute to the emulsion stability when present with asphaltenes. Evidence has been gathered to show that resins, derived from petroleum sources other than bitumen, increase water-in-oil emulsion stability (McLean et al., 1998). The role of resins was discussed by McLean et al. (1998): Resins may solvate asphaltene aggregates in crude oil and make smaller aggregates, which may improve the film forming capabilities. The smaller aggregates would be more mobile and would produce more organized films. The resins attached to asphaltene aggregates may be "shed" when the aggregates are adsorbed to an interface (McLean and Kilpatrick, 1997). The contributions of resins to interfacial films have been studied on the Langmuir trough and it has been shown that a mixture of resins and asphaltenes will form a less rigid film than the case for asphaltenes alone (Mohammed et al., 1993). The contribution of the entire maltene fraction is unknown but probably dominated by the resin component or natural surfactants from the bitumen.

2.2.3 Properties of Solids from Bitumen

Although fine solids exist in commercial diluted bitumen systems, little attention has been focused on solids-stabilized emulsions related to the oil sands industry. In particular, no studies have been conducted that use a Langmuir trough for this purpose. However, the role of fine solids in emulsion stability is important in many other industrial processes and has been under investigation for many years. Information from emulsion studies with other systems and which utilize other experimental devices may be applicable to this thesis. To obtain this information it is suggested that the reader refer to a review article of solids-stabilized emulsions research such as Lopetinsky, Masliyah and Xu (In press).

Solid particles present in industrial oil-water systems contribute to water-in-oil emulsion stability, such as the contribution of seawater particulates to emulsions in oceanic oil spills (Lee, 1999). The fine solids present in oil sands ore, which carry through processing to froth treatment, also contribute to the stability of water-in-oil emulsions (Yan et al., 1999). Emulsion stability in froth treated bitumen is in part due to the presence of these fine solids. This has been shown by the results from several researchers including Yan et al. (1999), Sztukowski and Yarranton (2004), and Gu et al. (2003).

Many properties of the solids present during oil sands processing have been investigated. Solids from oil sand ore in the –2 μm size fraction are composed of mostly clay particles (Camp, 1976). The ultrafine solids that remain in bitumen after extraction and froth treatment are mainly composed of single-layer clay particles such as kaolinite (Kotlyar et al. 1999; Sztukowski and Yarranton, 2004). The particle size distribution determined by dynamic light scattering (Malvern Mastersizer) shows that 90% of the particle diameters are smaller than 300 nm but the diameters range up to 1μm (Sztukowski and Yarranton, 2004). TEM micrographs show that the particles have a plate-like shape and that the thickness is usually less than 10 nm (Kotlyar et al., 1999). Figure 2.3 shows a TEM micrograph of fine solids extracted from coker feed bitumen. For samples of Athabasca coker-feed bitumen the weight fraction of fine solids obtained from studies specifically investigating the solids was 0.8-0.9% (Kotlyar et al., 1998; Sztukowski and Yarranton, 2004).

For model emulsions created in laboratories it has been shown that solid particle size is an important parameter affecting emulsion stability. To a certain extent, as particle size decreases, emulsion droplet size decreases and emulsion stability increases. Determining the effective size of fine particles from bitumen is difficult because when the particles are dispersed in froth treated bitumen and during laboratory removal the fine solids may aggregate. Yan et al. (1999) were able to remove a certain amount of solids from bitumen by filtering toluene-diluted bitumen through 8μm filter paper. The filtered product (i.e. solids-reduced bitumen) did not have a reduced ability to stabilize water-in-diluted bitumen emulsions. After filtering out particles with 0.22 μm filter paper, stability of emulsions formed with the filter product had been reduced. This suggests that particles in the –8 μm/+0.22 μm size range make the largest contribution to emulsion stability. However, for solids studied by Sztukowski and Yarranton (2004), about 90% of the particles are less than 0.3 μm in diameter when they are removed and fully dispersed with sonication. Particles removed by filter paper are probably aggregated together and may be held together with asphaltenes or other bitumen components. Research has indicated that particles will aggregate when dried (Sztukowski and Yarranton, 2004). It appears that particle aggregation plays a role in the emulsion stability of froth treated bitumen, and aggregates may form on the surface of emulsion droplets. Based on calculations of asphaltene monolayer coverage of model water-in-oil emulsion droplets, fine particles appear to lay flat at the interface and do not aggregate (Sztukowski and Yarranton, 2004). However, the actual behaviour of the fine solids at oil-water interfaces has not been determined.

Particle wettability determines whether or not particles remain at oil-water interfaces and whether the solids will reside in the continuous oil phase or dispersed water phase in a water-in-oil emulsion. Particles with an intermediate wettability (i.e. biwettable) will more strongly adhere to an interface and should produce more stable emulsions (Aveyard, Binks and Clint 2003). The fine solids in froth-treated bitumen are interfacially active and have been shown to be biwettable. The oil-water contact angles of solids obtained from froth treated bitumen have been studied by Chen et al. (1999). They observed that the solids are biwettable (by oil and water) and the wettability is dependant on the polarity of solvent used to wash the solids. Infrared spectroscopy measurements of the washing solvents showed that the surface of the fine solids were associated with surfactant particles, which were removed by toluene but not heptane. Cleaning of the fine solids with toluene reduces the ability of the solids to stabilize emulsions (Gu et al., 2003). Thus the surface properties (i.e. wettability) of the fine solids are determined by surfactants or other components in bitumen.

The emulsion stability can also be affected by the pH of the system. For both, water-in-toluene-diluted bitumen emulsions and water-in-heptol emulsions stabilized by solids, emulsion inversion was induced by pH changes (e.g. change from water-in-oil to oil-in-water) (Gu et al., 2003). Emulsion inversion due to pH change suggests that the wettability of the fine solids is dependant on pH, which was confirmed by contact angle measurements of commercial kaolinite clays at different pH levels (Gu et al., 2003). By measuring conductivity and surface tension of the aqueous phase from a water-in-diluted bitumen emulsion, the presence of both cationic and anionic surfactants was observed. The surfactants were released from the bitumen over an extended pH range and are likely responsible for the wettability change in the fine solids (Gu et al., 2003).

In addition to the presence of surfactants on fine solid surfaces, asphaltenes are likely to adsorb onto the solid surfaces. Metal analysis of the fine solids shows high nickel and vanadium concentrations, which is indicative of the presence of asphaltenes on the surface of fine solids from bitumen (Kotlyar et al., 1999). Most of the solids present in bitumen will be removed during precipitation of asphaltenes (Kotlyar et al., 1998). The adsorption of asphaltenes onto clean kaolinite clay particles causes a change in the particle contact angle and imparts the ability to stabilize oil-in-water emulsions on clay particles (Yan and Masliyah, 1993).

The composition, shape, size and wettability of fine solids in bitumen are varied. All of these factors have a role in the emulsion stability. However, the extent of this role has not been elucidated. Surfactants from bitumen have been found to alter the wettabilty of solid particles influencing the particles contribution to emulsion stability. The combination of solids and asphaltenes has some influence on emulsion stability as well. Little or no study of fine solids with the Langmuir trough has been performed in regards to interfacial film strength or the combination of solids and asphaltenes for emulsion stability. Literature on Langmuir trough studies of solids is reviewed in section 2.4.3 after the Langmuir trough apparatus is introduced.

2.3 Thesis Objective

The purpose of this thesis is to use the Langmuir trough and Langmuir-Blodgett deposition techniques to obtain information about the interaction between asphaltenes, maltenes and fine solids at an air-water and toluene-water interface. Investigating the interfacial film properties of these components and their mixtures provides valuable information about the interfacial films responsible for the stability of water-in-bitumen emulsions.

2.4 Langmuir Films

The Langmuir trough is a tool capable of investigating certain properties of interfacial films. This equipment was designed to conduct experiments on surface-active material that has the ability to form a monolayer film on a water surface. Irwing Langmuir developed the theory, technique and instruments related to the Langmuir trough nearly 100 years ago. The longevity of his technique is a testament to the significance of this Nobel Prize winner's research. In an article in 1917, Langmuir described the technique of measuring surface pressure and detailed his experimental apparatus (Langmuir, 1917). Langmuir's research into spread oil films on water surfaces is predated by Pockels (1891) and Rayleigh (1899), who studied the surface tension of clean and contaminated water using rectangular troughs. Langmuir refined the equipment and techniques and developed the theory behind the experimental results more thoroughly. For further detail on the techniques and history of insoluble monolayers refer to Gaines (1966). The basic measurement that the Langmuir trough makes is the change in interfacial pressure with a change in the interfacial area of a spread film. To explain the concept of the Langmuir trough and further describe the equipment and technique, a basic treatment of the underlying principles including, surfactants, surface tension, and surface pressure follows.

2.4.1 Theory

Surface Active Material

Surfactants are molecules with molecular structures that enable them to assemble at fluid-fluid interfaces. Most surfactants are amphiphilic in nature, containing hydrophilic and hydrophobic components. Additionally, fine particles with intermediate wettability can behave similar to surfactants (Lopetinsky et al., In press). It is the ability of the surfactants to form films/layers at an interface that allows them to stabilize emulsions. The films formed at the interface are thus an important area to study.

Surface Tension

One basic concept underlying Langmuir trough experiments is surface tension. At a fluid-fluid interface there is an imbalance in the cohesive forces acting on molecules at the molecular interfacial layer. The result is that molecules are pulled from the interface towards the bulk, which enhances the cohesive forces amongst molecules (of the same fluid) at the interface. The interfacial molecules thus resist the formation of new interfacial area giving rise to surface tension (Gaines, 1966, p. 8; Adamson and Gast, 1997, p. 56; KSV Instruments Ltd., n.d.). Surface (interfacial) tension can be considered as a free energy per unit area (e.g. erg/cm^2) or a force per unit length (e.g. mN/m) (Adamson and Gast, 1997). All liquids have a characteristic surface tension and the tension of water is particularly high (72.8 mN/m at 20°C). For further details on the theory of interfaces and a development of an expression for surface free energy using thermodynamics, many references are available, including those by Adamson and Gast (1997) and Gaines (1966).

Surface Pressure

One property of interfacial films formed by surface-active agents is their effect on the interfacial tension of a liquid-liquid interface. The surfactant layer will cause a decrease in the surface tension. In Gaines' book he elucidates a concept from Langmuir (1917) that the difference in surface tension can be thought of as the two-dimensional pressure exerted by the surface film (Gaines, 1966, p. 14). This explanation has led to the definition of surface (interfacial) pressure as the change in surface (interfacial) tension. Mathematically this is expressed by Equation 2.1 below:

$$\Pi = \gamma_o - \gamma \quad \text{[2.1]}$$

where Π is the interfacial pressure, γ_o is the interfacial tension of a "pure" interface and γ is the interfacial tension in the presence of an interfacial film formed by surfactants or particles. An increase in two-dimensional pressure is equivalent to a decrease in tension.

A Langmuir trough is an experimental device designed to measure the increase in surface pressure caused by a spread film while the interfacial area is decreased. One explanation for the increase in surface pressure at reduced areas is to consider that the molecules of surfactant act like a gas at the interface. The surfactants cause an increase in the two-dimensional pressure by pushing on the interfacial barriers similar to how gas molecules create pressure inside a container (Adamson and Gast, 1997, p. 81).

Langmuir Trough Set-Up

A drawing of a typical Langmuir trough set-up is shown in Figure 2.6. The Langmuir trough consists of a shallow container (trough), and a mechanical means to decrease the interfacial area available for the molecules/particles. In this study this was accomplished by a set of barriers perpendicular to the length of the trough (as in Figure 2.6) that simultaneously compress the film of material. Such a barrier system provides symmetrical compression of the film. Common terminology for the lower liquid in the trough is subphase, and the upper liquid can be referred to as the supraphase (or topphase). Another important component of the Langmuir trough is the method of surface pressure measurement. Several variations on the Langmuir trough design are possible, including different methods of determining the change in pressure and only having one barrier for compression. Gaines (1966) discusses several experimental set-ups and procedures related to Langmuir troughs and the study of interfacial films. Mingins and Owens (1987) provide a more current assessment of experimental factors involved in Langmuir trough studies. Aston (1993) provides a brief but adequate introduction of surfactant monolayer studies with the Langmuir trough.

Wilhelmy Plate

For this study, measurements of the surface pressure are made with a Wilhelmy plate method. This method is well suited for measuring the surface tension of a film-covered surface. A thin plate is suspended from a balance so that the plate is partially submerged in the subphase and intersects the interface. For an air-water interface the liquid will wet the plate as shown in Figure 2.4. A simple force balance on the plate is as follows:

Net Force = gravitational force - buoyancy force + force from surface tension .... [2.2]

The force due to gravity and the buoyant force will remain constant for a plate that is stationary and remains submerged to the same level. Thus, any change in the net force on the plate can only be provided by a change in the force from surface tension. The change in force due to a change in surface tension is given by the following equation:

$$\Delta\mathbf{F} = 2(t + w)(\gamma - \gamma_o)\cos\theta \quad [2.3]$$

where **F** is the force measured by the balance, ***t*** and ***w*** are the plate thickness and width, θ is the contact angle (assumed to be constant), γ_o is the initial surface tension, and γ is the final surface tension. When the plate is completely wetted by the liquid the contact angle is equal to zero and $\cos\theta$ equals unity. Using this simplification and rearranging Equation 2.3 to calculate the change in surface tension gives:

$$(\gamma_o - \gamma) = -\frac{\Delta\mathbf{F}}{2(t + w)} \quad [2.4]$$

If the initial surface tension, γ_o, is that of a clean surface and the final surface tension, γ, is that of a film covered surface, a measured change in force on the Wilhelmy plate corresponds to a change in surface pressure, as shown by Equation 2.5.

$$\Pi = -\frac{\Delta\mathbf{F}}{2(t + w)} \quad [2.5]$$

In order to determine the change in surface tension an initial force reading must be taken so that the change in force can be measured. Experimentally the surface pressure is determined by making the initial force equal to zero providing a reference to detect surface tension changes. For the present experiments an accurate electronic balance is used to measure the force on the Wilhelmy plate, which is made of filter paper to ensure complete wetting and a contact angle of zero. There are also other methods of measuring surface pressure including the method used by Langmuir (1917). For a description of these other methods, consult Gaines (1966).

Pressure-Area Isotherms

Langmuir trough enables measuring the surface (interfacial) pressure while the interfacial area is reduced or expanded. Measurements resulting from experiments taken at a constant temperature and compression rate can be plotted as a pressure-area (π-a) isotherm. The (π-a) isotherm is a widely accepted method of characterizing the interfacial film. From this isotherm we can interpret the film rigidity and collapse point, and calculate the film compressibility.

For many substances the π-a isotherm is a distinctive curve with noticeable slope changes. Figure 2.5 is a π-a isotherm of arachidic acid ($CH_3(CH_2)_{18}COOH$) from an air-water interface. The isotherm contains two distinctive slope changes, which is typical of many substances such as fatty acids. For these film-forming substances, the slope changes signify phase transitions between different states or phases of the film, i.e. gaseous, liquid and solid (Gaines, 1966). It is common to use the term 'phase' even though the film is not in complete equilibrium because the films are stable in the experimental timescale (Peng et al., 2001). At the largest area the surface pressure is close to zero and the pressure does not increase as the area decreases. This flat region is representative of a gas-like phase in the Langmuir film. The molecules are relatively far apart and do not interact with each other. Upon further compression the pressure starts to increase abruptly. After this transition, there is a region that represents a liquid-like phase as film molecules start to interact with each other. Over this region the pressure increases in a nearly linear relationship with decreasing area. A second transition occurs and the slope of the curve increases so that there is a steep linear region. The Langmuir film is in a condensed solid-like phase where film molecules are closely packed. After the solid phase, the isotherm exhibits a collapse point (as illustrated in Figure 2.5) where the surface pressure stops increasing and a 'kink' in the curve is exhibited. Film collapse is usually signified by this isotherm characteristic. Physically, the collapse occurs when some part of the film is pushed out of the interfacial area, this could be due to individual molecule/particle expulsion or a folding of the film (Gaines, 1966, p.145 and 149). Occasionally, the collapse of a Langmuir film can be visually observed. Phase transitions usually appear on the isotherms of smaller molecules. However, isotherms of polymer films formed by large molecules with a broad molecular weight distribution do not have distinctive transitions or regions that correspond well to the different states (Gaines, 1966, p.173). For films without distinctive phase transitions qualitative interpretations of the phases are common.

Another characteristic of π-a isotherms is the initial molecular area or limiting area (**A_o**) of the film. This is the point where the initial increase in pressure occurs. For films where it is hard to determine the initial point of pressure increase, **A_o** can be determined by extrapolating a best fit-line to the abscissa. The **A_o** for different phases can also be determined in a similar manner as shown in Figure 2.5 where the **A_o** of the solid phase is approximately 17 Å^2/molecule. For fatty acids of various chain lengths (including arachidic acid) the limiting area at the solid state is approximately 20 Å^2/molecule (Peng et al., 2001). The difference between Figure 2.5 and previously published results is discussed in section 4.2.1. The initial area can be used to compare the size of molecules of different film forming substances. For amphiphilic molecules the limiting area in the solid state corresponds to the size of the hydrophilic head group.

Compressibility

The slope of the isotherm provides meaningful information about the film. A film with an isotherm that is steep (i.e. larger slope) is more rigid/less flexible than a film with a shallow (i.e. smaller slope). In addition to a qualitative comparison of isotherm slope the film compressibility can be determined from π-a isotherm data. Monolayer compressibility is analogous to bulk compressibility and is defined by Equation 2.6 (Gaines, 1966),

$$C_s = -\frac{1}{A_t}\frac{dA_t}{d\pi} \quad \text{[2.6]}$$

where **C_s** is the film compressibility, **A_t** is the trough area and **π** is the surface pressure. The film compressibility gives information about the film structure, as a highly compressible film is more likely to have an expanded structure and a condensed film would be less compressible (Ese, 1999b). When considering interfacial films surrounding emulsion droplets, one can propose that a more rigid film provides a larger steric hindrance to coalescence. Thus, a highly incompressible film is more likely to produce a more stable emulsion. In practice this correlation may not always hold as steric hindrance is not the only mechanism of emulsion stability and an extremely rigid film may sometimes be less stable.

2.4.2 Asphaltenes on the Langmuir Trough

The Langmuir trough is a useful method of characterizing interfacial films of asphaltenes. Several studies investigating the properties of spread films of asphaltenes extracted from bitumen have been conducted at the University of Alberta. These studies focus on the film properties at air-water (Zhang et al., 2003a), *n*-heptane-water (Lawrence et al., 2004), toluene-water (Zhang et al., 2005b), and heptol-water (Zhang et al., 2003b) interfaces. As well, one of those studies investigated the effects of demulsifiers on the asphaltene film properties (Zhang et al., 2003b). Results show that asphaltenes form insoluble monolayers at the interfaces, including the toluene-water interface studied. Similar studies were reported by Ese and coworkers. Others include those by Leblanc and Thyrion (1989), and Mohammed et al. (1993).

Many of these publications provide π-a isotherms of asphaltene films at an air-water interface. The shape of isotherms from asphaltenes is fairly consistent in literature even though the asphaltenes in each study are derived from different petroleum sources. Figure 2.7, taken from Zhang et al. (2003a), is provided for an example of a π-a isotherm of asphaltenes at an air-water interface. No distinct phase transitions are shown in isotherms of asphaltenes, providing evidence that asphaltenes are a mixture of surface-active molecules that exhibit different phase transitions (Zhang et al., 2003a). Collapse pressures shown by the different isotherms vary, although most reported pressures are in the range of 50-70 mN/m. The surface pressure continues to increase after the film collapse, possibly due to the elastic nature of the asphaltene film produced by the entanglement of molecules (Zhang et al., 2003a).

Although the shape of the isotherms is fairly consistent, the position of the isotherm in regards to the area changes between studies. No single consistent limiting molecular area (A_o) can be calculated from different π-a isotherms. In addition to the differences in film characteristics and different π-a isotherms reported by each source, the variance in the molecular weight of the sample contributes to discrepancy in A_o calculations. Molecular weights of asphaltenes vary depending on the oil sample they are derived from, the extraction procedure and the method of molecular weight determination. The variation in molecular weight is thus reflected in the limiting molecular area (area per molecule) calculated from an isotherm. Comparison of different molecular weight fractions of Athabasca asphaltenes with different Langmuir trough experiments showed that the low molecular weight fraction is a more condensed fraction (Zhang et al., 2003a). The isotherms presented in Figure 2.7 show that the behaviour of the different fractions is similar but differences do exist in hysteresis and relaxation curves and in the structures observed with atomic force microscope imaging (Zhang et al., 2003a). Comparisons have also been made for films adsorbed to a heptol-water interface, with similar findings (Zhang et al., 2005a). Subphase pH has no effect on the shape and position of the π-a isotherm of asphaltene films at an air-water interface (Zhang et al., 2003a).

Langmuir trough studies have also been used to investigate the films of asphaltenes mixed with another component. Films of mixtures of resins and asphaltene films are less rigid than films of asphaltenes alone (Ese, 1999a, 1999b; Ese et al., 1998, 1999; Mohammed et al., 1993). Demulsifiers have been shown to have a similar effect as resins by causing asphaltene films to become more compressible (Ese 1999a, 1999b; Ese et al., 1999; Lawrence, 2003; Zhang et al., 2003b). Analysis of the π-a isotherms of asphaltenes mixed with demulsifiers has shown that their mixing behaviour is close to ideal (Zhang et al., 2003b).

Information obtained from Langmuir trough experiments of asphaltenes at oil-water interfaces is more applicable to emulsion stability since air-water interfaces are not present in emulsions. Studies have shown that spread asphaltene films are more compressible at heptol-water interfaces (Lawrence, 2003; Zhang et al., 2003b). More recently, experiments have shown that spread asphaltene films at toluene-water interfaces are not dissolved by the toluene and can be compressed to obtain π-a isotherms (Zhang et al., 2005b). Furthermore, when isopropanol is added to the toluene phase, isopropanol penetrates the asphaltene monolayer and significantly alters the isotherm.

There are limited reports on using the Langmuir trough to investigate asphaltenes and other related components. As shown there are some recent investigations conducted at both air-water and oil-water interfaces. These Langmuir trough studies have provided information on the film properties of asphaltenes and petroleum, which can be related to emulsions. Deposited films from the Langmuir trough provide more qualitative information about the structure and organization of the asphaltene interfacial films. At the time this thesis was written, no studies were devoted to investigating the combination of petroleum components and fine solids on the Langmuir trough.

2.4.3 Solid Particles on the Langmuir Trough

The Langmuir trough was originally designed to study monomolecular layers of surfactants. Theories behind Langmuir film formation, and analysis of film properties such as the gas, liquid, solid states in an isotherm were developed to explain the behaviour of insoluble monolayers of surfactants. However, applications of the Langmuir trough and related experiments have been extended to studies of solid particle behaviour at interfaces. The Langmuir films of solid particles have recently been studied primarily for the development of nanostructured materials (Stine and Moore, 2002; Fendler, 1996). But, work has also been conducted to examine particle behaviour at interfaces. In these studies Langmuir trough experiments such as π-a isotherm measurements and Langmuir-Blodgett deposition are used to study particle behaviour at a planar interface. Most studies were conducted with particles at an air-water interface but some of the studies utilized an oil-water interface. The behaviour of solid particles at an oil-water interface can be different due to the particle interactions in oil being different than in air.

Interpretation of the π-a isotherms is the basis of many studies. Various analyses of the measured isotherms have been undertaken. Analysis of particulate film behaviour includes determining the particles size based on π-a isotherms (Clint and Taylor, 1992; Sheppard and Tcheurekdjian, 1968), contact angles based on collapse pressure (Aveyard et al., 1994; Clint and Taylor, 1992; Hórvölgyi et al., 1996) and interaction energies between particles (Aveyard et al., 2000a; Hórvölgyi et al., 1993, 1996). The following sections review different contributions that use a Langmuir trough to study particle behaviour at interfaces.

Typical π-a Isotherms

Pressure-area isotherms have been measured for monolayers (Langmuir films) of many different solid particles, such as, gold nanoparticles (Paul et al., 2003), foam polystyrene balls (Schuller, 1967; Kumaki, 1988; Aveyard et al., 2000b), and Stöber silica with various surface treatments (Tolnai et al., 2001). In most cases the isotherm of the particulate film is similarily shaped. For example, the isotherms in Figure 2.8 are from various sources and all of them have a similar shape. There are no distinct phase transitions with only narrow gas and liquid regions in the curve. The isotherm is steep in all cases showing that solid films are rigid and have low compressibility. Most particulate films have a high collapse pressure, ranging from up to ~60 mN/m at the air-water interface.

It is difficult to compare isotherms from different sources because of the manner in which they are presented. For monolayers of surfactant molecules the convention is to plot the surface or interfacial pressure against the area per molecule. The measured trough area is normalized by the number of molecules spread at the interface. An equivalent presentation for particulate films is to show the area normalized by the number of particles spread at the interface. This requires the number of particles to be known or calculated. For instance, if the density and size of a sample of monodisperse spherical particles is known, the number of particles in a set mass can be calculated. In many cases the particle size is unknown and so the interfacial pressure is plotted against the measured trough area or area per mass.

'Surface Pressure' of Particulate Films

In literature there have been some discussions on the meaning of the pressure measured during Langmuir trough experiments for solid particle films. In this case, π-a isotherms with π measured by a Wilhelmy balance can vary with changes to the orientation of the Wilhelmy plate (Aveyard et al., 2000b; Kumaki, 1988). Kumaki (1988) suggested that the measurements made by the Wilhelmy plate were not truly "surface pressures" because he obtained different results when the plate orientation was changed from parallel to perpendicular to the compression direction. depending on plate orientation. The applied pressure from the Langmuir trough barriers does not distribute equally across particulate films because of the strength of particle attractions and the result is surface pressure gradients (Maté et al., 1998). It is possible these surface pressure gradients are the cause of discrepancies in π-a isotherms when the Wilhelmy plate orientation is varied. Kumaki (1988) used a platinum plate, and suggested that contamination of the plate, not a change in surface tension, was responsible for an apparent surface pressure. The use of a paper Wilhelmy plate may reduce this contamination effect, as the plate is wetted more easily. Despite the conclusions made by Kumaki (1988), investigations continued into Langmuir films of particles. Pressure-area isotherms can provide valuable information the strength of particulate films and the particle size and wettability.

Particle-Size Determination from Isotherms

One of the earliest applications of π-a isotherms of particulate films was to estimate particle size. In order to make these calculations it must first be assumed that the particles are spherical and monosized. A second assumption is that the particles will form a close packed arrangement (cubic or hexagonal) at the interface at some point during compression. The particle size is then calculated from the trough area based on geometry. Sheppard and Tcheurekdjian (1968) used the limiting area in their calculations and assumed particles were closed packed at the onset of surface pressure increase. Another method is to assume the particles become close-packed at the collapse area (Clint and Taylor, 1992). This is perhaps a better assumption since it has been observed that particulate films are not completely continuous at the onset of surface pressure (Hórvölgyi et al., 1993). Particle sizes calculated using trough areas are roughly equal to the sizes measured by other means, but because of the assumptions of shape and size distribution, the applications of this method are limited. Other methods of interpreting π-a isotherms usually use well-characterized particles in order to simplify analysis of the particle behaviours.

Contact Angle Determination from Isotherms

Particles need to have an "intermediate" wettability in order to form interfacial films. Within the "intermediate" range, wettability will affect particle behaviour at the interface. Hórvölgyi et al. (1993) observed π-a isotherms and spreading behaviour of silica beads of different hydrophobicities at an air-water interface. Hydrophobicity determines interfacial position (see Figure 2.2), dispersability and aggregation behaviour of the particle, which affect the monolayer structural strength and collapse behaviour (Hórvölgyi et al., 1993). In addition, variations in particle hydrophobicity can change the ordering of particles in a monolayer. Particles up to a certain level of hydrophobicity will form ordered monolayers and particles more hydrophobic will form disordered monolayers (Horozov et al., 2003).

Monolayer collapse due to compression can result in particle ejection from the interface. If this condition holds the pressure at collapse can be equated to the work required to overcome the adhesion of particles to the interface (Aveyard et al., 1994). Using this concept several authors have used the collapse point from π-a isotherms to determine the contact angle of the film-forming particles such as detergents (Clint and Taylor, 1992). Clint and Taylor (1992) derived an expression[1], as given by Equation 2.7, to calculate the air-water contact angle (θ) of spherical, monodisperse particles from the collapse pressure (Π_c) of the monolayer.

$$\theta = \cos^{-1}\left[\pm\left(\sqrt{\frac{\Pi_C 2(3)^{1/2}}{\pi\gamma_{aw}}}-1\right)\right] \quad \text{..................................... [2.7]}$$

Differences in authors' approaches are based on the inclusion of new information or extra complications such as using compensating calculations for the effect of surface pressure gradients (Maté et al., 1998), implementing a correction for particle repulsion at close range (Aveyard et al., 1994), or by using different methods of surface pressure measurement like a Wilhelmy balance (Hórvölgyi et al., 1999) or Langmuir balance (Hórvölgyi et al., 1996). Usually the calculated contact angles did not agree with the values obtained using other measurements. Maté et al (1998) showed that extrapolating Wilhelmy plate measurements to represent the surface pressure change next to the moving barriers improved the agreement of calculated contact angles. The discrepancy between contact angle measurements is possibly due to collapse behaviour inconsistent with particle ejection.

---

[1] Clint et al. (1992) presented a rearranged form of Equation 2.7. Their equation is of the form $\pi_c = f(\theta)$.

Collapse of Langmuir Films of Particles

Collapse of a particulate film can occur by particle expulsion into a bulk fluid phase (Hórvölgyi et al., 1996) and by folding (buckling or creasing) of the film without particle expulsion (Aveyard et al., 2000b). Similar behaviours occur in surfactant films. Folding, for example, occurs when interactions between surfactant chains are strong (Gaines, 1966, p.149). Folding of particulate films has been observed by electron microscopy of deposited, collapsed films (Sheppard and Tcheurekdjian, 1968) and optical microscopy of films during compression (Aveyard et al., 2000b). Figure 2.9 shows optical micrographs of a buckling monolayer at an air-water interface. In addition, buckling behaviour of interfacial films was used to explain results of an ellipsometric study of nanosized silica particles at a toluene-water interface (Binks et al., 2003), which is indirect evidence of buckling in films of nanoparticles. The buckling behaviour occurs in particulate films at air-water interfaces (Sheppard and Tcheurekdjian, 1968) (Hórvölgyi et al., 1993), and oil-water interfaces (Aveyard et al., 2000a; 2000b). Further evidence of buckling has been obtained at oil-water droplet interfaces, indicating that the mechanism is not limited to planar interfaces. In a recent study images were obtained of a creased particle layer surrounding a pendant drop of oil or water (Asekomhe et al., 2005).

Collapse pressure has also been shown to depend on the interfacial tension of the fluids being studied. After adjustments of the oil/water interfacial tension with surfactants the resulting π-a isotherm showed collapse at an interfacial pressure equal to the new interfacial tension (Aveyard et al., 2000b). This means the interfacial tension in the presence of particles approaches zero when collapse occurs.

Particle Interactions

Information about particle-particle interactions in 2-dimensional monolayers has been attained from Langmuir trough studies. Hórvölgyi et al. (1993) calculated the interparticle energies of hydrophobic microspheres using DLVO theory. In their calculation total interaction energy was the sum of van der Waals attraction, hydrophobic interaction and double layer repulsion. Calculations of energies for different particle spacing and wettabilities showed that strong repulsion amongst particles commonly exists and prevents particle-particle contact. They concluded that mechanisms during film spreading were responsible for the observation of patch-like monolayer structures. Aveyard et al. (2000a) included the contribution of residual surface charges on the solid particles in a model of interparticle interactions of latex particles at oil-water interface. They concluded that additional repulsive energies due to electrostatic interactions can occur at oil-water interfaces and these energies are responsible for different monolayer structures being observed. Calculation of particle interaction energies can be used to explain why long range ordering occurs in some particle monolayers but not in others (Horozov et al., 2003). Hydrophobic attractive forces appear to be the source of aggregation of hydrophobic silica at an air-water interface as the aggregation decreases with decreasing hydrophobicity (Tolnai et al., 2001). A comparison of particle aggregation for three different types of silica is shown in Figure 2.10.

Particle-particle interaction can become very complex. Fractals and patterned structures form in colloidal monolayers when subjected to external fields such as the application of electric current (Ghezzi et al., 2001). Controlled modification of interparticle forces and observation of the results may lead to explanations of more complex particle interactions that can occur. Ghezzi et al. (2001) provided some qualitative explanations for complex pattern formation. An example of the complex patterns formed by particle monolayers is shown in Figure 2.11.

2.5 Langmuir-Blodgett Films

Langmuir-Blodgett (LB) Films are formed by depositing a Langmuir film onto a solid substrate. Cohesive forces between molecules of the interfacial film allow them to stay together and transfer from the interface to a substrate. Experimentally the LB films are constructed by submerging a thin solid plate into the lower phase. The interfacial film is then spread at the interface and compressed to a desired pressure. The substrate is drawn upwards until it has completely passed through the interface. As the substrate is withdrawn upwards the pressure is held constant by varying the interfacial area of the film. Figure 2.12 is a diagram of the LB deposition process. For this diagram amphiphilic molecules are present at the interface. When an upwards deposition is performed, usually the substrate is hydrophilic so an attraction exists between the hydrophilic head groups of the molecules and the substrate. This helps ensure that molecules transfer to the substrate as shown in Figure 2.12. Choices for substrate materials include freshly cleaved mica, which is naturally hydrophilic, and silicon or glass, which can be treated to be hydrophobic or hydrophilic.

The Transfer Ratio (***TR***) is a measure of the deposition efficiency. The TR is calculated for each deposited LB film by Equation 2.8 below.

$$TR = \frac{Interfacial\ Area\ Reduction}{Substrate\ Area\ Available\ for\ Depostion} \qquad [2.8]$$

During a 100% efficient transfer the change in interfacial area during deposition will equal the area of the substrate that passed through the interface (i.e. TR=1). A TR near 1 is desirable as the resulting LB film will more closely resemble the original Langmuir film. If films are non-reactive there exists an entrained water layer between the interfacial material and the solid substrate (Gaines, 1966). This water layer evaporates leaving only the interfacial film-forming material. Once deposited LB films are very stable and can be stored without the film structure changing.

As stated by Knobler and Schwartz (1999) several studies have shown that the structure of Langmuir films can survive transfer during Langmuir-Blodgett deposition. LB films can be studied with imaging techniques that are difficult or impossible to perform on Langmuir films. This includes atomic force microscopy and scanning electron microscopy.

2.5.1 Atomic Force Microscopy

Atomic Force Microscopy (AFM) is a useful tool for studying atomic scale features of substances. Originally developed by Binnig, Quate and Gerber in 1986, AFM has progressed to become a commercially available tool (Binnig et al., 1986). One use of the AFM is to obtain images of LB films. A sketch and some basic details of the operation of a common AFM are provided in Figure 2.13. Variations to this set-up exist, but this description applies to the current study. During operation of the AFM the sample to be studied is placed under a sharp tip at the end of a cantilever. A piezo crystal scanner is used to carefully control the sample movements. As the sample moves the cantilever tip responds to the surface of the sample. The simplest response is obtained by contacting the tip with the sample. During the appropriately named "contact-mode" the cantilever tip moves up and down with the sample topography. In order to measure the deflection of the cantilever and produce an image from the deflections a laser and photodiode detector are employed. The laser is reflected off of the top of the tip and onto a position-sensitive photodiode detector. Movements of the cantilever tip cause the laser to move its position on the detector causing a variation in current output from the photodiode detector. The current is registered with a computer and an AFM image of the sample topography is constructed. Peripheral equipment aids in the operation of the AFM. A vibration platform is needed to reduce fluctuations in the tip movement, which can cause interference and noise in the images. Cantilevers of different stiffness are available and different sizes of piezo scanners can be used depending on the sample features and desired resolution of images. It is also possible to obtain images from samples by operating the AFM in tapping mode and non-contact mode. These modes rely on the surface forces between the sample and cantilever tip. AFM images are useful for determining short-range structure of molecules.

2.5.2 Scanning Electron Microscopy

Scanning electron microscopy (SEM) was used as a secondary imaging method to confirm AFM images of films and to provide different information. Atomic force microscopy usually provides higher resolution images, but the SEM still has great resolving power. However, the AFM used in the experiments was limited because of its small capture area. A wider view was needed in order to "see the forest through the trees". SEM provides a wider view of the LB films and a greater depth of field (in this study). SEM images are useful for determining long-range structure between groups of molecules.

The first commercial SEM device was available in 1964 (Flegler, Heckman, and Klomparens, 1993). SEM is a sophisticated technique, and entire books are devoted to the explanation of SEM operations, theory and applications. For a practical introduction refer to Flegler et al. (1993). In this study SEM is only used for an imaging technique and other capabilities of the SEM, such as sample composition, were not utilized. Only a brief introduction into the instrument is warranted by the limited application of this technique.

One of the widespread uses of the SEM is for metal and material characterization. As such, the SEM is introduced in various textbooks on materials characterization. The following introduction to the technique is summarized from two such sources, Exner (2002) and Bindle (1992). The basic principle behind the SEM imaging method is that an electron beam replaces the light beam in optical microscopy. Figure 2.14 shows the basic setup of an SEM. An electron gun generates a monochromatic beam of electrons. The beam is narrowed and focused with magnetic lenses. A set of magnetic coils then deflects the focused beam in a raster pattern. The surface of the sample is scanned by this raster pattern deflection. When the energetic electrons contact the sample, interactions between the sample and electrons occur. Stated simply, electrons in the sample are excited and emitted (other emissions like x-ray can occur). An electron detector then captures the emitted electrons. Equipment is used to amplify the current and utilize their characteristics to produce an image (e.g. characteristic energy of Auger electrons). SEM operation requires conductive surfaces and must operate in a vacuum. A conductive material such as carbon or gold can be used to coat non-conductive surfaces. Organic films such as asphaltene films require this sample preparation before imaging with an SEM is possible.

2.5.3 Review of Langmuir-Blodgett Film Literature

LB deposition is useful for construction of nanotechnology. In fact, LB deposition was one of the first procedures useful for constructing materials on a molecular scale (Zasadzinski et al., 1994). Stine and Moore (2002) have recently reviewed the work using Langmuir and LB films in nanotechnology applications. Although much LB film research is focused directly on deposited films, LB deposition is a valuable technique to gain information about interfacial (Langmuir) films. Both SEM and AFM have been used to investigate the structure and organization of deposited Langmuir films. Information from images of LB films is usually directly applicable to the film when it is at the interface.

SEM is useful for studying LB films of inorganic and especially conductive materials. For nanotechnology applications, SEM images can be used to determine the uniformity of the deposition process. SEM images of spherical silica particles deposited from an air-water interface showed a close packed hexagonal arrangement of particles, but with incomplete ordering (Szekeres et al., 2002). By imaging several films the effect of variables such as spreading solvent on the particle arrangement were gauged. An early example of SEM use on LB films is the imaging of latex emulsion particles deposited from an air-water interface (Sheppard and Tcheurekdjian, 1968).

Since the advent of the AFM, study of LB films with SEM has been limited, especially when working with organic films. The AFM usually provides better resolution and the small thickness of interfacial films makes the AFM better suited because there are no tall features to scan. For these thin films the greater depth of field provided by the SEM is unnecessary. AFM images have been obtained for LB films of asphaltenes and resins. From the images of asphaltene films at an air-water interface it was shown that aggregates of asphaltene molecules are present (Zhang et al., 2003a). AFM imaging of LB films has also been used to show the effects of a demulsifier on an asphaltene film

(Zhang et al., 2003b). Ese and coworkers obtained AFM images of asphaltene films mixed with resins (Ese et al., 2000). AFM has also been used to image films of asphaltenes adsorbed from toluene (Toulhoat et al., 1994) and oil residues left on substrates after evaporation of light ends (Batina et al., 2003).

AFM images of deposited asphaltene films were used to determine the structural characteristics of the film at various interfacial pressures. Presented in Figure 2.15 are two images from Zhang et al. (2003a) showing disc and rod-like asphaltene aggregates. At lower surface pressures the structure was more open and the aggregates were larger. Zhang et al. (2003b) showed that mixing a demulsifier with asphaltenes creates a film that is less rigid when measured by π-a isotherms. AFM images of these films reveal that the decrease in rigidity is not due to breaking of asphaltene aggregates but the presence of demulsifier molecules at the interface changing the packing and continuity of the film (Zhang et al., 2003b). During AFM imaging, a comparative measurement of film thickness can be made by the z-scale of cantilever deflection. Taller structures in the film will have a larger z-scale. By comparing the height of cantilever deflection the thickness of asphaltene films is found to be greater at higher interfacial pressure (Zhang et al., 2003b). Langmuir films can be deposited from an oil-water interface just as easily as an air-water interface. This allows for the comparison of LB film morphology from different interfaces. Films of Athabasca asphaltenes have similar structures at a heptol-water interface as at an air-water interface (Zhang et al., 2003b). AFM images of an asphaltene film from a toluene-water interface are shown in Figure 2.16. Similar structures can be seen in the AFM images of films from air-water and toluene-water interfaces.

2.6 Chapter Summary

The theory behind the experimental devices utilized in thesis experiments has been introduced. A review of solids stabilized emulsions and an introduction to bitumen processing show the industrial relevance of this thesis. The Langmuir trough is a well-proven technique for investigating spread surface and interfacial films. This technique has been used for studying asphaltenes and resins derived from petroleum sources, including work conducted at the University of Alberta. The Langmuir trough has also been used to study fine particles at interfaces. An extension of the Langmuir trough technique is Langmuir-Blodgett deposition, which involves deposition of Langmuir films onto a solid substrate. Imaging methods such as AFM and SEM can be used to investigate the deposited interfacial films. Combining Langmuir-Blodgett deposition with an imaging technique provides useful information about interfacial film structure not obtainable from pressure-area measurements.

2.7 References

Adamson, A.W., Gast A.P., Physical chemistry of surfaces, 6th ed, New York, Wiley-Interscience, 1997.

Asekomhe, S.O., Chiang, R., Masliyah, J.H., Elliott, J.A.W., *Some observations on the contraction behaviour of a water-in-oil drop with attached solids,* Industrial & Engineering Chemistry Research, 44(5), 1241-1249, 2005.

Aston, M.S., *The study of surfactant monolayers by surface pressure–area measurement,* Chemical Society Reviews, 22(1):67-71, 1993.

Auflem, I.H., *Influence of Asphaltene aggregation and pressure on crude oil emulsion stability*. Ph. D. Thesis, Norwegian University of Science and Technology, 2002. Retrieved November 16, 2004 from http://www.chemeng.ntnu.no/research/polymer/ugelstadlab/thesis/ihauflem.pdf

Aveyard, R., Binks, B.P., Clint, J.H., *Emulsions stabilised solely by colloidal particles,* Advances In Colloid and Interface Science, 100:503-546, 2003.

Aveyard, R., Binks, B.P., Fletcher, P. D. I., Rutherford, C. E., *Measurement of contact angles of spherical monodisperse particles with surfactant solutions,* Colloids and Surfaces A: Physicochemical and Engineering Aspects, 83(1):89-98, 1994.

Aveyard, R., Clint, J.H., Nees, D., Paunov, V.N., *Compression and Structure of Monolayers of Charged Latex Particles at air/water and oil/water interfaces,* Langmuir, 16(4):1969-1979, 2000a.

Aveyard, R., Clint, J.H., Nees, D., Quirke, N., *Structure and collapse of particle monolayers under lateral pressure at the octane/aqueous surfactant solution interface*, Langmuir, 16(23):8820-8828, 2000b.

Batina, N., Manzano-Martinez, J.C., Andersen, S.I., Lira-Galeana, C., *AFM characterization of organic deposits on metal substrates from Mexican crude oils,* Energy & Fuels, 17(3):532-542, 2003.

Bindle, J.B., *Scanning electron microscopy* In Encyclopedia of materials characterization - Surfaces, interfaces, thin films, R.C. Brundle, C.A. Evans Jr., S. Wilson (Eds.), Elsevier, pp.70-84, 1992.

Binks, B.P., Clint J.H., Dyab, A.K.F., Fletcher, P.D.I., Kirkland, M., Whitby, C.P., *Ellipsometric studies of monodisperse silica particles at an oil-water interface,* Langmuir, 19(21):8888-8893, 2003.

Binning, G., Quate, C.F., Gerber, Ch., *Atomic Force Microscope*, Physical Review Letters, 56(9):930-933, 1986.

Camp, F.W., The Tar Sands of Alberta,Canada, 3rd Ed., Cameron Engineers Inc., Colorado, USA, 1976.

Chen, F., Finch, J.A., Xu, Z., Czarnecki, J., *Wettability of fine solids extracted from bitumen froth*, Journal of Adhesion Science Technology, 13(10):1209-1224, 1999.

Clint, J.H., Taylor, S.E., *Particle size and interparticle forces of overbased detergents - a Langmuir trough study*, Colloids and Surfaces, 65(1):61-67, 1992.

Ese, M.-H., *Compressibilities and excess surface areas of mixed asphaltene/resin monolayers. Influence of demulsifiers.*, Journal of Dispersion Science and Technology, 20(7):1849-1859, 1999a.

Ese, M.-H., *Langmuir film properties of indigineous crude oil components. Influence of demulsifiers*, PhD. Thesis, University of Bergen, 1999b.

Ese, M.-H., Galet, L., Clausse, D., Sjöblom, J., *Properties of Langmuir surface and interfacial films built up by asphaltenes and resins: Influence of chemical demulsifiers*, Journal of Colloid and Interface Science, 220(2):293-301, 1999.

Ese, M.-H., Sjöblom, J., Djuve, J., Pugh, R., *An atomic force microscopy study of asphaltenes on mica surfaces. Influence of added resins and demulsifiers*, Colloid and Polymer Science, 278(6):532-538, 2000.

Ese, M.-H., Yang, X., Sjöblom, J., *Film forming properties of asphaltenes and resins. A comparative Langmuir-Blodgett study of crude oils from North Sea, European continent and Venezuela*, Colloid and Polymer Science, 276(9):800-809, 1998.

Exner, H.E., *Scanning electron microscopy*, In ASM Handbook, Volume 9, Metallography and Microstructures, 1985.
Retrieved November 4, 2004 from
http://products.asminternational.org/hbk/index.jsp

Fendler, J.H., *Nanoparticles at air/water interfaces*, Current Opinion in Colloid and Interface Science, 1:202-207, 1996.

Flegler, S.L., Heckman, J.W., Klomparens, K.L., *Scanning and transmission electron microscopy: an introduction*, New York, W.H. Freeman, 1993.

Gaines, G. L., *Insoluble monolayers at liquid-gas interfaces,* New York, Interscience Publishers, 1966.

Ghezzi, F., Earnshaw, J.C., Finnis, M., McCluney, M., *Pattern formation in colloidal monolayers at the air-water interface*, Journal of Colloid and Interface Science, 238(2):433-446, 2001.

Gu, G., Xu, Z., Nandakumar, K., Masliyah, J.H., *Influence of water-soluble and water-insoluble natural surface active components on the stability of water-in-toluene-diluted bitumen emulsion*, Fuel, 81(14):1859-1869, 2002.

Gu, G., Zhou, Z., Xu, Z., Maslyah, J.H., *Role of fine kaolinite clay in toluene-diluted bitumen/water emulsion,* Colloids and Surfaces A: Physicochemical and Engineering Aspects, 215(1-3):141-153, 2003.

Horozov, T.S., Aveyard, R., Clint, J.H., Binks, B.P., *Order-Disorder transition in monolayers of modified monodisperse silica particles at the octane-water interface*, Langmuir, 19(7):2822-2829, 2003.

Hórvölgyi, Z., Máté, M., Dániel, A., Szalma, J., *Wetting behaviour of silanized glass microspheres at water-air interfaces: a Wilhelmy film balance study*, Colloids and Surfaces A: Physicochemical and Engineering Aspects, 156:501-508, 1999.

Hórvölgyi, Z., Nemeth, S., Fendler, J.H., *Monoparticulate layers of silanized glass spheres at the water-air interface: particle-particle and particle-subphase interactions*, Langmuir, 12(4):997-1004, 1996.

Hórvölgyi, Z., Németh, S., Fendler, J.H., *Spreading of hydrophobic silica beads at water--air interfaces*, Colloids and Surfaces A: Physicochemical and Engineering Aspects, 71(3):327-335, 1993.

Knobler, C.M., Schwartz, D.K., *Langmuir and self-assembled monolayers*, Current Opinion in Colloid and Interface Science, 4(1):46-51, 1999.

Kotlyar, L.S., Sparks, B. D., Woods, J. R., Chung, K. H., *Solids associated with the asphaltene fraction of oil sands bitumen*, Energy & Fuels, 13(2):346-350, 1999.

Kotlyar, L.S., Sparks, B. D., Woods, J. R., Raymond, S., Le Page, Y., Shelfantook, W., *Distribution and types of solids associated with bitumen*, Petroleum Science and Technology, 16(1-2):1-19, 1998.

KSV Instruments Ltd., *KSV Minitrough: Instruction manual for Windows 95/98/NT/2000*, Helsinki, Finland.

Kumaki, J., *Monolayer of polystyrene monomolecular particles on a water surface studied by Langmuir-type film balance and transmission electron microscopy*, Macromolecules, 21(3):749-755, 1988.

Langmuir, I., *The constitution and fundamental properties of solids and liquids. II. Liquids*, Journal of American Chemical Society, 39:1848-1906, 1917.

Lawrence, S.A., *Characterisation of asphaltene monolayers using a Langmuir trough and an atomic force microscope at air-water and n-heptane-water interfaces*, MSc. Thesis, University of Alberta, 2003.

Lawrence, S., Zhang, L.Y., Xu, Z., Masliyah, J.H., *Langmuir and Langmuir-Blodgett asphaltene films at heptane-water interface,* Canadian Journal of Chemical Engineering, 82(4), 821-828, 2004

Leblanc, R.M., Thyrion, F.C., *A study of monolayers of asphalts at the air water interface*, Fuel, 68(2):260-262, 1989.

Lee, R.F., *Agents which promote and stabilize water-in-oil emulsions*, Spill Science & Technology Bulletin, 5(2):117-126, 1999.

Lopetinsky, R., Masliyah, J.H., Xu, Z., *Solids-Stabilized emulsions: A review* in B.P. Binks and T.S. Horozov (Ed.), Colloidal Particles at Liquid Interfaces, Cambridge University Press, In press.

Masliyah, J.H., Gray, M.R., *Intensive Short Course Extraction and Upgrading of Oilsands Bitumen*, Department of Chemical and Materials Engineering, University of Alberta, Edmonton, October 2004.

Maté, M., Fendler, J.H., Ramsden, J.J., Szalma, J., Hórvölgyi, Z., *Eliminating surface pressure gradient effects in contact angle determination of nano- and microparticles using a film balance*, Langmuir, 14(22):6501-6504, 1998.

McLean, J.D., Kilpatrick, P.K., *Effects of asphaltene solvency on stability of water-in-crude-oil emulsions*, Journal of Colloid and Interface Science, 189(2):242-253, 1997.

McLean, J.D., Spiecker, P.M., Sullivan, A.P., Kilpatrick, P.K., *The role of peteroluem asphaltenes in the stabilization of water-in-oil emulsions*, In O.C. Mullins, E.Y. Sheu (Eds.), Structures and Dynamics of Asphaltenes. Plenum Press, New York, pp. 377-422, 1998.

Mingins, J., Owens, N.F., *Experimental considerations in insoluble spread monolayers*, Thin Solid Films, 152(1-2):9-28, 1987.

Mohammed, R.A., Bailey, A.I., Luckham, P.F., Taylor, S.E., *Dewatering of crude oil emulsions 2. Interfacial properties of the asphaltic constituents of crude oil*, Colloids and Surfaces A: Physicochemical and Engineering Aspects, 80(2-3):237-242, 1993.

Paul, S., Pearson, C., Molloy, A., Cousins, M.A., Green, M., Kolliopoulou, S., Dimitrakis, P., Normand, P., Tsoukalas, D., Petty, M.C., *Langmuir-Blodgett film deposition of metallic nanoparticles and their application to electronic memory structures*, Nanoletters, 3(4):533-536, 2003.

Peng, J.B., Barnes, G.T., Gentle, I.R., *The structures of Langmuir-Blodgett films of fatty acids and their salts*, Advances In Colloid and Interface Science, 91(2):163-219, 2001.

Pockels, A., *Surface tension (Letter to the Editor)*, Nature, 43(1115):437-439, 1891.

Rayleigh, L., *Investigations in capillarity*, Philosophical Magazine, 48:321-337, 1899.

Schuller, H., *Modellversuche zur spreitung von kolloid-partikeln*, Kolloid Zeitschrift, 216-217:380-383, 1967.

Sheppard, E., Tcheurekdjian, N., *Monolayer studies IV. Surface films of emulsion latex particles*, Journal of Colloid and Interface Science, 28 (3-4):481-486, 1968.

Stine, K.J., Moore, B.G., *Langmuir monolayers: Fundamentals and relevance to nanotechnology*, In M. Rosoff (Ed.), Nano-Surface Chemistry. New York, Marcel Dekker, pp. 59-140, 2002.

Szekeres, M., Kamalin, O., Schoonheydt, R.A., Wostyn, K., Clays, K., Persoons, A., Dékany, I., *Ordering and optical properties of monolayers and multilayers of silica spheres deposited by the Langmuir-Blodgett method*, Journal of Materials Chemistry, 12:3268-3274, 2002.

Sztukowski, D.M., Yarranton, H.M., *Characterization and interfacial behavior of oil sands solids implicated in emulsion stability*, Journal of Dispersion Science and Technology, 25(3):299-310, 2004.

Tolnai, Gy., Csempesz, F., Kabai-Faix, M., Kálmán, E., Keresztes, Zs. Kovács, A.L. Ramsden, J.J. Hórvölgyi, Z., *Preparation and characterization of surface-modified silica-nanoparticles*, Langmuir, 17(9):2683-2687, 2001.

Toulhoat, H., Prayer, C., Rouquet, G., *Characterization by atomic force microscopy of adsorbed asphaltenes*, Colloids and Surfaces A: Physicochemical and Engineering Aspects, 91(3):267-283, 1994.

Yan, Y., Masliyah, J.H., *Solids-stabilized oil-in-water emulsions- scavenging of emulsion droplets by fresh oil addition*, Colloids and Surfaces A: Physicochemical and Engineering Aspects, 75:123-132, 1993.

Yan, Z.L., Elliott, J.A.W, Masliyah, J.H., *Roles of various bitumen components in the stability of water-in-diluted-bitumen emulsions*, Journal of Colloid and Interface Science, 220(2):329-337, 1999.

Yarranton, H.W., Hussein, H., Masliyah, J.H., *Water-in-hydrocarbon emulsions stabilized by asphaltenes at low concentrations*, Journal of Colloid and Interface Science, 228(1):52-63, 2000.

Zasadzinski, J. A., Viswanthan, R., Madsen, L., Garnaes, J., Schwartz D. K., *Langmuir-Blodgett films*, Science, 263(5154):1726-1733, 1994.

Zhang, L.Y., Lawrence, S., Xu, Z., Masliyah, J.H., *Studies of Athabasca asphaltene Langmuir films at air-water interface*, Journal of Colloid and Interface Science, 264(1):128-140, 2003a.

Zhang, L.Y., Xu, Z., Masliyah, J.H., *Langmuir and Langmuir-Blodgett films of mixed asphaltene and a demulsifier*, Langmuir, 19(23):9730 -9741, 2003b.

Zhang, L.Y., Xu, Z., Masliyah, J.H., *Characterization of adsorbed Athabasca asphaltene films at solvent-water interfaces using a Langmuir interfacial trough*, Industrial & Engineering Chemistry Research, 44(5):1160-1174, 2005a.

Zhang, L.Y., Lopetinsky, R., Xu, Z., Maslyah, J.H., *Asphaltene monolayers at a toluene-water interface*, Energy and Fuels, To Be Published, 2005b.

2.8 Figures

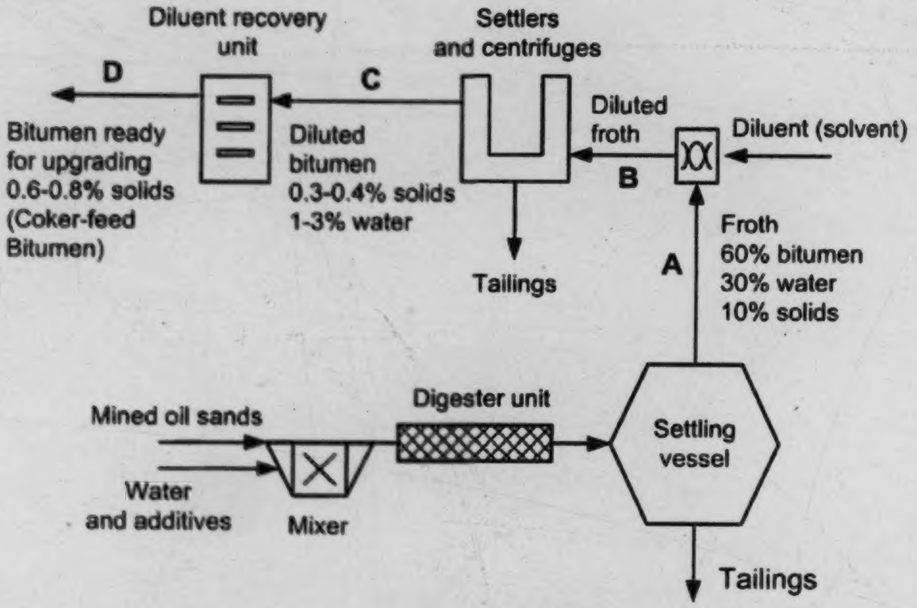

Figure 2.1: Process flow of a bitumen extraction plant (reproduced from Yan et al., 1999)

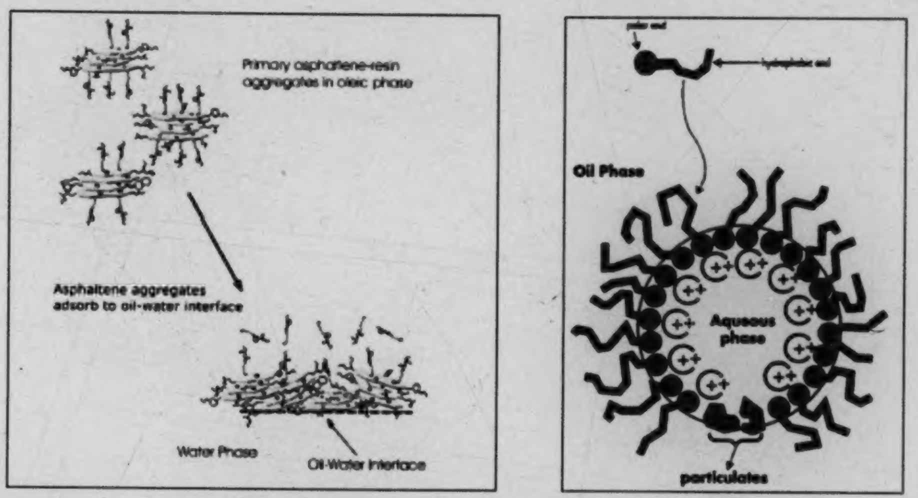
Primary asphaltene-resin aggregates in oleic phase
Asphaltene aggregates adsorb to oil-water interface
Water Phase
Oil-Water Interface
polar end
hydrophobic end
Oil Phase
Aqueous phase
particulates

(a) (b)

Figure 2.2: Two possible compositions of the interfacial film formed by asphaltenes a) asphaltene aggregates form a network at the interface (reproduced from Auflem, 2002), and b) asphaltenes behave as surfactants and form an interfacial film (reproduced from Lee, 1999)

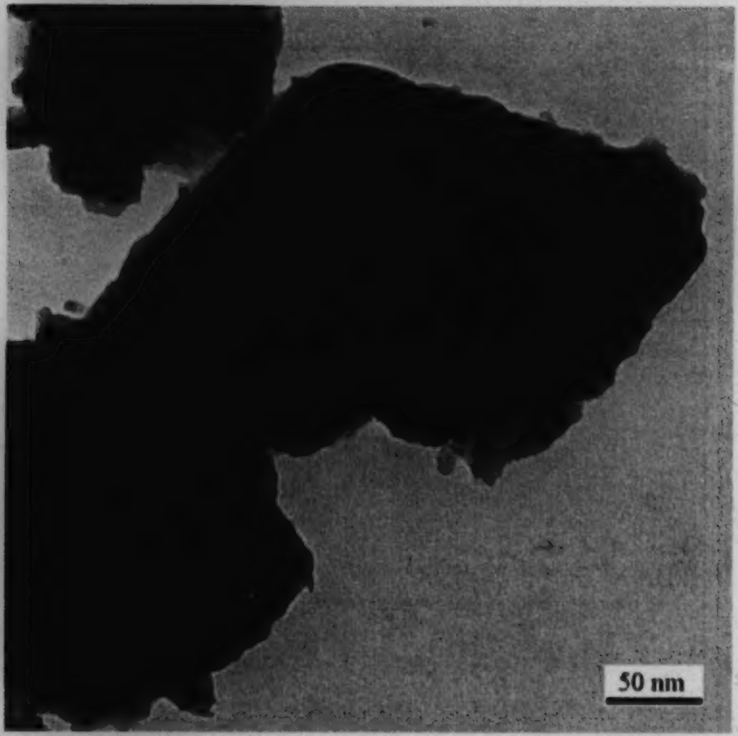

Figure 2.3: TEM micrograph of fine solid particle obtained from coker feed bitumen (reproduced from Sztukowski and Yarranton, 2004)

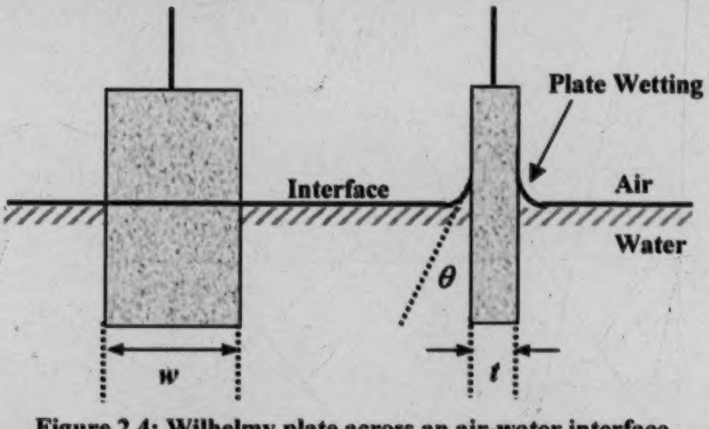

Figure 2.4: Wilhelmy plate across an air-water interface.

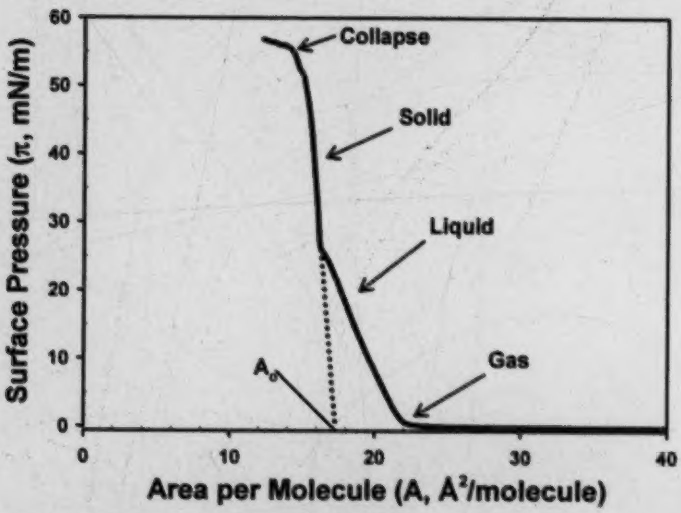

Figure 2.5: Surface pressure-area isotherm of arachidic acid at an air-water interface.

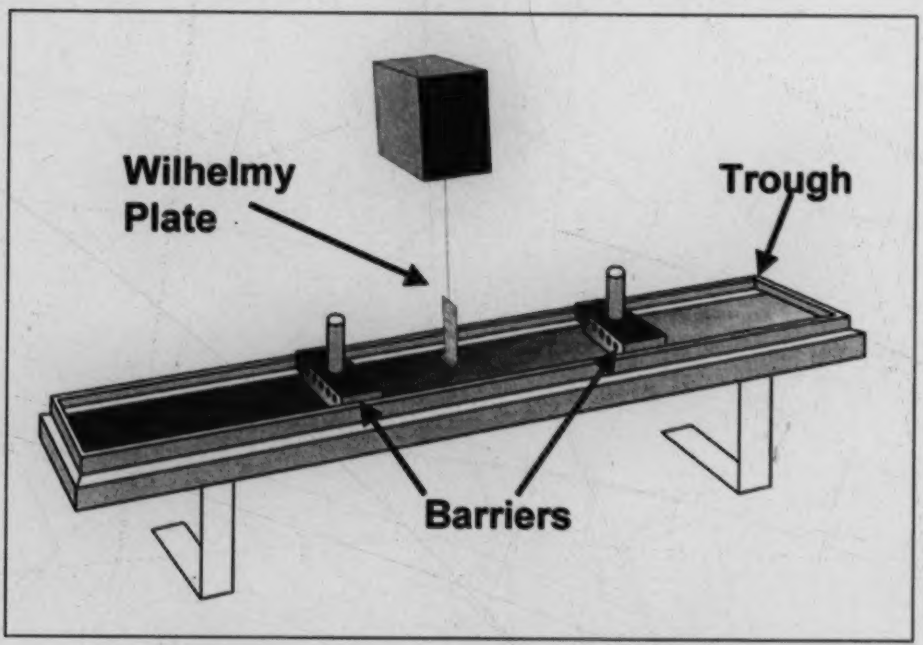

Figure 2.6: Sketch of a typical Langmuir trough device

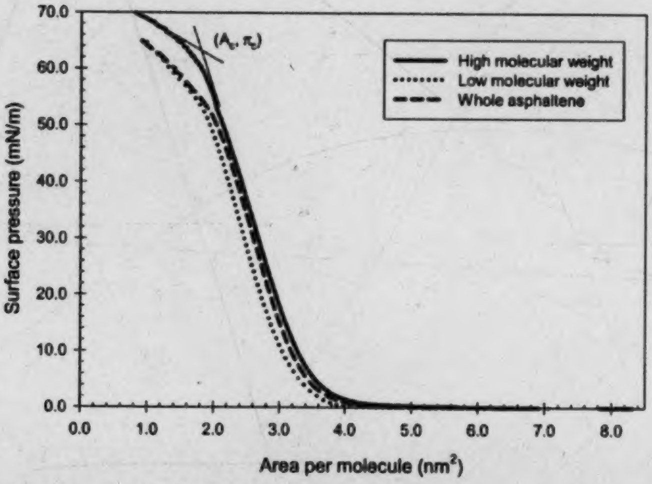

Figure 2.7: Surface pressure-area isotherms for different asphaltene fractions extracted from Athabasca bitumen. (reproduced from Zhang et al., 2003a)

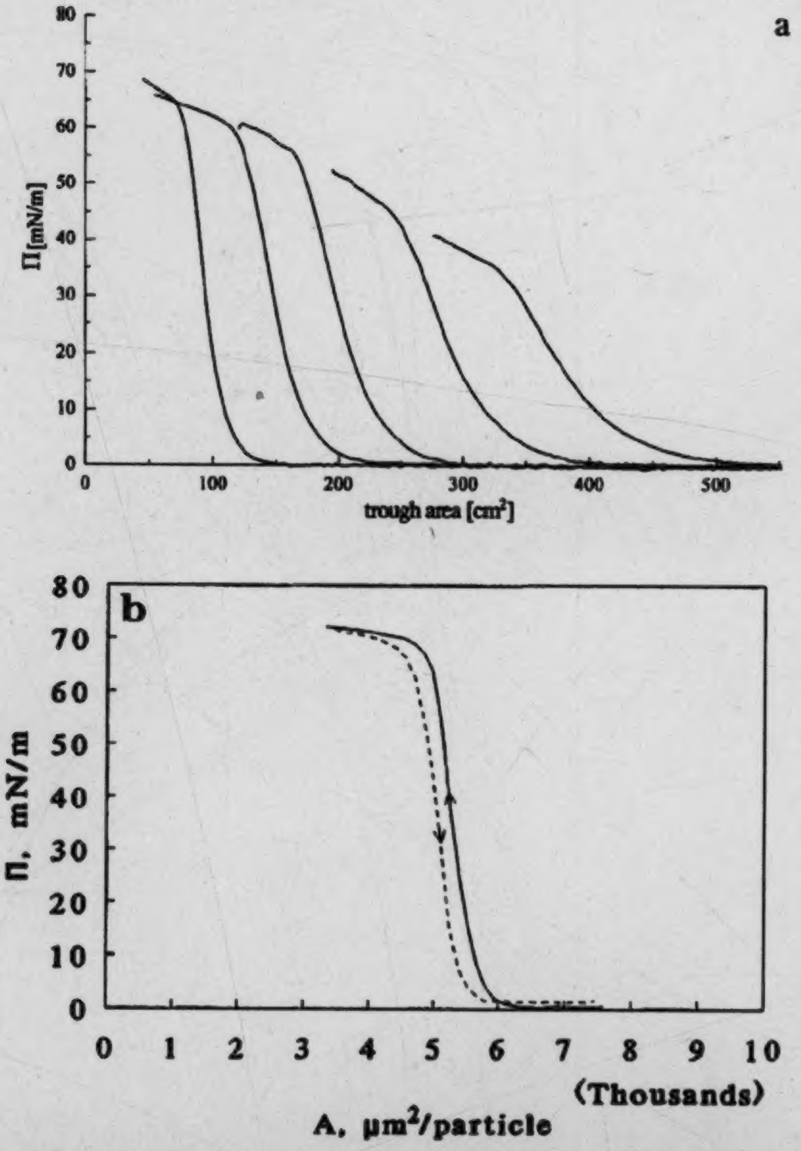

Figure 2.8:a) Isotherms of various amounts of Cab-O-Sil silica nanoparticles where pressure is plotted against trough area (reproduced from Maté et al., 1998), and b) Isotherm of silanized glass spheres (d~3μm). The trough area has been normalized by the number of particles spread on the water surface (reproduced from Hórvölgyi et al., 1996)

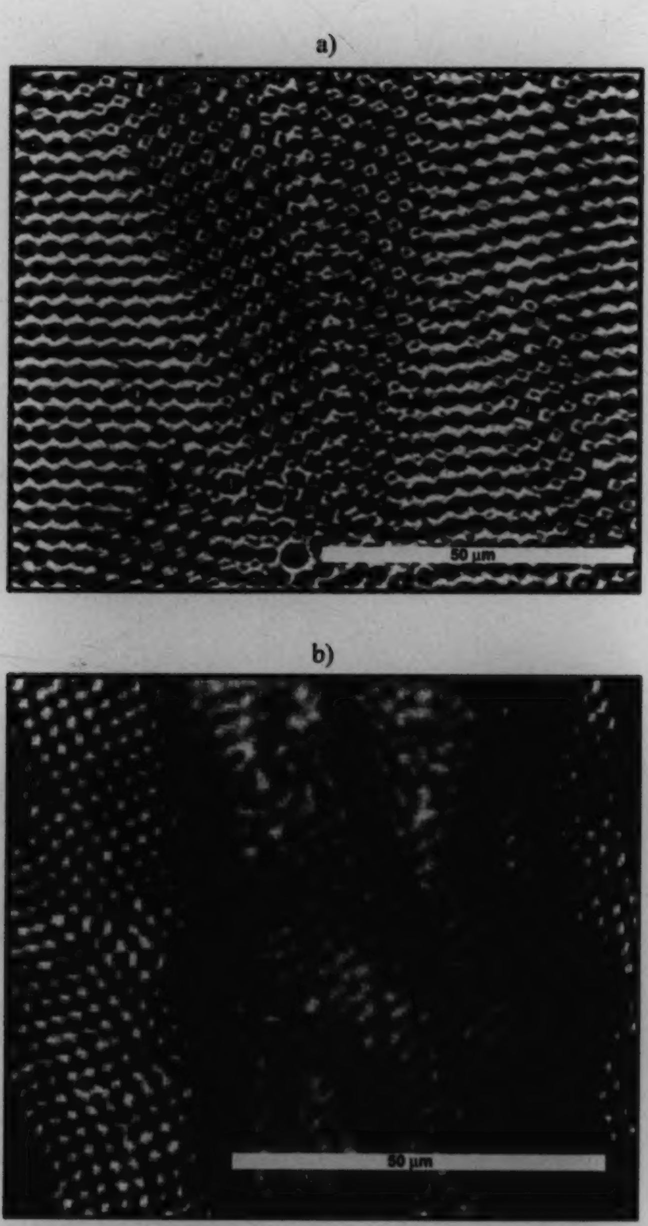

Figure 2.9: Microscopic images of the collapse of a polystyrene particulate film: a) some monolayer is folding soon after collapse is seen in the π-a isotherm, and b) upon further compression the folds expand and deepen. White scale bars are 50µm wide. (reproduced from Aveyard et al., 2000b)

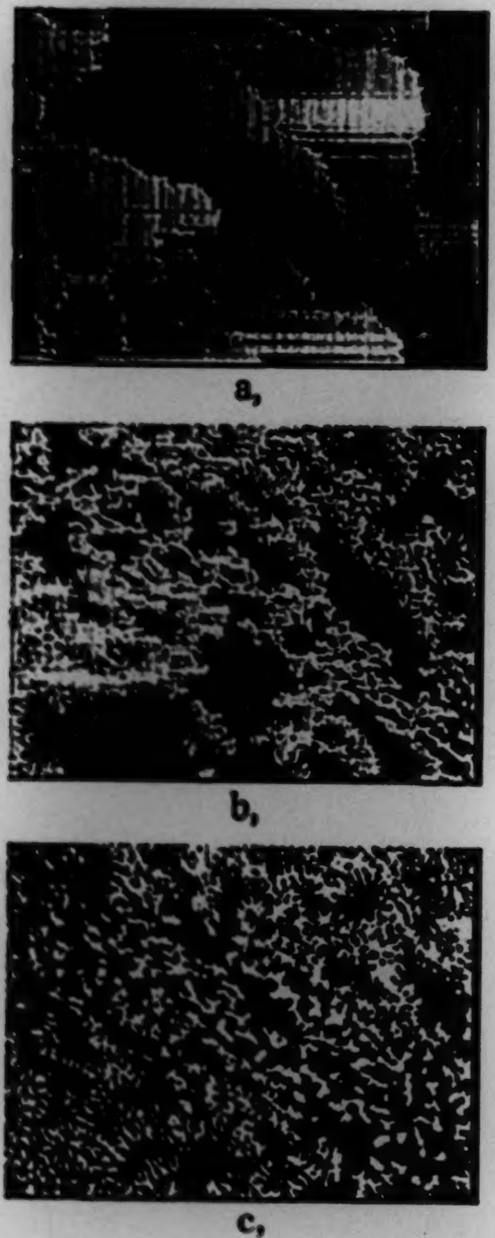

Figure 2.10: Brewster angle microscope images showing clusters of hydrophobic silica particles at an air-water interface. Hydrophobicity decreases from a) to c). Image width is 550 μm. (Reproduced from Tolnai et al., 2001)

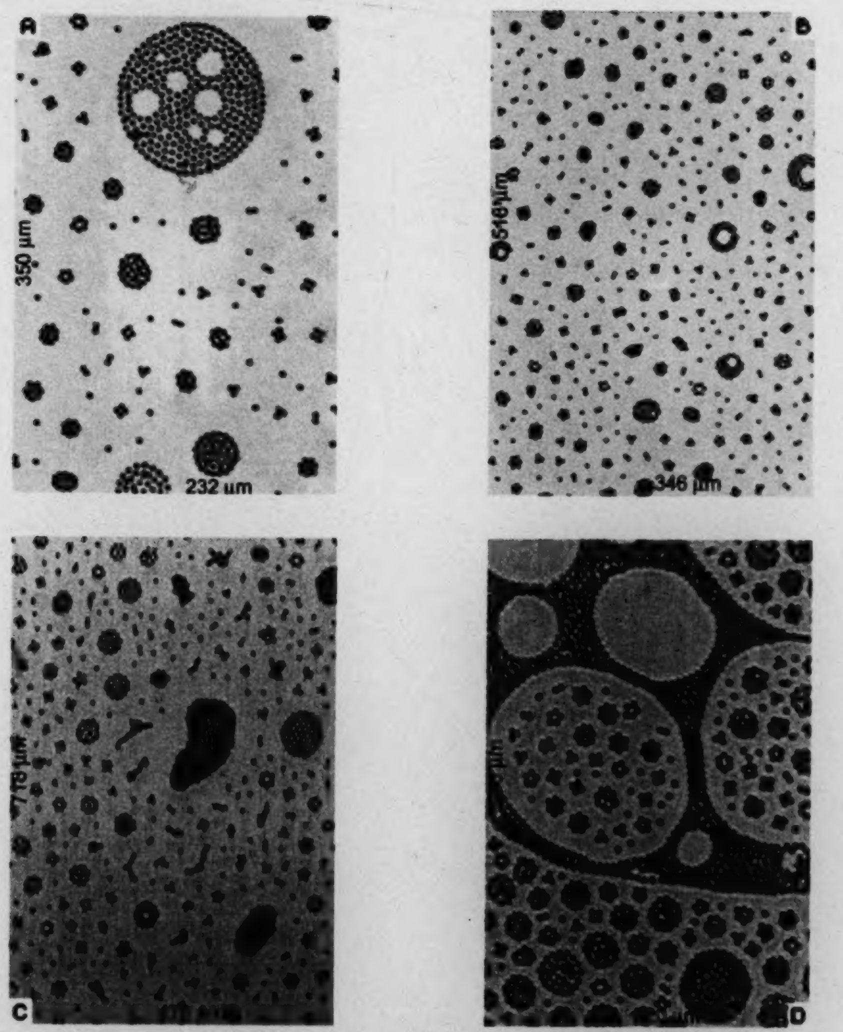

Figure 2.11: Microscopic images showing complex pattern formation in monolayers of 3μm latex particles. Approximate image dimensions are as shown. (reproduced from Ghezzi et al., 1999)

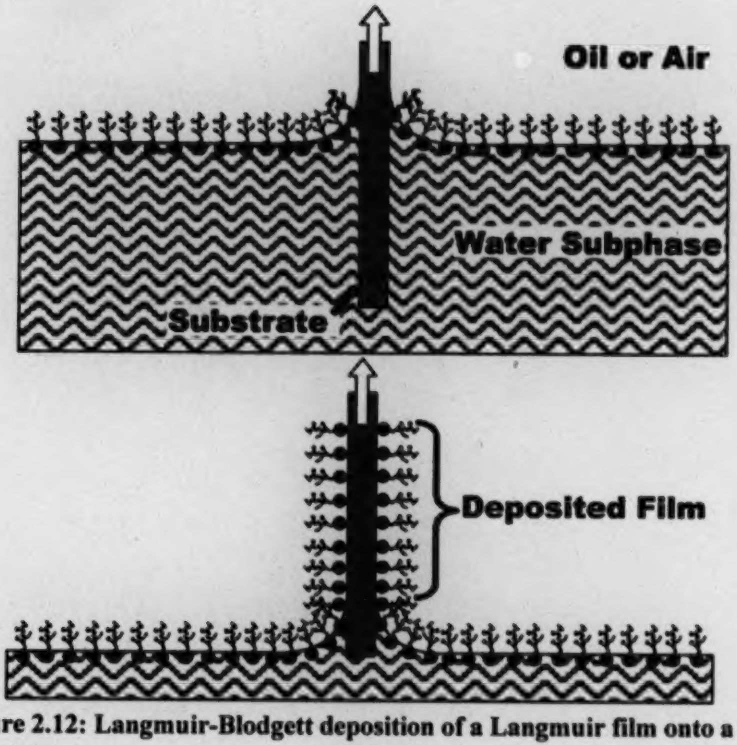

Figure 2.12: Langmuir-Blodgett deposition of a Langmuir film onto a solid substrate

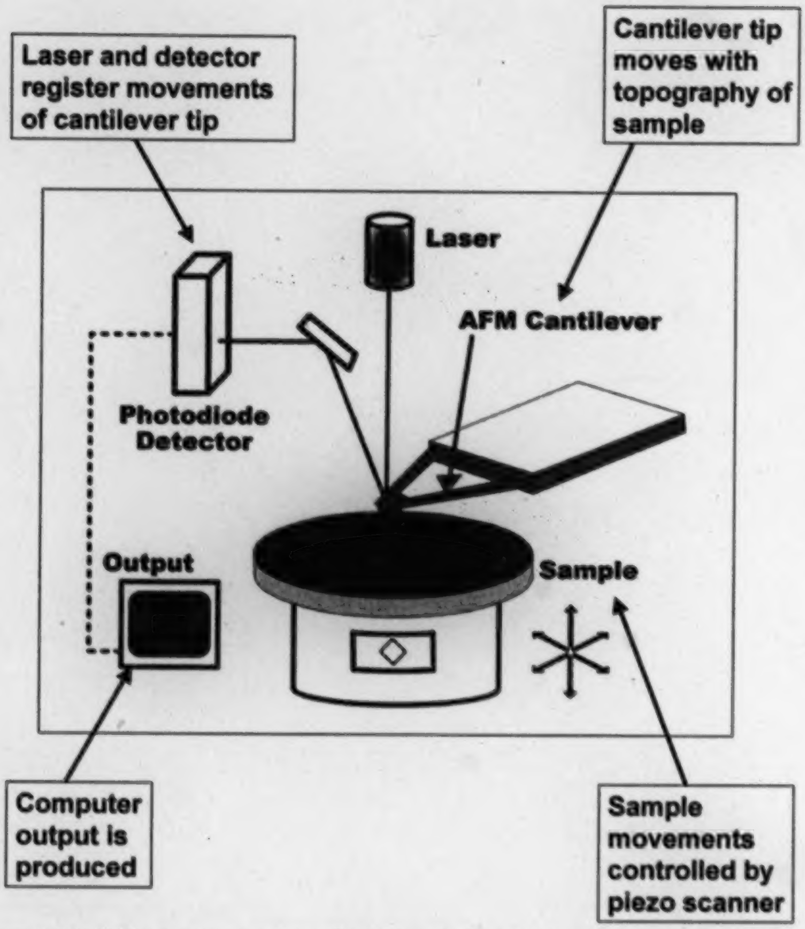
Laser and detector register movements of cantilever tip
Cantilever tip moves with topography of sample
Laser
AFM Cantilever
Photodiode Detector
Output
Sample
Computer output is produced
Sample movements controlled by piezo scanner

Figure 2.13: Major components of an atomic force microscope and details of its operation

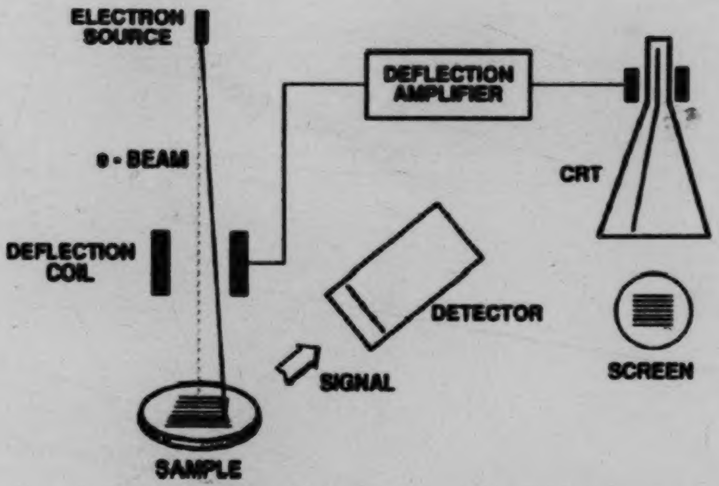

Figure 2.14: Major components of a scanning electron microscope. (reproduced from Bindle et al., 1992)

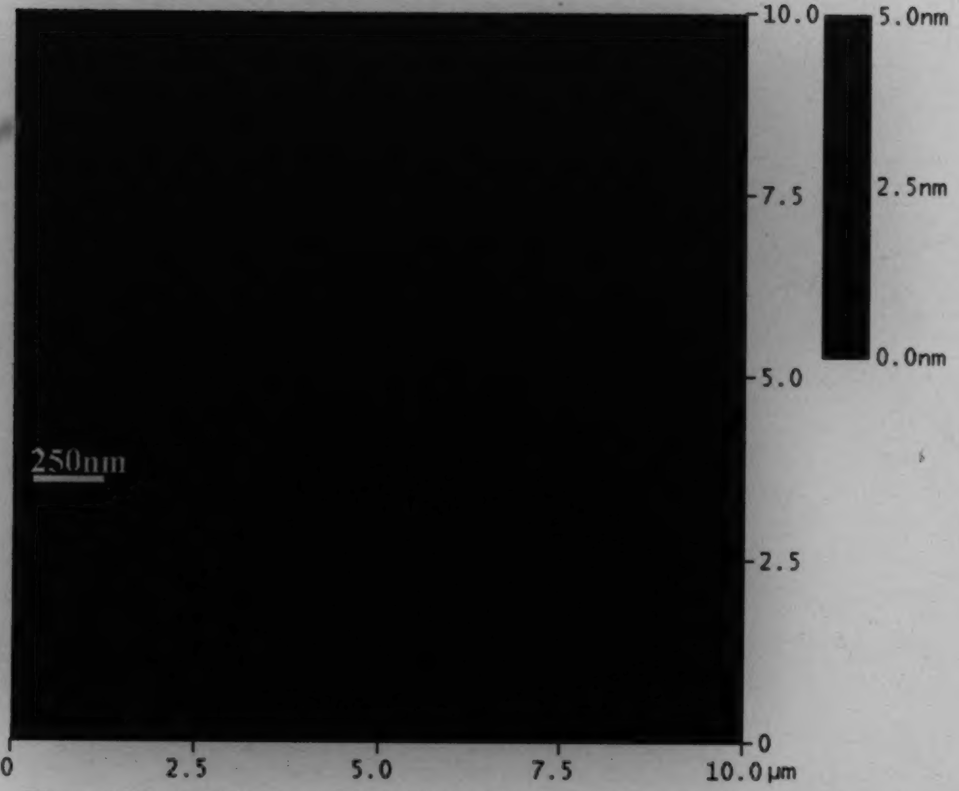

Figure 2.15: AFM images of Athabasca asphaltenes deposited from an air-water interface. Π= 30mN/m (reproduced from Zhang et al., 2003b)

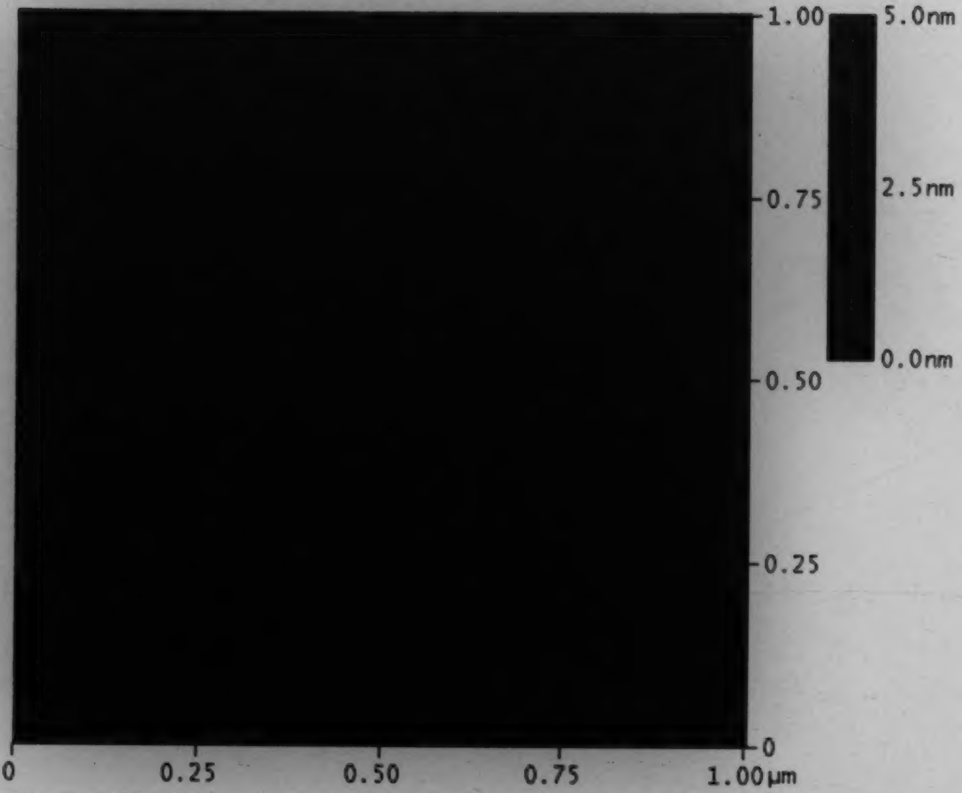

Figure 2.16 AFM images of Athabasca asphaltenes deposited from a toluene-water interface. Π= 20mN/m (reproduced from Zhang et al., 2005b)

"Not everything that counts can be counted, and not everything that can be counted counts."

-Albert Einstein

3

Experimental Materials and Methods

3.1 Introduction

This chapter describes the materials used and the experimental procedures followed for thesis research. Many materials were obtained through various chemical suppliers, but some materials required specific laboratory preparation. The procedures for all preparatory laboratory work, and the work producing results shown in subsequent chapters, are included in order to provide a script to follow in future work.

3.2 Materials

3.2.1 Reagents

Due to the importance of cleanliness and avoiding contamination when investigating surface chemistry, high-grade chemicals were used whenever possible. Optima grade toluene (99.9%), HPLC (High Performance Liquid Chromatography) grade *n*-heptane (99.4%), and HPLC grade acetone (99.6%) were obtained from Fisher Scientific. All chemicals were used as received, without any further purification. High purity water was obtained from an in-house Milli-Q filtration system (Millipore), which purifies water with an electrolyisis method, followed by a filtration process, and then an ultraviolet photo-oxidation process. Water used for experiments has a resistivity greater than 18.2 mΩ·cm. Bitumen, designated as vacuum distillation feed bitumen, was obtained from Syncrude Canada Limited. The bitumen had been through extraction and froth treatment processes, and was ready to be used in the Syncrude upgrading process.

3.2.2 Asphaltenes and Maltene Preparation

Bitumen was used to prepare samples of asphaltenes and maltenes to be used in the tests. The procedure followed was developed by Dr. Li Yan Zhang and is provided in detail in a 2003 article (Zhang et al., 2003a). The procedure requires several steps but essentially involves dissolving the bitumen in toluene and precipitating the asphaltenes with *n*-heptane. First a sample of bitumen was dissolved in toluene at a bitumen to toluene volume ratio of 5:1. Solids were removed by centrifugation for 30 min at 20,000 rpm (35,000g). The dissolved bitumen was placed under ambient conditions to allow the toluene to fully evaporate. The "solids-free" bitumen was then dissolved in *n*-heptane at a volume ratio of 40 parts heptane to 1 part bitumen. After precipitation, the asphaltenes were washed repeatedly with *n*-heptane and the supernatant containing deasphalted bitumen was collected. Both the asphaltenes and deasphalted bitumen were placed in a fume hood to allow the toluene and *n*-heptane to fully evaporate. When dissolved in toluene for use on the Langmuir trough, additional solids were removed by filtration with 1μm and 0.2μm Whatman PTFE (polytetrafluoroethylene) filters (Fisher).

Molecular weight determination and elemental analysis of asphaltenes and maltenes samples were performed at the Spectral Services and Microanalytical Laboratory in the Department of Chemistry at the University of Alberta. Vapour Pressure Osmometry (VPO) was used to determine the molecular weight of each sample. A Corona Westcan vapour pressure osmometer was used. Toluene was used as the solvent and measurements were taken at 50°C. The nitrogen, carbon, hydrogen and oxygen contents of the samples were determined with a Carlo-Erba 1108 Elemental Analyser. Sulfur content of the samples was determined with a dry ashing technique where samples are burned in a flask filled with oxygen and then titration with barium perchlorate is used to determine the amount of (SO_4) ions. Results from the elemental analysis are summarized in Table 3.1

Table 3.1: Elemental analysis of asphaltenes (Zhang et al., 2003b) and deasphalted bitumen.

Sample	C	H	N	O	S	H/C
Asphaltene	79.71	8.25	1.20	1.33	7.81	1.23
Maltene	82.72	10.46	0.32	1.61	4.36	1.50

Density measurements were conducted with an Anton Paar DMA 45 density meter. The device was calibrated using high-purity water and air, and then the density of pure toluene was measured. Samples of the asphaltenes and maltenes were dissolved in toluene at known concentrations and the densities of the respective solutions were measured. At low concentrations of asphaltenes or maltenes in toluene it is reasonable to assume the solution will behave as an ideal solution such that volume is conserved and the following equation is applicable (Yarranton and Masliyah, 1996).

$$\frac{1}{\rho_{mix}}=\frac{x_{sample}}{\rho_{sample}}+\frac{1-x_{sample}}{\rho_{tol}} \quad \text{..................................[3.1]}$$

The density of the hydrocarbon sample can then be calculated using (Lawrence, 2003)

$$\rho_{sample}=\frac{1}{\left[\frac{1}{\rho_{tol}}+\left(\frac{1}{\rho_{mix}}-\frac{1}{\rho_{tol}}\right)\frac{1}{x_{sample}}\right]} \quad \text{............................[3.2]}$$

where ρ_{tol} is the measured density of toluene, ρ_{mix} is the measured density of the solution and x_{sample} is the mass fraction of sample in the solution. Results of molecular weight and density measurements are given in Table 3.2

Table 3.2: Molecular weight and density of asphaltenes and deasphalted bitumen (a- from Zhang et al. (2003b))

Sample	MW (g/mol)	ρ (g/cm^3)
Asphaltene	7072^a	1.21
Maltene	559.3	0.99

Asphaltenes and maltenes were carefully weighed and dissolved in toluene at a desired concentration for use in Langmuir trough experiments.

3.2.3 Silica Nanoparticles

Degussa Corporation donated the silica nanoparticles used in this study. All products were produced by flame hydrolysis of silicon tetrachloride and are referred to as fumed silica. These particles are marketed under the brand name AEROSIL®. Several product types were initially obtained. Product types were differentiated by particle size and chemical treatment. A summary of the significant product details is presented in Table 3.3. Product details and related information that follow were obtained from two technical bulletins produced by Degussa (Deguss AG, 2001, 2003).

Table 3.3: Properties of fumed silica nanoparticles used in experiments. Surface treatments are a) Dimethyldichlorosilane, b) Hexamethyldisilazane, and c) Aminosilane

	AEROSIL® Product Name		
	200	R974	R504
Primary Diameter (nm)	12	12	12
Specific Surface Area (m^2/g)	200±25	170±20	200±25
Surface Treatment	None	DDS[a]	HMDS[b] & AS[c]
Methanol Wettability	n/a	40-50%	30-40%
Toluene-Water Contact Angle θ_{ow}	0°	75°	n/a
Air-Water Contact Angle θ_{aw}	14°	117±4°	n/a

Average primary diameters were determined by analysing TEM micrographs. Specific surface areas are another measure of the particle size. The values provided by Degussa are determined by measuring the adsorption of nitrogen onto the surface of the particle. The three fumed silica products are smooth and nonporous, so the surface area determined by adsorption corresponds well to the calculated area from TEM micrographs.

The silica nanoparticles can be treated in order to change the surface properties. AEROSIL® 200 particles are hydrophilic, the others are treated with Dimethyldichlorosilane (DDS) or Hexamethyldisilazane (HMDS) and Aminosilane (AS). During treatment of the hydrophilic silica in a fluidized-bed reactor with desired chemicals, the surface silanol groups on the hydrophilic silica are replaced by different functional groups. For AEROSIL® R974, the silanol groups are replaced by methyl groups. The end result of the surface treatment is to render the particles hydrophobic. The methanol wettability exhibited by the particles (refer to Table 3.3) is a measure of the degree of hydrophobicity. The value of methanol wettability is determined by the percent of methanol in a methanol/water solution required to wet the silica particles. A higher methanol concentration corresponds to a more hydrophobic sample. Further details of the silica products can be found in literature provided by Degussa or on the World Wide Web at http://www.aerosil.com and sites contained in this domain.

A common measure of the wettability of solids is contact angle. Figure 3.1 shows the difference in air-water contact angles of a hydrophilic and hydrophobic solid surface. Yan et al. (2000) determined the air-water and toluene-water contact angles for the same fumed silica types using enthalpy of immersion techniques. The technique involved mixing the particles in a desired fluid and measuring the heat released with a calorimeter. The contact angles were calculated from the measured enthalpies of wetting.

Particle Size Distribution

During the flame hydrolysis process, primary particles of silica tend to fuse together. The resulting aggregation of primary particles is shown by a transmission electron micrograph of AEROSIL® product in Figure 3.2. The average primary particle sizes given in Table 3.3 were determined by analysis of TEM images. In addition to the aggregation shown in Figure 3.2, agglomeration occurs so that the silica particles form a loose network structure. In order to obtain another measure of the particle size, hydrophobic silica-in-toluene dispersions (AEROSIL® R974) were analyzed using an Acoustic Spectrometer (Model DT-1200 – Dispersion Technology). This device uses the attenuation of ultrasonic waves to determine the particle size distribution of desired samples. Results from this device provide a measurement of the apparent particle size of the silica aggregates when the silica is dispersed in toluene.

The procedure for obtaining the particle size distribution of silica-in-toluene dispersions for various concentrations of silica is as follows. 110 ml of 3 wt% silica suspension was prepared. The suspension was sonicated in a 130W ultrasonic bath for 60 minutes and cooled with an ice bath to maintain a temperature near 20°C. This suspension was then analyzed with the acoustic spectrometer and the particle size distribution was recorded. The device software fitted a monomodal log-normal distribution to the collected data. During particle size measurement, the suspension was constantly agitated by a stirring mechanism. To investigate the effects of varying the solids concentration, the suspension was diluted several times and particle sizes were obtained for each concentration. Dilution was performed by extracting a 30 ml sample of the suspension and replacing it with toluene. This was an efficient method of varying the concentration, keeping the volume of the suspension within limits of the device and avoiding problems with cleaning the equipment chamber between readings.

Figure 3.3 shows the monomodal fitted particle-size distribution obtained for a 1.05 wt% suspension of silica in toluene. The particle size distribution in this suspension is log-normal with a mean diameter of 26 nm and standard deviation of 0.413. Also shown in Figure 3.3 is the cumulative particle size distribution by weight. From this curve, 5 % (by weight) of the particles will have a diameter of 2.7 nm or less and 95% (by weight) of the particles will have a diameter of 117 nm or less. Thus, the range 3-120 nm is a representative range of particle sizes measured by the acoustic spectrometer. Such size range well reflects the fact that most silica particles are in the form of aggregates as previously discussed.

A plot of the mean diameter versus the concentration shows that there is very little change in the particle size when the suspension is diluted. Figure 3.4 shows that the mean diameter ranges between 25 nm and 37 nm for concentrations between 0.29 wt% and 2.97 wt%. Further dilution was not performed because the lowest concentration that the device could measure was reached. There appears to be a trend, shown in Figure 3.4, where the mean particle diameter of the silica increases at lower concentrations. It is more likely that this variation is caused by flocculation of silica due to a longer stirring time. After the final dilution from 0.48 wt% to 0.29 wt% silica, particle size measurements were made at regular time intervals for an extended length of time. During these measurements the suspension was constantly stirred. Figure 3.5 shows the mean particle diameter measured at different times. Time zero corresponds to the time at which the final dilution was made. As shown in Figure 3.5 the mean particle diameter increases with time, most likely due to flocculation of particles during stirring.

The variation in mean particle diameter between different concentrations and different times is small compared to the distribution in each measurement (i.e. all mean particle sizes fall within the range 3-120 nm). Silica-in-toluene mixtures used in Langmuir trough experiments were also sonicated prior to use, and the most used silica concentration was approximately 1.16 wt% (10 mg/ml). Therefore, the results presented in Figure 3.3, for a suspension with silica concentration of 1.05 wt%, are useful as a measurement of the effective particle size of the silica particles dispersed in toluene. During Langmuir trough experiments with silica, prior to film formation, the particle size can be said to be 26 nm in diameter.

3.2.4 Solution Preparation

In general, solutions used for the formation of monolayers on the Langmuir trough consist of a surface-active component (e.g. asphaltenes, maltenes, particles) dissolved or dispersed in a spreading solvent (e.g. toluene). In order to study Langmuir films formed by mixtures of asphaltenes, maltenes and silica particles bulk solutions of each substance were created and small volumes of these bulk solutions were mixed together. Samples of the bulk solutions or mixtures were used to form Langmuir films on the Langmuir trough.

Bulk Solutions

First, asphaltenes and maltenes were extracted from bitumen by the procedure described in section 3.2.2. The desired substance (asphaltenes, maltenes or silica) was carefully weighed out in a volumetric flask and the flask was filled with toluene. Asphaltene solutions were made at 1 mg/ml and 2 mg/ml concentrations; maltene solutions were made at 2 mg/ml concentrations; and silica suspensions were made at 1 mg/ml and 10 mg/ml concentrations. Once the toluene had been added, the flask was shaken by hand for initial mixing and placed in an ultrasonic bath (130W). In order to avoid raising the temperature of the solution, ice was added to the ultrasonic bath. The solution was agitated for more than 30 minutes to ensure good dispersion/dissolution. The resulting asphaltene solution was of a clear brown colour; the maltene solution, a lighter brown; and the silica suspension, a bluish white. To aid in the use of the solutions on the Langmuir trough, small samples were transferred from the volumetric flask to small vials. All solutions were refrigerated at a temperature of approximately 4°C.

Classical Mixtures

Experiments in this study also involved the use of mixtures of asphaltenes, maltenes and silica nanoparticles. These mixtures were prepared by mixing the desired volumes (measured with pipettes) of each bulk solution. The initial concentrations of the bulk solutions were 10 mg/ml for the silica suspension and 2 mg/ml for the asphaltene and maltene solutions. The mass ratio of the two components and the resulting concentration of each component are listed in Table 3.4 for each of the mixtures used. In order to ensure that the silica particles were adequately dispersed in the suspension, the silica bulk solution was sonicated for at least 30 minutes prior to extracting a volume for mixing. The combination of bulk solutions was again sonicated for at least 30 minutes to ensure adequate mixing. These mixtures are referred to as "classical mixtures" in reference to one of the two different spreading techniques used in Langmuir trough studies. Care was taken when preparing mixtures in order to lessen any error that could be introduced when using small volume pipettes. In addition, some Langmuir trough experiments were repeated for mixtures made from bulk solutions of different concentrations. Results obtained (π-a isotherms) were similar for separate mixtures and within the results of individual mixtures.

Table 3.4: Summary of mixtures of silica, asphaltenes and maltenes used in Langmuir trough experiments

	Mixture Name					
	M-1	M-2	M-3	M-4	M-5	M-6
Mass Ratio Mal:Sil	10:90	20:80	25:75	30:70	40:60	50:50
Maltene Concentration (mg/ml)	0.71	0.40	1.25	0.60	0.80	1.00
Silica Concentration (mg/ml)	6.43	1.60	3.75	1.40	1.20	1.00
	MA-1	MA-2	MA-3	MA-4	MA-5	
Mass Ratio Asp:Mal	10:90	30:70	50:50	70:30	90:10	
Asphaltene Concentration (mg/ml)	0.20	0.60	1.00	1.40	1.80	
Maltene Concentration (mg/ml)	1.80	1.40	1.00	0.60	0.20	
	A-1	A-2	A-3			
Mass Ratio Asp:Sil	25:75	50:50	75:25			
Asphaltene Concentration (mg/ml)	1.25	1.67	1.88			
Silica Concentration (mg/ml)	3.75	1.67	0.62			

3.3 Langmuir Trough Experiments

3.3.1 Langmuir Trough Set-up

Experiments to obtain surface pressure-area isotherms and Langmuir-Blodgett films were conducted with a KSV Langmuir mini-trough system (KSV instruments, Finland) shown by the photograph in Figure 3.6. Refer to section 2.4.1 for a description of the basic design of a Langmuir trough. The KSV mini-trough system consists of a Langmuir trough and barriers, electronic balance and Wilhelmy plate, and a computer controlled motor driving the barriers. Experiments were run by computer with software provided by KSV instruments. The software recorded the change in surface pressure detected by the electronic balance and allowed for the manipulation of barrier speed and compression regime (constant rate vs. stepwise, compression vs. expansion etc.). After market modifications of the system were carried out in order to improve the experimental controls and maintain the environment for trough experiments. The trough was placed on an anti-vibration block to limit vibrations from other equipment in the laboratory and physical jarring of the countertop. The effects of dust and air currents on trough experiments were reduced by enclosing the trough in a vented chamber. Temperature controlled water circulation was added to the trough in order to maintain a constant temperature during trough experiments. Two different troughs were used, one designed for experiments at an air-water interface, the other designed for an oil-water interface. Figure 3.7 shows the different trough designs.

The air-water trough is made of Teflon with solid barriers made of Delrin (polyacetal). The trough is designed to hold one liquid only and the barriers rest on the top edges of the trough. The hydrophobic Teflon surface allows the water contained in the trough to maintain a level surface, and the hydrophilic Delrin keeps the Langmuir film from leaking past the barriers. In contrast, the oil-water trough is constructed of Delrin and has a two-level design so that the bottom can be filled with water and a top oil phase can be contained above the water phase. Barriers for the oil-water trough are also made of Delrin and are designed with holes in order to allow compression of the interfacial layer while allowing the top phase to flow freely. The barriers are designed to slide on the trough surface and provide a tight fit against the trough edges. Each trough has a different maximum area between the barriers. The air-water trough has a maximum area of 237 cm^2 and the oil-water trough has a maximum area of 170 cm^2.

During Langmuir trough experiments the electronic balance measures the change in force pulling the Wilhelmy plate downwards. In all experiments a rectangular shaped piece of Whatman chromatography paper (Fisher) is used as the Wilhelmy plate. Chromatography paper is well suited for use as a Wilhelmy plate in experiments at the oil-water interface because it is completely wetted by both liquids. In addition, use of chromatography paper allows the Wilhelmy plates to be changed frequently, decreasing contamination between experiments. Each piece is carefully cut so that the perimeter of the submerged portion is 30 mm.

3.3.2 Pressure-Area Isotherm Procedure

Pressure-area isotherms from air-water and toluene-water interfaces were obtained with very similar procedures. In both cases the procedure consisted of the following steps: trough cleaning, water phase addition, Langmuir film creation, spreading solvent evaporation and film compression. For air-water isotherms solvent evaporation is followed by Langmuir film compression. Toluene-water isotherm experiments required addition of an oil phase and a waiting period after oil phase addition before the Langmuir film compression. Trough cleaning was performed for every isotherm measured. Between individual experiments the trough was filled with ultra-pure water. After emptying the trough after an experiment, the trough and barriers were flushed with toluene dispensed from a rinse bottle. Excess toluene was removed with the suction of a glass pipette attached to a vacuum line, which contained an in-line liquid trap. After washing with toluene, the trough was rinsed in a similar manner with *n*-heptane and finally acetone. The trough and barriers were then wiped with an acetone-soaked Technicloth TexWipe. After rinsing and wiping, the solvents were allowed to evaporate under the suction of a fume hood. Once dry of solvents, the trough and barriers were rinsed with ultra-pure water several times. Water droplets remaining on the barriers and oil-phase compartment of the oil-water trough were removed with the "suction pipette".

Once cleaned, the trough was filled with approximately 250 ml or 120 ml of ultra-pure water for the air-water or toluene-water experiments respectively. The temperature and pH of the water were measured with a Fisher Scientific temperature/pH probe. The temperature was maintained at 20 °C throughout the experiment by a circulation bath. The initial water pH was 5.8.

The desired solution, suspension, or mixture was sonicated for 10 min in a 130W ultrasonic bath. The temperature of the bath was maintained at 20 °C by the addition of ice and/or cold water. Prior to spreading of the film-forming substance, the "suction pipette" was used to remove the surface layers of the water while compressing the surface to a minimum area. The minimum area corresponded to the barrier position that was closest to the Wilhelmy plate without barrier-plate contact. The minimum area was 21.75

cm^2 (9 % of max area) for the air-water trough and 15.12 cm^2 (9 % of max area) for the oil-water trough. The procedure of closing the barriers and removing the surface layers was repeated until the change in surface pressure was less than 0.10 mN/m.

Once the water surface was cleaned, the desired material was spread on the water surface. A 100 µl Hamilton gastight microsyringe was filled with the a desired volume of the newly sonicated solution. Droplets of the solution were formed at the end of the syringe needle and then touched to the water surface. Dispensing the solution in this manner reduced the possibility that material from the solution would enter the bulk water phase. Typical amounts of maltenes, asphaltenes and hydrophobic silica that were spread on the water surface are given in Table 3.5. For experiments that used the mixtures described in Table 3.4, the typical mass of each component at the interface is shown in Table 3.6.

Table 3.5: Typical amounts of substances used for pressure-area isotherm experiments

	Air-Water Interface	Toluene-Water Interface
Mass of Maltenes (µg)	60/30	40
Mass of Asphaltenes (µg)	60/30	30
Mass of Silica (µg)	540/700	540

Table 3.6: Typical amounts of individual components from mixtures used for pressure-area isotherm experiments

Maltene- Silica Mixtures

Mass Ratio Mal:Sil	10:90	20:80	25:75	30:70	40:60	50:50
Air-Water						
Mass of Maltenes (μg)	60	60	75/60	60	60	60
Mass of Silica (μg)	540	240	225/180	140	90	60
Toluene-Water						
Mass of Maltenes (μg)	-	-	60/44	-	-	100/200
Mass of Silica (μg)	-	-	180/131	-	-	100/200

Maltene-Asphaltene Mixtures

Mass Ratio Asp:Mal	10:90	30:70	50:50	70:30	90:10
Air-Water					
Mass of Asphaltenes (μg)	6	18	30	42	30.6
Mass of Maltenes (μg)	54	42	30	18	3.4
Toluene-Water					
Mass of Asphaltenes (μg)	-	12/9	20/10	14	-
Mass of Maltenes (μg)	-	28/21	20/10	6	-

Asphaltene-Silica Mixtures

Mass Ratio Asp:Sil	25:75	50:50	75:25
Air-Water			
Mass of Asphaltenes (μg)	60	60	60
Mass of Silica (μg)	180	60	20
Toluene-Water			
Mass of Asphaltenes (μg)	50	50	37.6
Mass of Silica (μg)	150	50	12.4

After spreading, 10 minutes (unless experiment was part of evaporation time tests) was allowed for evaporation of the spreading solvent (toluene). For air-water experiments, compression of the Langmuir film was started and recording of the surface pressure-area isotherm initiated. For toluene-water experiments, a toluene-water interface was created by carefully pouring approximately 75 ml of toluene onto the water phase. The toluene was poured down an inclined funnel that was pointed onto the ridge between the lower and upper compartments of the trough. Efforts were made to minimize the disruption of the spread film by slowly pouring the toluene. Once the toluene had been poured and a new toluene supraphase was formed, a waiting period of 10 minutes was allowed before compression. During film compression the barriers moved at a constant rate of 10 mm/min (unless part of compression rate tests). The pressure and area measurements were recorded at 1-second intervals by the Langmuir trough software and a pressure-area isotherm was plotted with the measured data. Unless otherwise stated, at least three isotherm experiments were conducted at the same set of conditions for every reported isotherm. In order to determine which isotherm to present, the averaging procedure outlined in Appendix C was carried out. In some cases the average isotherm is used, and in others an experimental isotherm that aligned with the average is used.

3.4 Langmuir-Blodgett Film Imaging

Langmuir films were transferred onto solid substrates using the Langmuir-Blodgett deposition technique. Images of the Langmuir-Blodgett films (deposited films) were then obtained with a Scanning Electron Microscope and an Atomic Force Microscope.

3.4.1 Substrate Preparation

For all Langmuir-Blodgett films, polished silicon wafers were used as the substrate for deposition. Silicon wafers obtained from Silicon Valley Microelectronics Inc. were prepared for deposition by cutting them to shape, cleaning, and surface treating. Rectangles approximately 10mm x 30mm were cut from a large wafer using a glass cutter. The cut wafers were soaked in soapy water overnight and cleaned with gentle rubbing. After copious rinsing with ultra-pure water, the wafers were soaked in a solution of sulphuric acid (95-98%, Fisher Scientific) and NOCHROMIX® (Fisher) overnight. The wafers were thus rendered hydrophilic and were retained as "hydrophilic wafers" for later film deposition. Some wafers were taken from the sulphuric acid solution rinsed with ultra pure water and soaked in a 10% solution of dichlorodimethylsilane (DDS) in toluene in order to make them hydrophobic. Hydrophilic wafers were stored in ultra-pure water and hydrophobic wafers were stored in a dry closed container. Immediately prior to film deposition, wafers were taken from storage and rinsed with ultra pure water and blown dry with nitrogen to remove dust and other contaminants.

3.4.2 Film Deposition

The same procedure was followed for deposition of Langmuir films from air-water and toluene-water interfaces. The KSV minitrough system was equipped with a "dipping mechanism", which allowed substrates to be raised and lowered through the liquids in the Langmuir trough. The dipping mechanism was computer controlled, which allows the transfer ratio (***TR***) to be calculated for each deposited film. Precise dimensions of the substrates were recorded in order for calculation of the transfer ratio of the deposition. Prepared silicon wafers were placed into the dipping mechanism as shown in Figure 3.8.

First, the substrate was lowered into the water phase. Then the Langmuir film was spread on the water surface as in the pressure-area isotherm experiments. If necessary, the toluene supraphase was added forming a toluene-water interface. Appropriate waiting periods were allowed. The Langmuir film was then compressed to the desired pressure (usually 10 mN/m) and the pressure was maintained for the duration of the deposition. The silicon wafer was then lifted through the interface at a speed of 5 mm/min. During deposition, the barrier positions were automatically adjusted by computer controls to maintain a constant surface pressure. Deposited films were allowed to dry in a clean ambient environment and stored in a desiccant chamber until used in imaging analysis.

3.4.3 Scanning Electron Microscopy

Imaging was performed with the SEM equipment in the Department of Chemical and Materials Engineering at the University of Alberta. Deposited films were carbon-coated with a sputtering device in order to make the sample surface conductive. Real time imaging allowed the entire surface of the film to be scanned to determine areas of interest on the film. Images were captured at 10,000 and 3,000 times magnification from an area of the film deemed representative of the sample and any areas with significant features.

3.4.4 Atomic Force Microscopy

Images were obtained with a Nano Scope IIIa – Digital Instruments AFM. The microscope was equipped with a 'J' type scanner, which has a maximum scan size of 125 μm x 125 μm and a vertical range of 5 μm. Images were obtained while using silicon nitride cantilever tips operating in contact mode. The tips varied in cantilever length (100 or 200 μm) and width, and had an approximate spring constant of 0.06, 0.12, 0.38, or 0.58 N/m. Different cantilever tips were used in order to obtain the clearest images, and the tip that gave the best results varied from sample to sample. Deposited films were removed from the desiccant chamber and then scanned with the AFM under ambient conditions. In order to ensure a representative image of the deposited films, AFM scans were performed at several locations on each deposited film.

3.5 Chapter Summary

In this chapter, important aspects of experimental procedures have been outlined and details of several procedures are provided. Asphaltenes and maltenes were extracted from Athabasca bitumen by dissolving the bitumen and precipitating out the asphaltene molecules. Molecular weight measurements (by VPO) and density measurements were made for both bitumen components. Hydrophobic fumed silica nanoparticles were provided by Degussa. An acoustic spectrometer was used to obtain an apparent particle size for the silica particles.

Asphaltenes, maltenes and silica particles were dissolved or dispersed in toluene separately or as mixtures. Films formed at air-water and toluene-water interfaces from these solutions and mixtures were studied with Langmuir trough experiments, which are used to obtain pressure-area isotherms. In addition, films were deposited onto silicon wafers using a Langmuir-Blodgett deposition technique, and AFM and SEM were used to obtain images of the deposited films.

Subsequent chapters present results obtained with the procedures and equipment described above. Results of some preliminary experiments conducted to establish different experimental parameters are presented and discussed in Chapter 4. Chapter 5 contains results and discussion about results from an air-water interface and Chapter 6 focuses on results from a toluene-water interface.

3.6 References

Degussa AG, *Special Hydrophobic Aerosil® (SHA) for Toners*, Technical Information TI 1222, Nippon Aerosil Co, 2001.

Degussa AG, *Technical Bulletin Fine Particles Number 11*, Aerosil & Silanes, Degussa AG, 2003.

Yan, N., Maham, Y., Masliyah, J.H., Gray, M.R., Mather, A.E., *Measurement of contact angles for fumed silica nanospheres using enthalpy of immersion data*, Journal of Colloid and Interface Science, 22:1-6, 2000.

Yarranton, H.W., Masliyah, J.H., *Molar mass distribution and solubility modeling of asphaltenes*, AIChE Journal, 42(12):3533-3543, 1996.

Zhang, L.Y., Lawrence, S., Xu, Z., Masliyah, J.H., *Studies of Athabasca asphaltene Langmuir films at air-water interface*, Journal of Colloid and Interface Science, 264(1):128-140, 2003a.

Zhang, L.Y., Xu, Z., Masliyah, J.H., *Langmuir and Langmuir-Blodgett films of mixed asphaltene and a demulsifier*, Langmuir, 19(23):9730 -9741, 2003b.

3.7 Figures

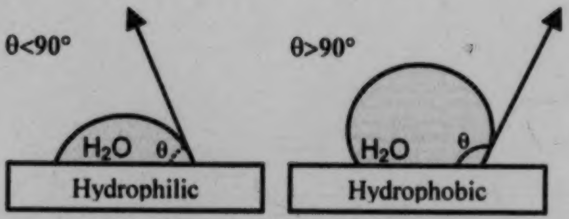

Figure 3.1: Measurement of contact angle from the shape of a sessile drop on a solid surface. Shown is the air-water contact angle of hydrophilic and hydrophobic solids

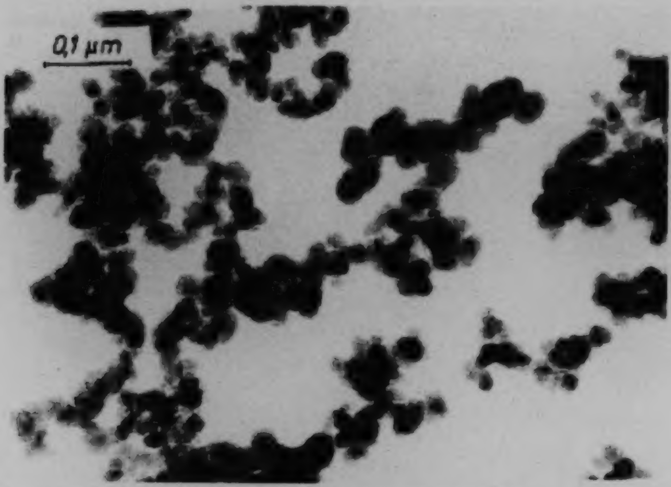

Figure 3.2: Transmission Electron Micrograph (TEM) of fumed silica nanoparticles (modified from Degussa Corporation website)

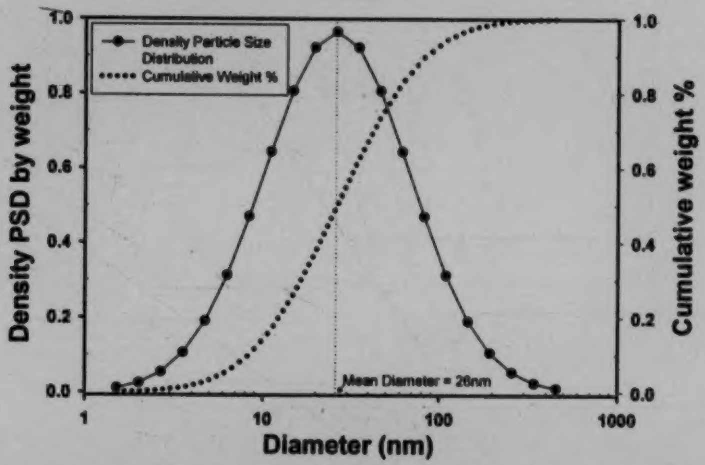

Figure 3.3: Density particle size distribution on weight basis of R974 hydrophobic silica in toluene (1.05 wt%) measured with acoustic spectrometer device.

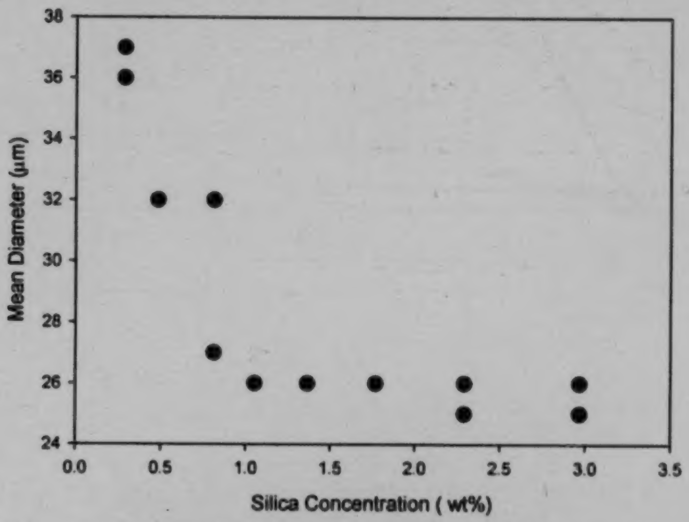

Figure 3.4: Mean diameter of silica in toluene measured with acoustic spectrometer at various concentrations of silica in toluene.

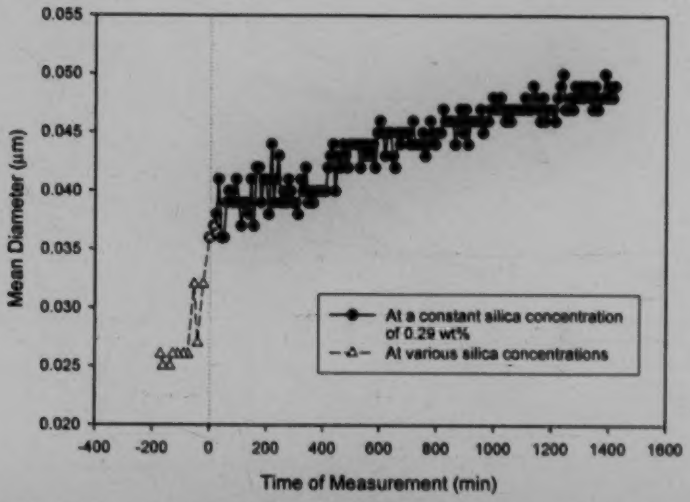

Figure 3.5: Variation of mean diameter of silica in toluene with an increase in the age of the suspension. Values from before time zero correspond to the values from the dilution graph in Figure 3.4. Measurements made after time zero are at a concentration of 0.29 wt%.

Figure 3.6: KSV mini-trough system.

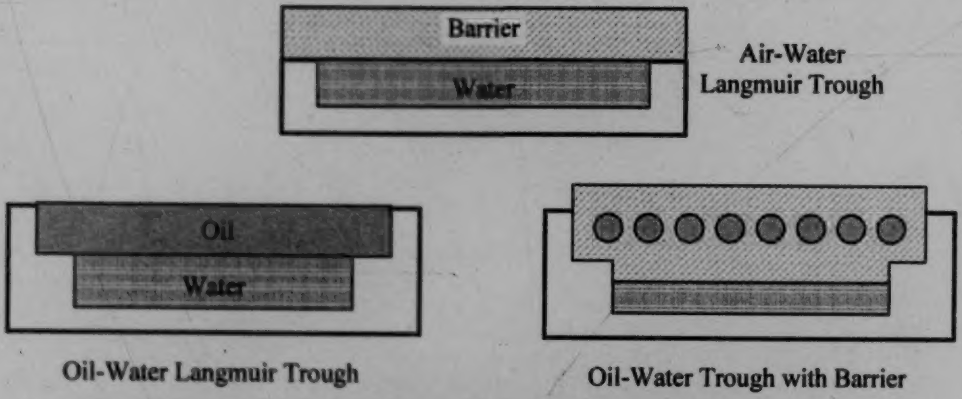

Figure 3.7: Cross section of the two Langmuir trough designs. Sketch shows the position of the barriers in the trough and the basic design of each trough.

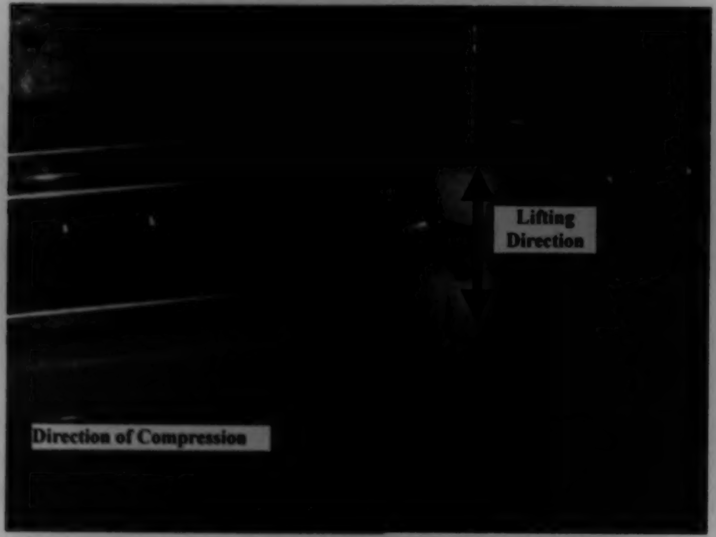

Figure 3.8: Image of silicon wafer loaded into the dipping mechanism prior to Langmuir-Blodgett deposition.

"I have yet to see any problem however complicated, which, when looked at in the right way, did not become even more complicated"

-Poul Anderson

4

Preliminary Experiments

4.1 Introduction

Several investigations into the operation of this particular Langmuir trough set-up were performed at the University of Alberta (Lawrence, 2003; Lawrence et al., 2004; Zhang et al., 2003a, 2003b, 2005a, 2005b). These investigations established the effectiveness of using the KSV Langmuir trough for investigating asphaltene films and the effectiveness of various control measures such as the temperature and vibration control. In addition to their investigations, for this thesis, several preliminary experiments were conducted to establish control over experimental variables that are related to tests performed with the mixtures described above. Some additional Langmuir trough experiments are discussed in Appendix A. Outcomes of these experiments have given directions to some areas of the research and in some cases yield important results. In order to have more effective discussion in later chapters, some results are presented and discussed in this chapter.

4.2 Langmuir Film Experiments

4.2.1 Comparison to Published Results

In order to establish the quality of the techniques used in Langmuir-Trough experiments, tests were conducted with arachidic acid to make a comparison with previously published results. The pressure-area isotherm of arachidic acid has a very distinct shape, and can be easily compared to previously published data. To perform this controlled test a 1 mg/ml solution of arachidic acid (99.9%, Sigma-Aldrich) in chloroform (99.9%, Sigma-Aldrich) was prepared. Shown in Figure 4.1 is the surface pressure-area isotherm obtained using this solution and isotherms of arachidic acid from several published articles.

There are considerable differences in the published results surveyed as shown in Figure 4.1. The positional change in isotherms (i.e. shift left or right along the x-axis) is evidence of experimental differences between the studies reviewed. When using a Langmuir trough like the KSV minitrough with a small trough area there is a chance for errors in the isotherm measurement. The discrepancies shown in Figure 4.1 suggest that there is not much agreement between experiments conducted by different researchers. There could be many reasons for this discrepancy, for example, the arachidic acid purity, trough cleanliness, water subphase purity or variations in the trough design. Because the results are shown as the area per molecule, very small changes in the amount of material at the interface can cause a shift in the isotherm. Figure 4.1 shows the difficulty in producing an isotherm that matches the results of other groups.

Repeat experiments using the same conditions were performed in order to obtain isotherms that closely match each other. This shows that experimental procedures give consistent results. In this thesis isotherms are used for comparison amongst different films. Thus, obtaining an exact match of the arachidic acid isotherm with previous published results is not as critical as ensuring that results can be repeated. However, the shape of isotherms obtained from experiments is common to most literature results presented including the data from Gaines (1966), which is considered a classic reference.

As well, one result matches very closely to that published by Santos et al. (2001). This demonstrates that the procedures followed during Langmuir trough operation generate accurate data, because, in general, the experimental isotherm was within the range of published values from different research groups. In addition to the results obtained with arachidic acid, results obtained by the author using Athabasca asphaltenes much more closely match results previously published by researchers at the University of Alberta.

4.2.2 Hydrophilic Silica

Different types of silica were available from Degussa as outlined in Table 4.3. The particle wettability has been shown to affect the Langmuir film characteristics of a particulate film (refer to section 2.4.3). To investigate the difference between the hydrophilic and hydrophobic particles (i.e. AEROSIL® 200 and AEROSIL® R974), attempts were made to form a film of AEROSIL® 200 particles and obtain a surface pressure-area isotherm. As expected, no film was formed on the water surface because the particles were too hydrophilic and sank when place on the water surface.

In addition to investigating the hydrophilic particles alone, a mixture of 20 wt% maltenes and 80 wt % hydrophilic silica particles was prepared and a surface pressure-area isotherm was obtained for the mixed film. As shown in Figure 4.2, there is very little change in the isotherm of a film of maltenes when the maltenes are mixed with hydrophilic silica before spreading of the Langmuir film. The presence of hydrophilic silica causes a slight shift to the left in the position of the isotherm, which indicates a more compact film or less material at the interface. However, the presence hydrophilic silica causes no significant change in the shape of the isotherm. (Refer to Chapter 5 for evidence of a significant change in isotherm shape when hydrophobic silica is present in a surface film). The shift in the initial area of the isotherm is probably due to some adsorption of the maltenes onto the hydrophilic silica particles, which then sink and do not remain at the interface. This would decrease the amount of maltenes present at the interface. Thus when the isotherms are normalized by the mass spread, the isotherm shifts to the left.

To test the possibility that adsorption of maltenes onto the silica is a contributing factor, a surface pressure-area isotherm was obtained for the supernatant of the mixture. The mixture was allowed to stand for a few days and significant settling of particles was observed. The supernatant was then extracted from the top of the mixture to ensure that no particles would be present. The maltene concentration of the supernatant was assumed to be the same as the original prepared solution in calculating the area per mass of maltenes. The isotherm of the supernatant normalized by the mass of maltenes spread on the water surface, is comparable to the isotherm of the original mixture without removal of particles. This finding suggests that it is adsorption of maltenes onto the particles that causes the isotherms to shift to the left from the isotherm of a maltene only film. Hydrophilic silica was not used for other experiments due to the lack of success in obtaining a surface-pressure area isotherm for the case when only hydrophilic silica was used and the case using maltene-hydrophilic silica mixtures.

4.2.3 Compression Rate

One parameter that can be manipulated during measurement of surface pressure-area isotherms is the barrier speed or area compression rate. To investigate the effect of compression rate on the isotherms of silica particle films, a series of tests were performed. In these tests, a standard set of conditions was used, while the rate of compression was varied. For each of the four isotherms 54 μl of a 12.5 mg/ml dispersion of hydrophobic silica (AEROSIL® R504) in toluene was spread on the water surface. The barrier speed was varied between 5 mm/min to 100 mm/min for the experiments. Results of the four surface pressure-area isotherms are presented in Figure 4.3.

Results show that rate of compression has little effect on the observed isotherm for silica particulate films. Since the variability inherent to the isotherm measurement is greater than the noticed differences between the isotherms shown in Figure 4.3, no distinct trend can be discerned amongst the four isotherms. The highest compression rate (barrier speed of 100 mm/min) had a slightly lower collapse pressure, which could be due to experimental error, but there are no other noteworthy findings. A barrier speed of 10 mm/min was chosen as the compression rate for all other isotherms reported.

Compression rate was also shown to have little effect on the shape of the surface-pressure area isotherm of asphaltenes (Lawrence, 2003).

4.2.4 Evaporation Time

All solutions prepared for the Langmuir trough tests used toluene as the spreading solvent. This choice was made because of the solubility of asphaltenes and maltenes in toluene, the availability of high purity toluene in the laboratory, and the common use of toluene in studies with bitumen. To ensure complete evaporation of the spreading solvent, time is allotted for evaporation of the toluene after spreading of the Langmuir film. Although the amount of toluene spread on the water surface was very small (between 20-150 μl) it is possible that not all of the toluene would evaporate before compression of the film was started. In addition, some other process may have occurred while the toluene evaporates. To investigate the effect of evaporation time, several isotherms were obtained for a film of maltenes. Maltenes were chosen for this investigation because they are most likely to retain toluene in their chemical structure.

Figure 4.4 shows isotherms from 3 tests with 10 minutes evaporation and 3 tests with 30 minutes evaporation. In each of these tests 30 μl of a 2 mg/ml solution was spread on the water surface. It is evident that there is no substantial change in the isotherms when the evaporation time is extended to 30 minutes. For practical purposes 10 minutes of evaporation time was used for all other experiments.

4.2.5 Aging of Mixtures

Mixtures prepared for study on the Langmuir trough were stored in glass containers with tight fitting, Teflon-lined lids. (A comparison of results obtained from silica suspensions held in different container types is provided in Appendix A) The process of extracting asphaltenes and maltenes from bitumen and preparing the mixtures is difficult and lengthy. Therefore, prepared mixtures were used for several isotherms. Two sets of experiments were performed to investigate if the age of the mixture (i.e. the length of time passed from original preparation) has any affect on the resulting surface pressure-area isotherm. The interactions between silica and asphaltenes, and silica and maltenes when in solution with toluene could be time-dependent and could change the properties of the resulting Langmuir film produced from the mixture. A silica-asphaltene mixture and a silica-maltene mixture were prepared with the procedure described in section 3.2.4. Timing for the age of the mixture was started immediately after sonication of the mixture. Surface-pressure isotherms were obtained at different storage times of the mixture, which was defined as the time passed from the end of the sonication to the film spreading. Unlike other surface pressure-area isotherms, the mixture was not sonicated prior to the spreading of each film. The mixtures were sonicated only once at the time of mixture preparation. Results from the surface pressure-area isotherms for different aging of mixtures are presented in Figure 4.5 for the silica-maltene mixture and Figure 4.7 for the silica-asphaltene mixture. A mixture with maltene:silica mass ratio of 25:75 (mixture M-3 in Table 3.4) and a mixture with asphaltene:silica mass ration of 50:50 were used for isotherms in Figure 4.5 and 4.7 respectively. The same volume of the mixture was spread on the water surface for each isotherm. Thus, 75 μg of maltene and 225 μg of silica were used for maltene-silica isotherms, and 60 μg of asphaltene and 60 μg of silica were used for asphaltene-silica isotherms.

To facilitate comparison of the various ages of the mixture, the surface pressure of the silica-maltene films at an area of 7 A^2/molecule maltene, and the film area at a surface pressure of 20 mN/m were determined for each isotherm. Figure 4.6 shows plots of the surface pressure and film area vs. mixture aging. A similar comparison was done for the silica-asphaltene mixtures at an area of 250 A^2/molecule, and surface pressure of 35 mN/m with the results presented in Figure 4.8.

Results show that aging has little effect on the isotherms of maltene-silica and asphaltene-silica mixtures. Isotherms of the silica-maltene mixture in Figure 4.5 are very similar with little variation among them. The same is true of the isotherms of silica-asphaltene mixtures in Figure 4.7. It is reasonable to suggest that there is not any significant settling or separation of the mixture for the time scales investigated. To be prudent, the mixtures were still sonicated for 10 min prior to film formation for all other tests. If prepared mixtures were stored for periods of time longer than 30 days, isotherm results were only used if they closely matched results from earlier dates. Otherwise new mixtures were prepared and experiments were repeated.

4.3 Langmuir-Blodgett Deposition Experiments

4.3.1 Carbon Coating of LB Films

For deposited films containing silica AFM scans were conducted after the film had been carbon coated and studied with the SEM. It was found that without this carbon coating, the cantilever tip displaced the silica particles, which resulted in blurred images. Images containing silica particles were much clearer after the film was carbon coated. Figure 4.9 shows AFM images obtained from (a) uncoated and (b) carbon coated deposited asphaltene-silica films. Figure 4.9a illustrates the image blurring caused by silica particle displacement.

It is possible that the carbon coating may produce features in the AFM images that would not be present in images of uncoated films. However, comparison of the two AFM images in Figure 4.9 shows that there are no major differences in the features of each AFM image. In addition, AFM images of coated and uncoated silicon wafers (without any deposited films) are shown in Figure 4.10. The image of the bare silicon wafer (Figure 4.10a) shows no discernable features, only some noise likely caused by outside interference. By comparison, Figure 4.10b shows that the carbon coating introduces few, very small features into AFM images.

Because it is expected that features of maltene and asphaltene films are smaller than features of silica films, a final comparison of images from uncoated and coated films is shown in Figure 4.11. AFM images of a mixed maltene-asphaltene film deposited from the same Langmuir film are shown in Figure 4.11. Figure 4.11a is an uncoated sample and Figure 4.11b is a carbon-coated sample. Comparison of the two AFM images shows that the carbon coating does not change the basic features of the maltene-asphaltene film. Unlike films containing silica, the image from the uncoated film is clear likely because the bitumen components stick to the silicon wafer better than the silica particles. Carbon coating is not necessary to obtain good AFM images for these films. Therefore, AFM images of films without silica were obtained from uncoated samples. By and large, carbon coating of LB films has been shown to have negligible effects on the features resolved by AFM scanning. In the context of this thesis the carbon coated films are considered comparable to uncoated films.

4.4 Conclusions

Preliminary Langmuir trough experiments were conducted in order to: compare experimental data to published results, study hydrophilic silica films, establish a standard compression rate, and investigate the aging of mixtures. For the LB films, a comparison of AFM images from uncoated and carbon coated films showed that carbon coating has negligible effects on AFM images.

4.5 References

Gaines, G. L., *Insoluble monolayers at liquid-gas interfaces,* New York, Interscience Publishers 1966.

Lawrence, S.A., Characterisation of asphaltene monolayers using a Langmuir trough and an atomic force microscope at air-water and n-heptane-water interfaces, MSc. Thesis, University of Alberta, 2003.

Lawrence, S.A., Zhang, L.Y., Xu, Z., Masliyah, J.H., *Langmuir and Langmuir-Blodgett asphaltene films at heptane-water interface*, Canadian Journal of Chemical Engineering, 82(4):821-828, 2004.

Lu, W.X., Zhou, H.L., He, P.S., Guo, W.H., *LB films formed from arachidic acid monolayers on an aqueous solution of a ruthenium(II) complex*, Thin Solid Films, 365 (1):67-71, 2000.

Santos, J.P., Zaniquelli, M.E.D., Batalini, C., De Giovani, W.F., *Modified electrodes using mixed Langmuir-Blodgett films containing a ruthenium complex: Features of the monolayers at air-liquid interface*, Journal of Physical Chemistry B, 105(9):1780-1785, 2001.

Sostarecz, A.G., McQuaw, C.M., Wucher, A., Winograd, N., *Depth profiling of Langmuir-Blodgett films with a Buckminsterfullerene probe*, Analytical Chemistry, 76(22):6651-6658, 2004.

Zhang, L.Y., Lawrence, S., Xu, Z., Masliyah, J.H., *Studies of Athabasca asphaltene Langmuir films at air-water interface*, Journal of Colloid and Interface Science, 264(1):128-140, 2003a.

Zhang, L.Y., Xu, Z., Masliyah, J.H., *Langmuir and Langmuir-Blodgett films of mixed asphaltene and a demulsifier*, Langmuir, 19(23):9730 -9741, 2003b.

Zhang, L.Y., Xu, Z., Masliyah, J.H., *Characterization of adsorbed Athabasca asphaltene films at solvent-water interfaces using a Langmuir interfacial trough*, Industrial & Engineering Chemistry Research, 44(5):1160-1174, 2005a.

Zhang, L.Y., Lopetinsky, R., Xu, Z., Maslyah, J.H., *Asphaltene monolayers at a toluene-water interface*, Energy and Fuels, 19(4):1330-1336, 2005b.

4.6 Figures

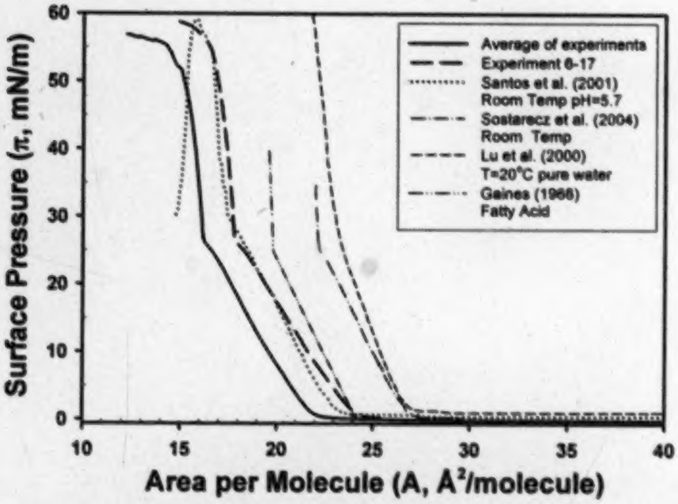

Figure 4.1: Surface pressure-area isotherms of arachidic acid at air-water interface. Comparison of experimental data with published results.

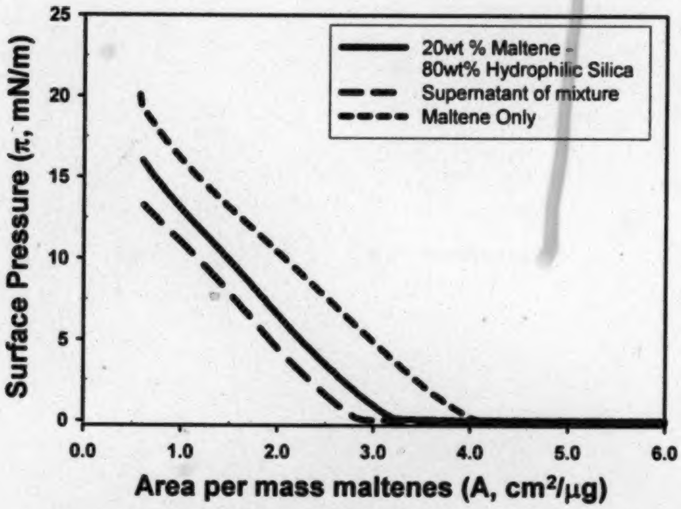

Figure 4.2: Surface pressure-area isotherms of maltenes and maltenes mixed with hydrophilic silica. Films formed at air-water interface.

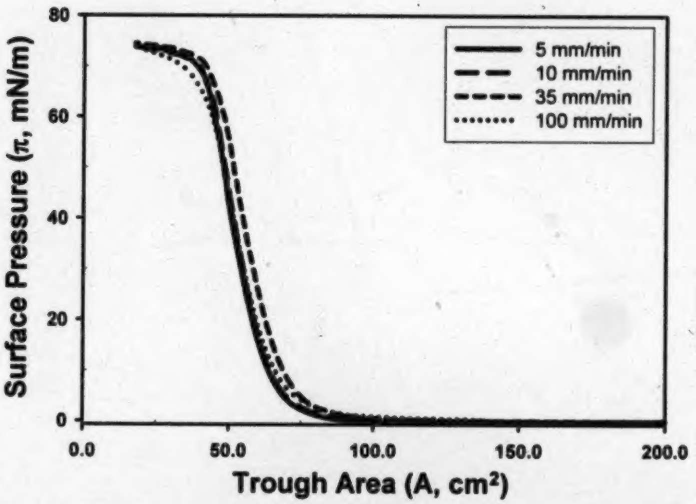

Figure 4.3: Surface pressure-area isotherms of R504 hydrophobic silica obtained with various film compression rates. Films formed at air-water interface

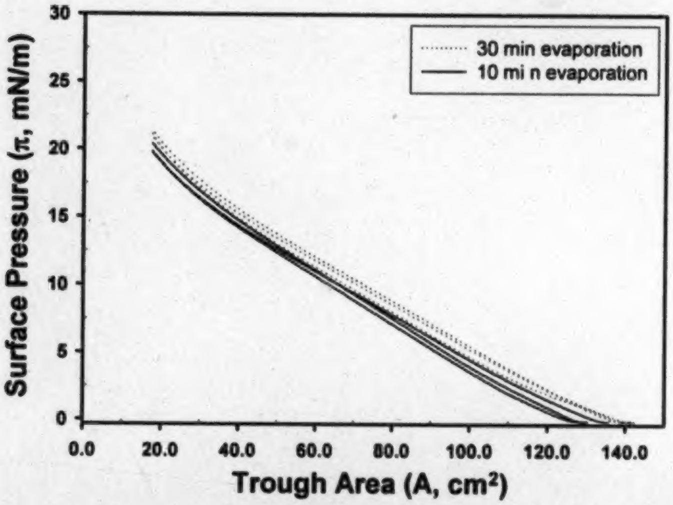

Figure 4.4: Surface pressure-area isotherms of maltenes for films that had different evaporation times (time between film spreading and initial compression). Films formed at air-water interface.

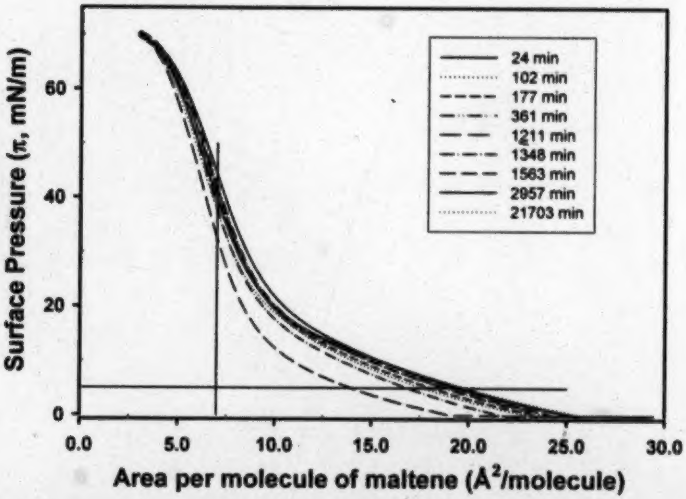

Figure 4.5: Surface pressure-area isotherms of mixtures of hydrophobic silica (θ_{aw}=117°) and maltenes. Each isotherm represents a film formed at a different time measured from the initial combination of the 2 substances.

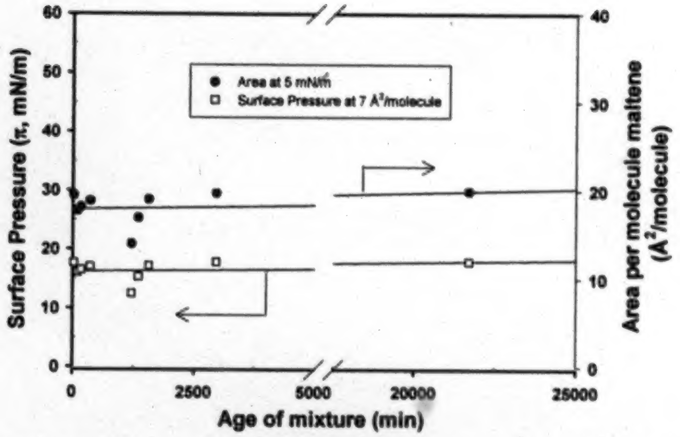

Figure 4.6: Variation in surface pressure and film area for maltene-silica mixtures of different ages

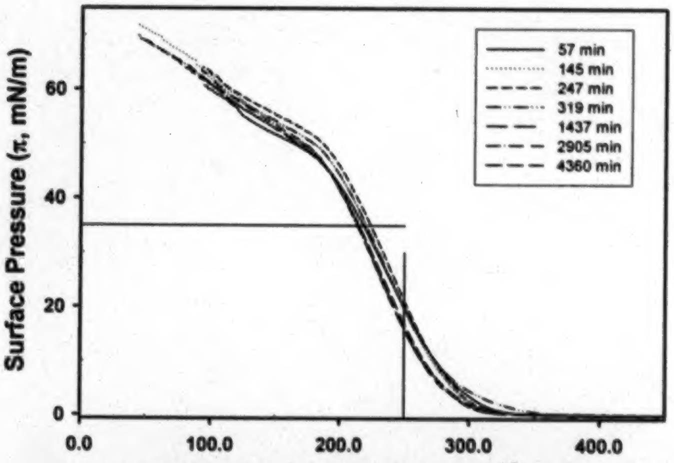

Figure 4.7: Surface pressure-area isotherms of mixtures of hydrophobic silica (θ_{aw}=117°) and asphaltenes. Each isotherm represents a film formed at a different time measured from the initial combination of the 2 substances.

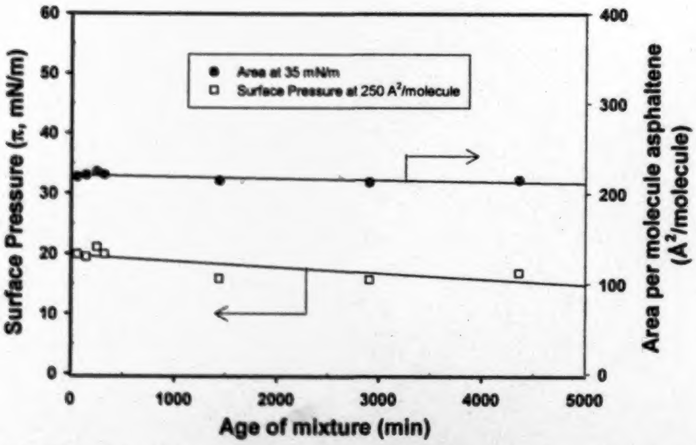

Figure 4.8: Variation in surface pressure and film area for asphaltene-silica mixtures of different ages

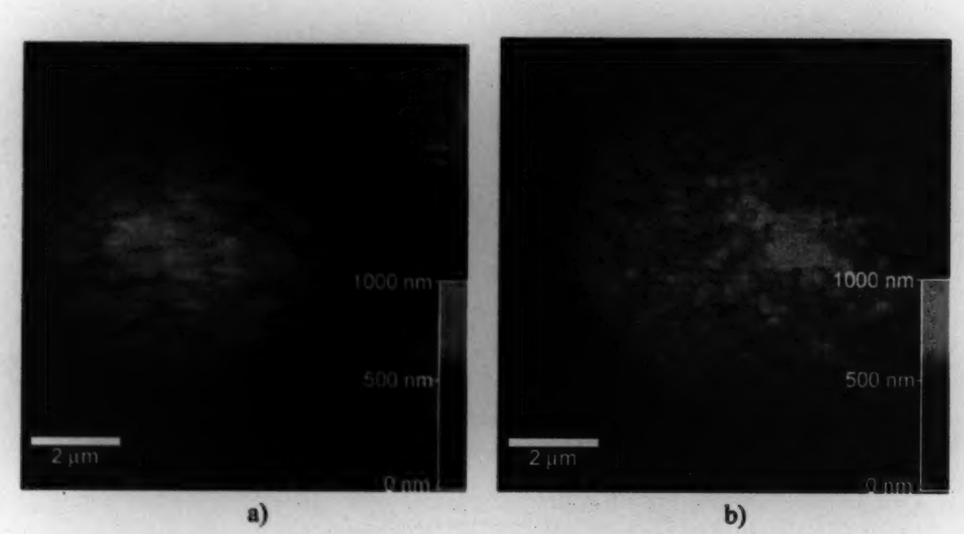

a) b)

Figure 4.9: AFM images of a 50 wt % asphaltene – 50 wt% silica mixture deposited from an air-water interface a) uncoated film and b) carbon coated film.

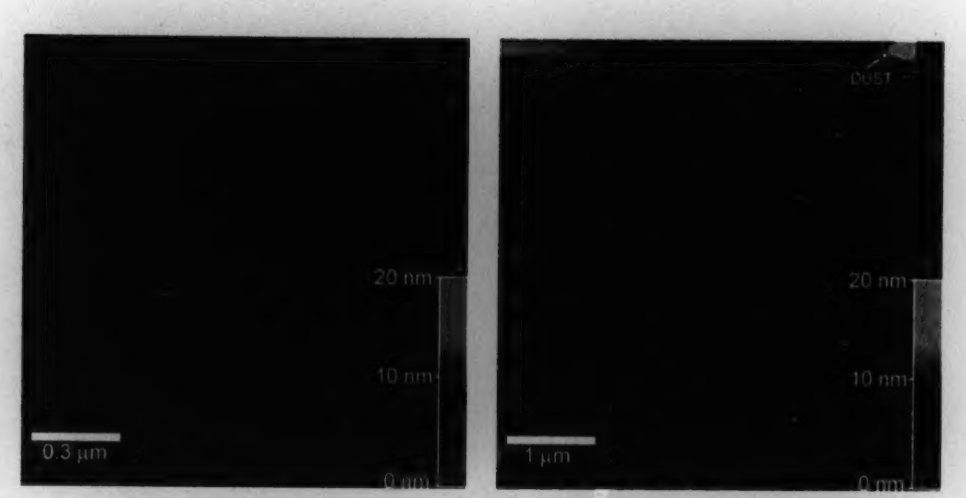

a) **b)**

Figure 4.10: AFM images of an (a) uncoated and (b) carbon coated silicon wafer.

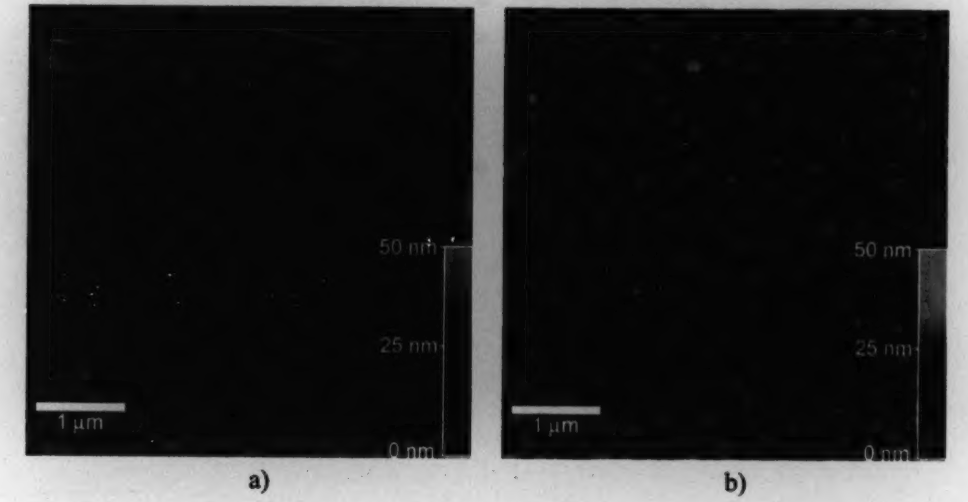

a) **b)**

Figure 4.11: AFM images of a 50 wt % maltene – 50 wt% asphaltene mixture deposited from an air-water interface a) uncoated film and b) carbon coated film.

"So there's no simple explanation for anything important any of us do"
-From the song "Courage" by The Tragically Hip

5

Nanoparticles, Deasphalted Bitumen, Asphaltenes and Their Mixtures at Air-Water Interface

5.1 Introduction

The present study uses Langmuir trough and Langmuir-Blodgett deposition techniques to examine the behaviour of fumed silica nanoparticles at an air-water interface. The objective is to compare the behaviour of fine particles to that of asphaltenes at the interface and to investigate the role of bitumen components in stabilizing surface films of fine particles. Combinations of silica particles and bitumen components were used to form films at an air-water interface and the effects of varying the composition of these mixed films on the film characteristics were determined. By combining the solid particles with bitumen components it was hoped to obtain a new perspective on the role of fines in stabilizing water-in-oil emulsions such as those in solvent diluted bitumen.

5.2 Isotherms of Silica, Asphaltenes, and Maltenes

Typical π-a isotherms of silica asphaltenes and maltenes are presented in Figure 5.2. As listed in the figure legend, different masses of each substance were spread at the interface. No sharp transition points are observed for any of the substances, but different regions in the isotherms correspond to phases of the films. Gas (G), liquid (L) and solid (S) phases are apparent for the asphaltene film but only gas and liquid phases are apparent for the maltene film, and the silica film exists in only gas and solid phases. Film collapse, marked by a kink (sharp change in slope) in the isotherm is shown for silica and asphaltenes at $\pi \approx 70$ mN/m and $\pi \approx 40$ mN/m, respectively. Above these pressures film material is forced out of the interface signifying the collapse of the Langmuir film. For both substances, the sharp change in the isotherm was accompanied by the appearance of streaks or creases in the film that were observed visually. According to Gaines (1966) the appearance of streaks is an indication of film collapse. For silica, the film collapse was apparent as the film was whitish and buckling was easily seen. Maltenes did not show film collapse; it appears that the small area of the trough prevented the film from being compressed sufficiently to reach such a point. Comparison of the three isotherms shows that the isotherm of maltenes has a much less steep slope than that of the asphaltenes or silica, suggesting that the film is more compressible.

5.3 Isotherms of Mixed Films

Surface pressure isotherms of mixed films that contain monomolecular film-forming substances such as fatty acids are usually presented with area per molecule on the abscissas. This provides a means of normalizing the data for comparison of the effects of each substance. In these cases the density and molecular weight is known for each substance in the mixture. Isotherms for films with solid particles cannot be normalized in this manner since the number of molecules at the interface is not easily estimated. Furthermore the particles used in this study are not monodispersed or spherical. Therefore, normalizing the surface area by the number of particles is not feasible. Attempts were made to estimate the number and mass of particles at the interface and deduce a particulate weight to use in place of molecular weight for the silica, without much success. A technique used for marine films by Pogorzelski (2001) to estimate the molecular weight of an unknown substance from the pressure-area isotherm was proven unsuccessful. Therefore, results are presented in this study as surface pressure versus area normalized by the mass of material at the interface. Scaling of the area values in this manner allows comparison of films of different compositions on the same plot. For the purpose of our study, this is proven suitable.

5.3.1 Maltene-Silica Mixtures

Six separate mixtures of maltenes and silica in toluene were tested. The concentration of maltenes and silica was varied to produce mixtures with different maltenes:silica ratios. Concentrations of the components are given in Table 3.4. Prior to spreading at the air-water interface mixtures were sonicated for 10 min with other variables being the same as that described previously. Figure 5.3 shows surface pressure-area isotherms for each of the maltene-silica mixtures with the trough area normalized by the amount of silica in each mixture. Typical amounts of silica are given in Table 3.6. Presenting the isotherms in this manner allows the effect of adding increasing amounts of maltenes on an equal amount of silica to be studied. Starting from the left side of the graph to the right, each curve represents an increase in the amount of maltenes present in the film. As the amount of maltenes present in the film increases, the isotherms shift to the right. In addition to the position shift, the shape of the isotherm changes with the addition of maltenes. A transition between two distinct slopes appears in the curves when the mass fraction of maltenes is 0.2 or greater. The position ($\pi_{transition}$, $A_{transition}$) of this transition is located by fitting linear lines to each of the two slopes and determining the intersection of these lines. This transition appears to be the transition from a maltene-dominated, liquid phase to a silica-dominated, solid phase. The extrapolated limiting area of each of the phases is determined by extending the line to a zero surface pressure. For films that demonstrate collapse, the critical points (π_c, A_c) was also determined in a similar manner and an example of the line fitting is shown in Figure 5.2. Results of the extrapolated limiting areas, the transition points and collapse points are presented in

Table 5.1. It is interesting to note that films containing more than 25% maltenes did not collapse, behaving just like maltene films due to the large initial area occupied by the film. As the fraction of maltenes increases the transition pressure and transition area increase.

Table 5.1: Extrapolated limiting area (A_o), collapse areas, and collapse pressures determined from intercepting lines fit to π-a isotherms of maltene-silica mixtures.

Mass Fraction Silica	A_0 Liquid Phase ($cm^2/\mu g$)	Transition Area ($cm^2/\mu g$)	Transition Pressure (mN/m)	A_0 Solid Phase ($cm^2/\mu g$)	Collapse Area ($cm^2/\mu g$)	Collapse Pressure (mN/m)
0.00	3.9	--	--	--	--	--
0.50	1.4	--	--	--	--	--
0.60	1.1	0.27	16	0.32	--	--
0.70	0.77	0.23	15	0.27	--	--
0.75	0.58	0.25	14	0.28	0.12	66
0.80	0.46	0.26	10	0.29	0.13	64
0.90	--	--	--	0.16	0.09	62
1.00	--	--	--	0.11	0.05	70

When the pressure-area data obtained for the maltene-silica mixtures are normalized by the mass of maltenes at the interface, isotherms emphasize the effect of adding silica to a film of maltenes. For the five maltene-silica mixtures tested, plots of surface pressure vs. area per μg of maltenes are shown in Figure 5.4. The typical amount of maltenes at the interface is listed in Table 3.6. There is some overlap in the curves, as the liquid phase does not change position with the addition of silica. The shape of the π-A isotherms does change though; mixtures with higher concentration of silica have a steeper curve and a larger solid phase beginning at lower area.

The change in isotherm position due to the addition of various amounts of maltene is further explored in Figure 5.5. The area shift (ΔA), from the isotherm of a silica film and each mixture was calculated at several surface pressures. The area shift for the 50 wt% maltenes mixture at a surface pressure of 10 mN/m is shown schematically in Figure 5.3. A plot of the area shift vs. the maltenes:silica ratio is shown in Figure 5.5. Because the area has been normalized by the mass of silica, the ratio of maltenes:silica also represents the amount of maltene added to the silica film. The area shift increases linearly with the amount of maltenes at lower surface pressure. At higher surface pressure there appears to be a limit for the area shift. Also, for a given amount of maltenes, the area shift at higher pressures is smaller than at lower pressures.

For each of the maltene-silica mixtures the area shift from a maltene isotherm at different surface pressures is shown in Figure 5.6. At surface pressures of 5 and 10 mN/m there is a negative area shift (isotherm shifts to the left) when the ratio of silica:maltenes increases. In both cases the magnitude of the area shift is larger at first but then levels off. At a higher surface pressure of 20 mN/m a positive area shift (isotherm shifts to the right) occurs when the silica:maltenes ratio is increased. The area shift appears to reach a maximum. At all three surface pressures the area shift does not change linearly with increasing silica content in the mixture.

5.3.2 Asphaltene-Silica Mixtures

Surface pressure-area isotherms of mixed asphaltene and silica films at the air-water interface are shown in Figures 5.7 and 5.8. Details of the three mixtures are given in Table 3.4 and amounts of each component used to obtain the isotherms are given in Table 3.6. In Figure 5.7 the abscissa is the trough area normalized by the mass of asphaltenes at the interface, illustrating the change in the isotherm of an asphaltene film associated with the addition of silica to the film. The isotherms have a similar shape but with the position of the curves for the mixtures to the left of asphaltene only, i.e. the films occupy less area per asphaltene. Isotherms for the asphaltene-silica mixtures also have a slightly steeper slope, with similar shape to the curve of asphaltene only. Figure 5.8 presents isotherms with the trough area normalized by the mass of silica at the interface, illustrating the change in the isotherm of a film of silica nanoparticles associated with the addition of asphaltene to the film. Mixtures of silica and asphaltene have isotherms positioned at larger area per mass of silica. The shape of the isotherms deviates from a silica-only film. Asphaltene-silica mixtures exhibit decreasingly less steep isotherms as the ratio of asphaltenes:silica increases. Collapse points of the asphaltene-silica mixtures, determined with the procedure mentioned before, are shown in Figure 5.8. Values of the collapse pressures and collapse areas are listed in Table 5.2. The collapse pressures of the asphaltene-silica mixtures are between the collapse pressure of silica and asphaltene, but closer to the collapse pressure of asphaltene (π_c~ 40 mN/m). The extrapolated limiting area per mass for the solid phase of each asphaltene-silica mixture is presented in Table 5.2. Areas are presented as an area per total mass spread. As can be seen from Table 5.2, the extrapolated area at the solid state (A_0) and the collapse area (A_c) increase with increasing asphaltene fraction in the mixed films. However, the collapse surface pressure (π_c) does not follow any specific trend with increasing asphaltene mass fraction.

As with the maltene-silica mixtures the area shift from a single component isotherm has been calculated for each of the mixtures. The area shift from a silica isotherm is shown in Figure 5.9 and the area shift from an asphaltene isotherm is shown in Figure 5.10. As the ratio of asphaltenes:silica increases the area shift from silica only increases linearly. The rate of increase in area shift (the slope of the lines) decreases at higher surface pressure. The change in area from an asphaltene only film is negative for each of the mixtures. As the ratio of silica:asphaltenes increases, the area shift reaches a limit. This trend occurs for all four surface pressure values given in the legend boxes in Figures 5.9 and 5.10.

Table 5.2: Extrapolated limiting area A_o, collapse areas, and collapse pressures determined from intercepting lines fit to π-A isotherms of asphaltene-silica mixtures.

Mass Fraction Asphaltene	A_0 (cm^2/μg)	Collapse Area (cm^2/μg)	Collapse Pressure (mN/m)
0.00	0.11	0.06	68
0.25	0.51	0.36	49
0.50	1.1	0.74	44
0.75	1.8	1.1	48
1.00	2.9	2.0	40

5.3.3 Maltene-Asphaltene Mixtures

Five mixtures of maltenes and asphaltenes in toluene were prepared and studied on the Langmuir trough. The isotherms for the maltene-asphaltene mixtures are shown in

Figures 5.11 and 5.12. Typical amounts of maltenes and asphaltenes used to obtain these isotherms are given in Table 3.6. Surface pressure is plotted against area per molecule for these isotherms, because the molecular weight of both asphaltenes and maltenes were available from VPO measurements. The molecular weights of the mixtures were calculated by a weighted average ($MW_{mix}= X_a \cdot MW_a + X_m \cdot MW_m$), where X_a and X_m are the molar fractions of asphaltenes and maltenes. The composition of the five mixtures and the calculated molecular weights are listed in Table 5.3.

Table 5.3: Molecular weights of maltene-asphaltene mixtures

Weight Fraction Maltene	Weight Fraction Asphaltene	Molar Fraction Maltene	Molar Fraction Asphaltene	MW of Mixture (g/mol)
1.0	0.0	1.0	0.0	559.3
0.9	0.1	0.99	0.009	616.0
0.7	0.3	0.97	0.03	772.8
0.5	0.5	0.93	0.07	1036.6
0.3	0.7	0.84	0.16	1573.9
0.1	0.9	0.58	0.42	3267.3
0.0	1.0	0.0	1.0	7072

Figure 5.11 shows isotherms of all the mixtures, except the mixture with 90 wt% maltenes, and isotherms of the single components. Each of the isotherms of the mixtures lies in between the isotherms of a maltene film and an asphaltene film. In Figure 5.12 the scales used on the axes are decreased in order to show better detail of the isotherm shapes and in order that the isotherm of the mixture with 90 wt% maltenes can be shown. Figures 5.11 and 5.12 show that as the asphaltenes content of the mixture increases, the isotherm shifts to the right with the exception of the isotherm of the 90% maltenes-10% asphaltenes mixture which lies to the left of isotherm of 100% maltenes. In addition, the shape of the isotherm varies among the mixtures. The isotherm of maltenes alone and of the 10% asphaltenes mixture have less steep slopes than other isotherms. Isotherms of other mixtures have two different slopes representing liquid and solid phases. The phase transition points (π_t,A_t) have been estimated by fitting straight lines to each section of the curves. It appears that there is a transition point for the 10% asphaltenes mixture but it begins at very low area and so the compression is not sufficient to make the film

complete the transition into a solid phase. Other transitions are gradual and so the points are estimates. Also the surface pressure at which the transition occurs decreases with increasing amount of asphaltene until the asphaltene content is greater than 10 wt%. The transition only appears in the isotherms of intermediate mixtures. Outlined in Figure 5.12 are the estimated transition and collapse points for several isotherms. Area and surface pressure values of the points are given in Table 5.4. The collapse pressure changes with the composition of the mixture and appears to pass through a maximum at higher wt% asphaltene. The single component asphaltene film has a lower collapse pressure than mixtures with 30 wt% and 10 wt% maltenes. From the three mixtures where a phase transition was easy to identify it can be seen that the transition pressure decreases with increasing asphaltene content until no transition occurs.

Table 5.4: Transition and collapse points of maltene-asphaltene mixtures

Molar Fraction Maltene	Transition Area (Å^2/molecule)	Transition Pressure (mN/m)	Collapse Area (Å^2/molecule)	Collapse Pressure (mN/m)
1.00	--	--	--	--
0.99	--	--	--	--
0.97	14.5	12.1	9.37	38.7
0.93	31.2	8.58	22.6	36.8
0.84	61.6	4.50	43.2	43.8
0.58	--	--	99.6	57.1
0.00	--	--	231	40.3

Figure 5.13 shows a plot of the area per molecule for different films at three different surface pressures (5, 10, 15 mN/m). For monolayer mixtures that behave ideally or if the components are completely immiscible, the variation in area with molar fraction will follow a straight line between the areas of each single component. A straight line between the area per molecule of a film with molar fraction of maltenes of zero and one has been drawn for each surface pressure. The areas neither fall exactly on the straight line nor show any trend; some points lie above the line and some below. This would indicate that either, the maltenes and asphaltenes are immiscible, or that they form an ideal mixture. A composition dependency of the collapse pressure occurs, which shows that the two components likely are miscible and therefore form an ideal mixture.

An analysis of maltene-asphaltene mixtures using area per mass similar to that performed with maltene-silica mixtures is provided in Appendix E. Isotherms are plotted with the abscissa normalized by the mass of each component. The area shift from single component isotherms was also calculated for each mixture. A comparison of these figures with those from maltene-silica mixtures shows some similarities.

5.4 Compressibility

Figure 5.14 shows the compressibility of the maltene-silica mixtures and Figure 5.15 shows the compressibility of asphaltene-silica mixtures, all calculated from the surface pressure and area data presented previously. Compressibilities for all mixtures are similar in that the film compressibility decreases from a high value when the film is in a gas phase to a relatively constant, lower value at the solid phase. There is a difference between the compressibility of the maltene-silica mixtures starting with the most compressible (highest compressibility) maltene film with a solid phase compressibility around 0.06 m/mN and decreasing to the least compressible silica film with a solid phase compressibility around 0.01 m/mN. The value of compressibility changes for each mixture at positions that correspond to the transition points discussed earlier. Also, for films that collapsed, compressibility showed a sharp increase and/or scattered values near or after collapse. This is most likely due to artefacts introduced by slope calculations. In contrast to the maltene-silica mixtures, the difference between the compressibility of the asphaltene-silica mixtures is marginal with solid phase compressibility for all mixtures ranging from 0.006 m/mN for (75% asphaltenes-25% silica) and 0.012 m/mN (asphaltenes only). It is difficult to discern any trend in how the compressibility changes with a variation in asphaltenes:silica ratio, but the asphaltene only film exhibits the highest compressibility at the solid phase.

5.5 Deposited Film Images

Single layer Langmuir-Blodgett films were deposited on to hydrophilic silicon wafers. Transfer ratios (TR) obtained for each deposited film are given in figure captions and are tabulated below in Table 5.5. As discussed by Zhang et al. (2003) the deposition of asphaltene films is non-reactive due to the presence of a water film between the substrate and the depositing film. Transfer of the film of silica particles resulted in a reasonable TR, even though the particles were hydrophobic and a hydrophilic substrate was used.

Table 5.5: Transfer ratios of the Langmuir-Blodgett depositions

LB Film Composition	Transfer Ratio
100 wt% silica	0.51
100 wt% maltene	1.25
100 wt% asphaltene	0.57
50 wt% maltene – 50 wt% silica	1.39
50 wt% asphaltene – 50 wt% silica	2.46

Atomic force microscope images were taken for each deposited film from the air-water interface. Figure 5.16 shows the images obtained from films of (a) silica, (b) silica-maltene mixtures, (c) silica-asphaltene mixtures, and (d) asphaltene. All films were deposited at π=10 mN/m. Inset in each subfigure is a higher magnification image of the same film. For films with silica the magnification is centered on a silica cluster. Scales are given as horizontal bars and the vertical greyscale bars on each image show the height of the features. Figure 5.17 shows a magnified image of a lower (dark) area from Figure 5.16(b) and Figure 5.16(c). Films containing silica have much larger structures as compared to the film of asphaltene. AFM scanning in contact mode did not produce any discernable features for a single component maltene film, as the film was too smooth, so AFM images are not reported for these films. The transfer ratio for the maltene film is greater than one, so there should be maltenes on the silicon wafer to scan with the AFM.

SEM Images provide a lower magnification of the films enabling the study of any larger arrangement of particles in the film. Micrographs of the LB film of hydrophobic silica only, silica-asphaltene mixture and maltene-silica mixture are presented in Figures 5.18, 5.19 and 5.20. Higher magnification images are inset for each mixture. All SEM images presented are of films deposited at 10 mN/m. Deposits at other surface pressures were taken with little or no difference in the resulting images. It was difficult to obtain AFM images of films with silica particles as during both contact and tapping modes the film was moved by the AFM tip which blurred the images. The silica did not adhere well to the surface and the large differences in height for the silica clusters were hard to scan with the AFM tip.

5.6 Discussions

5.6.1 Single Component Films

The isotherms for silica films are of very similar shape to isotherms for monoparticulate layers of glass spheres presented by Hórvölgyi et al. (1996) and isotherms of fumed silica particles presented by Maté et al. (1998). The curve is very steep and can be compressed to a high surface pressure (π_c=68 mN/m) before collapse. AFM images show that the silica nanoparticles form clusters larger than the primary diameter of 12 nm, as indicated in the product literature (Degussa AG, 2003) and 26 nm, as determined by acoustic spectroscopy. SEM images show that the clusters are not ordered and no patterns formed, as was the case for monolayers of charged latex particles under certain conditions (Ghezzi et al., 2001). Particle aggregation likely occurs at the interface because the clusters are larger than the particle size determined by acoustic spectroscopy. Aggregation at the air-water interface is due to hydrophobic interactions. Similar aggregation into clusters occurred for monodisperse silica nanoparticles of high hydrophobicity, and smaller domains were observed for particles with lower hydrophobicity (Tolnai et al., 2001).

Figure 5.2 shows that the surface pressure-area isotherm for the maltene film was much less steep than the silica film or asphaltene film. This shows that the maltene film is much less rigid than asphaltenes films, which is anticipated because the molecular weight (as determined by VPO analysis) of maltenes is substantially smaller and maltene molecules are not expected to be highly surface active. In addition, the maltene molecules may be pushed out of the interface, resulting in increased film compressibility. Langmuir films of resins extracted from different crude oils are also less rigid than the asphaltenes from the same oil (Ese, Yang, and Sjöblom, 1998; Mohammed et al., 1993).

For the isotherms obtained from a film of maltenes, there is a period of zero surface pressure increase at trough areas greater than 125 cm^2 (39 $Å^2$/molecule). In addition, consistent isotherms were obtained with different masses spread at the interface. These two facts confirm that a monolayer of maltene molecules is formed and that the maltene fraction of bitumen contains some surface-active species.

Asphaltene isotherms are consistent with previous results reported by Zhang et al. (2003). The asphaltenes molecules are surface active and form a relatively incompressible film. The particle size of the silica is much larger than the expected molecule size of the bitumen components. Also the AFM and SEM images have shown that the silica forms clusters, which are most likely 3-dimensional extending out of the interface into the bulk phases. Thus, for a given mass of silica, asphaltenes or maltenes, the area occupied at the interface is smallest for the silica.

5.6.2 Maltene-Silica Mixtures

Mixtures of silica and maltenes produced isotherms that appeared to be a combination of isotherms from each of the pure substances. The isotherms have two distinct slopes that represent different phases of the film. No clear transition points are observed between the phases; instead a gradual transition is observed. The lack of a distinct transition point indicates that the components are mixed together. The liquid phase is dominated by maltenes, as the initial slope in the mixed isotherms is similar to the slope of a maltene isotherm. The silica does not appear to contribute to the film behaviour until the film has been compressed to the transition point. After the transition point the silica dominates the film behaviour and the appearance of a solid phase in the film is shown by the marked increase in the slope of the isotherm.

At a certain maltenes:silica mass ratio (near 20:80) the amount of maltenes present may not be enough to create a liquid phase in the isotherm. In this case, there are an insufficient number of maltene molecules to fill in between the solid particles. Therefore, compression of the film only results in a surface pressure increase when silica particles reach a point of interaction. The maltene molecules can fit into the space between silica clusters or adsorb onto the silica particles so that not enough maltenes are present at the interface to increase the surface pressure at greater trough areas. For mixtures with higher maltenes content (30 wt% maltenes for example) a liquid phase is shown by the isotherm because there are sufficient maltene molecules to occupy more interfacial area than the interstitial area among the solid particles. These maltene molecules at the interface respond to increase the surface pressure.

AFM and SEM images reveal that clusters of silica particles are embedded in a film of maltenes. However, there are some interactions between the silica particles and maltenes. From comparison of Figures 5.16a) and 5.16b), it can be seen that the clusters of silica are smaller when the film contains maltenes. As well, in the mixed film the silica clusters form a network in the film with more area in between clusters than in the silica film (at the same surface pressure of 10 mN/m). The SEM images in Figures 5.18 and 5.19 show the difference in film structures at a lower magnification. AFM imaging of an area between the clusters, shown in Figure 5.17a) reveals that there are no large features in between the clusters. Because AFM imaging of a maltene film did not reveal any discernable features, it is likely that the area between silica clusters is filled with maltenes. Maltene adsorption on the silica particles decreased the effect of interparticle forces that caused the silica particles to flocculate. Also, the maltene film present at the interface would provide an increase in the viscosity of the interface and provide a barrier to the movement of particles at the interface. Vignati, Piazza, and Lockhart (2003) have shown that particles trapped at an oil-water interface are subject to Brownian motion when unhindered by interparticle interactions. The maltene-silica interactions are likely to be a hindrance to silica particle flocculation.

From Figure 5.3 when the isotherms are normalized by the mass of silica spread, the area occupied by the film increases as maltenes are added to silica. Figure 5.5 shows that the increase in area (positive ΔA) varies linearly with the amount of maltenes added to the mixture. This area shift is larger at lower surface pressure, i.e., the isotherm shifts more when in a liquid phase. The area shift is likely due to the increased amount of maltenes at the interface forming a more expanded film. At higher surface pressures the area shift shown in Figure 5.5 is smaller than that at lower pressures. The solid phase, which is dominated by silica, appears to have a limiting area/mass. In Figure 5.3 the curves of films with >20% maltenes all have the solid phase in nearly the same position but the initial liquid phase continues to shift to the right. The smaller silica clusters appearing in the maltene-silica mixtures provide an explanation for the positive area shift at higher pressures. Although the dry LB film may not be representative of the original Langmuir film, the clusters appear to be 3-dimensional (i.e. they extend away from the interface into the bulk phases) as shown by the cross-sectional profile of a cluster in Figure 5.21. The peak shown by the cross-sectional profile and the circular shape of the clusters in AFM images suggests the clusters are roughly spherical. With this shape, a smaller cluster would occupy more area per mass than a larger one. As the amount of maltenes added to the film increases, the silica clusters decrease in size and take up more area per mass.

In contrast, adding more silica to the maltene film does not increase the area/mass maltene occupied by the film as shown by the overlapping isotherms in Figure 5.4. Figure 5.6 shows that there is a negative area shift from an isotherm of a maltene film for isotherms of maltene-silica mixtures. As the amount of silica increases in a maltene film, the area/maltene that the film occupies decreases. This can be explained if the maltene molecules are assumed to adsorb on to the silica particles. As the concentration of particles is increased there is more area available for maltenes to adsorb to. Thus there will be less maltenes available to occupy area at the interface and the area/mass of maltenes decreases.

The silica particles are miscible with the maltenes and films formed by the mixtures of the components share features of films of the individual components. The interactions between the silica and maltene films cause the film to become more expanded at higher surface pressures as the silica clusters occupy more area per mass. Silica makes the films of maltenes more rigid or less compressible shown by the changes in slope of Figure 5.4 and the compressibility curves in Figure 5.14. A decrease in the compressibility relates to an increase in mechanical strength of the film caused by the silica clusters embedded in the maltene films.

5.6.3 Asphaltene-Silica Mixtures

There are similarities in the behaviour of asphaltene-silica mixtures and maltene-silica mixtures. There is evidence that at the interface some mixing between the components occurs. In Appendix D further analysis of the mixtures shows that both the maltene-silica and asphaltene-silica mixtures behave as non-ideal mixtures. Results from section 5.3 also demonstrate that maltenes and asphaltenes are mixed with silica at the interface. Maltene-silica mixture isotherms are markedly different than the two single component isotherms and are combination of the two isotherms. However, because the isotherms from films of asphaltenes alone and silica alone are similar, the isotherm of the asphaltene-silica mixtures is also similar. Compressibility of a silica film is close to that of an asphaltenes film, and the shape of two isotherms is very similar.

As with the maltene-silica mixtures, increasing the amount of asphaltenes in the film causes the silica in the film to occupy more area per mass. AFM and SEM images show that asphaltenes make the silica clusters even smaller than maltenes. The asphaltenes also cause the silica clusters to separate, most of the silica clusters appearing in Figure 5.20 are not networked together as in Figure 5.19. The silica particles appear to adsorb some asphaltenes, which is shown by the negative area shifts in Figure 5.10. Values of the collapse pressure for the asphaltene-silica mixtures are between the collapse pressures of asphaltenes and silica. The collapse pressure is composition dependant but no trend can be observed. The pressure values are closer to the collapse pressure of asphaltenes, indicating that the collapse pressure of the mixtures is more dependent on asphaltenes in the film. There is little increase in the mechanical strength of the film with the addition of silica. However, addition of silica does decrease the film rigidity somewhat, since the slope of the isotherm and the compressibility of the film are lower for the mixtures than for an single component asphaltene film. AFM images show that the silica structures are much larger than the asphaltene structures in the film. The film areas between the silica clusters are filled with asphaltenes shown by the lower height structures in Figure 5.17b).

5.6.4 Maltene–Asphaltene Mixtures

Comparison of Figure 5.3 and Figure 5.12 shows that there are similarities between a maltene-asphaltene film and a maltene-silica film. The isotherms of the mixed films appear to be a combination of the isotherms of single component films. Maltenes create a more compressible liquid phase signified by a less steep slope. The asphaltenes (or silica particles) on the other hand, create a less compressible solid phase where the curve has a much steeper slope. As with the other mixtures, the phase transition in maltene-asphaltene films is gradual. The transition pressure decreases with increasing asphaltene (or silica) content. At a certain maltenes:asphaltenes ratio (near 70:30) the amount of maltene present is not sufficient to noticeably change the liquid phase that occurs for an asphaltene film. As such, no transition point can be determined. From Figure 5.13, the maltenes and asphaltenes are miscible and appear to form an ideal mixture. However, because of the appearance of two separate phases in the mixture isotherms the components may only be partially miscible. In this situation the film may be composed of asphaltene aggregates embedded in a film of maltenes, as in the case with maltene-silica mixtures. There is some miscibility between the two components because the collapse pressure is composition dependent. The interactions between maltenes and silica appear to be similar to those between maltenes and asphaltenes.

Since both fumed silica nanoparticles (Yan et al., 2001) and asphaltenes (Yan et al., 1999) can stabilize water-in-oil emulsions, it is not surprising to note that the film behaviour of the two substances is similar. What is of interest is to consider that asphaltene molecules are behaving as solid particles. Zhang, Xu and Masliyah (2005) have shown that asphaltenes contribute to an adsorbed Langmuir film at an oil-water interface in the form of particulate aggregates. Evidence presented here supports the similarities between fine solid particles and asphaltenes at air-water interface.

Midmore (1998) used a costabilizer and colloidal silica to create a stable oil-in-water emulsion with incomplete drop coverage by particles. Also recent studies have shown that solid particles can prevent droplets from coalescing with low surface coverage (Stancik, Koukhan and Fuller, 2004; Vignati et al., 2003). For the Langmuir films studied clusters formed by the silica at air-water interface do completely cover the interface. When mixed with asphaltenes or maltenes the silica clusters are separated and evenly dispersed across the interface, and the interface is still completely covered with a mixture of asphaltene-silica or maltene-silica. This could mean that fine particles would enhance the stability of an emulsion by increasing the mechanical strength of the interfacial film as they are evenly dispersed across the interface.

5.7 Conclusions

Interfacial behaviour of mixtures of silica with maltenes and silica with asphaltenes obtained from Athabasca vacuum feed bitumen was studied using a Langmuir trough. For hydrophobic fumed silica the aggregation of primary particles and irregular shapes did not prevent a surface pressure-area isotherm from being obtained. The fumed silica film had a surface pressure-area isotherm similar to that of other solid particles studied on a Langmuir trough. Deasphalted bitumen was able to form a monolayer at the air-water interface, showing that there are surface-active components present in bitumen even when asphaltenes have been removed. The film of maltenes was much more compressible than films of fumed silica and asphaltenes. All films containing silica formed silica clusters and the maltenes and asphaltenes reduced the size of these clusters. Silica clusters in maltene-silica films formed a network and clusters in asphaltene-silica films were evenly dispersed in the film. Many similarities in behaviour of the films containing asphaltenes and films containing fumed silica nanoparticles were observed. The isotherms of asphaltenes and silica were both rigid and when mixed with maltenes similarities in the isotherms, such as the appearance of a liquid phase, exist. The state of asphaltenes in molecular aggregates is likely responsible for the observed similarities.

5.8 References

Binks, B.P., Clint J.H., Dyab, A.K.F., Fletcher, P.D.I., Kirkland, M., Whitby, C.P. *Ellipsometric studies of monodisperse silica particles at an oil-water interface*, Langmuir, 19(21):8888-8893, 2003

Binks, B.P., Kirkland, M., *Interfacial structure of solid-stabilised emulsions studied by scanning electron microscopy*, Physical Chemistry Chemical Physics, 4(15):3727-3733, 2002.

Binks, B.P., Lumsdon, S.O., *Stability of oil-in-water emulsions stabilised by silica particles*, Physical Chemistry Chemical Physics, 1(12):3007-3016, 1999.

Binks, B.P., *Particles as surfactants - similarities and differences*, Current Opinion in Colloid and Interface Science, 7:21-41, 2002

Chen, F., Finch, J.A., Xu, Z., Czarnecki, J., *Wettability of fine solids extracted from bitumen froth*, Journal of Adhesion Science Technology, 13(10):1209-1224, 1999.

Degussa AG, *Special Hydrophobic Aerosil® (SHA) for Toners*, Technical Information TI 1222, Nippon Aerosil Co, 2001.

Degussa AG, *Technical Bulletin Fine Particles Number 11*, Aerosil & Silanes, Degussa AG, 2003.

Ese, M.-H., Yang, X., Sjöblom, J., *Film forming properties of asphaltenes and resins. A comparative Langmuir-Blodgett study of crude oils from North Sea, European continent and Venezuela*, Colloid and Polymer Science, 276(9):800-809, 1998.

Gaines, G. L., *Insoluble monolayers at liquid-gas interfaces*, New York, Interscience Publishers 1966.

Ghezzi, F., Earnshaw, J.C., Finnis, M., McCluney, M., *Pattern formation in colloidal monolayers at the air-water interface*, Journal of Colloid and Interface Science, 238(2):433-446, 2001.

Horozov, T.S., Aveyard, R., Clint, J.H., Binks, B.P., *Order-Disorder transition in monolayers of modified monodisperse silica particles at the octane-water interface*, Langmuir, 19(7):2822-2829, 2003.

Hórvölgyi, Z., Németh, S., Fendler, J.H., *Monoparticulate layers of silanized glass spheres at the water-air interface: particle-particle and particle-subphase interactions*, Langmuir, 12(4):997-1004, 1996.

Lawrence, S., Zhang, L.Y., Xu, Z., Masliyah, J.H., *Langmuir and Langmuir-Blodgett asphaltene films at heptane-water interface,* Canadian Journal of Chemical Engineering, 82(4), 821-828, 2004

Maté, M., Fendler, J.H., Ramsden, J.J., Szalma, J., Hórvölgyi, Z., *Eliminating surface pressure gradient effects in contact angle determination of nano- and microparticles using a film balance*, Langmuir, 14(22):6501-6504, 1998.

Mohammed, R.A., Bailey, A.I., Luckham, P.F., Taylor, S.E., *Dewatering of crude oil emulsions 2. Interfacial properties of the asphaltic constituents of crude oil*, Colloids and Surfaces A: Physicochemical and Engineering Aspects, 80(2-3):237-242, 1993.

Pickering, S.U., *Emulsions*, Journal of the Chemical Society, 91:2001-2021, 1907.

Pogorzelski, S.J., *Structural and thermodynamic characteristics of natural marine films derived from force-area studies*, Colloids and Surfaces A-Physicochemical and Engineering Aspects, 189 (1-3):163-176, 2001.

Ramsden, W., *Separation of solids in the surface-layers of solutions and 'suspensions' (observations on surface-membranes, bubbles, emulsions, and mechanical coagulation). -- Preliminary account*, Proceedings of the Royal Society of London, 72:156-164, 1903.

Sheppard, E., Tcheurekdjian, N., *Monolayer studies IV. Surface films of emulsion latex particles*, Journal of Colloid and Interface Science, 28(3-4):481-486, 1968.

Stancik, E.J., Koukhan, M., Fuller, G.G., *Coalescence of particle-laden fluid interfaces*, Langmuir, 20 (1):90-94, 2004.

Stine, K.J., Moore, B.G., *Langmuir monolayers: Fundamentals and relevance to nanotechnology*, In M. Rosoff (Ed.), Nano-Surface Chemistry. New York, Marcel Dekker, pp. 59-140, 2002.

Vignati, E., Piazza, R., Lockhart, T.P., *Pickering emulsions: Interfacial tension, colloidal layer morphology, and trapped-particle motion*, Langmuir, 19(17):6650-6656, 2003.

Yan, N.X., Gray, M.R., Masliyah, J.H., *On water-in-oil emulsions stabilized by fine solids*, Colloids and Surfaces A: Physicochemical and Engineering Aspects, 193(1-3):97-107, 2001.

Yan, N.X., Maham, Y., Masliyah, J.H., Gray, M.R., Mather, A.E., *Measurement of contact angles for fumed silica nanospheres using enthalpy of immersion data*, Journal of Colloid and Interface Science, 22:1-6, 2000.

Yan, N.X., Masliyah, J.H., *Characterization and demulsification of solids-stabilized oil-in-water emulsions part 2. Demulsification by addition of fresh oil*, Colloids and Surfaces A: Physicochemical and Engineering Aspects, 96(3):243-252, 1995.

Yan, Z.L., Elliott, J.A.W, Masliyah, J.H., *Roles of various bitumen components in the stability of water-in-diluted-bitumen emulsions*, Journal of Colloid and Interface Science, 220(2):329-337, 1999.

Zhang, L.Y., Lawrence, S., Xu, Z., Masliyah, J.H., *Studies of Athabasca asphaltene Langmuir films at air-water interface*, Journal of Colloid and Interface Science, 264(1):128-140, 2003.

Zhang, L.Y., Xu, Z., Masliyah, J.H., *Characterization of adsorbed Athabasca asphaltene films at solvent-water interfaces using a Langmuir interfacial trough*, Industrial & Engineering Chemistry Research, 44(5):1160-1174, 2005.

5.9 Figures

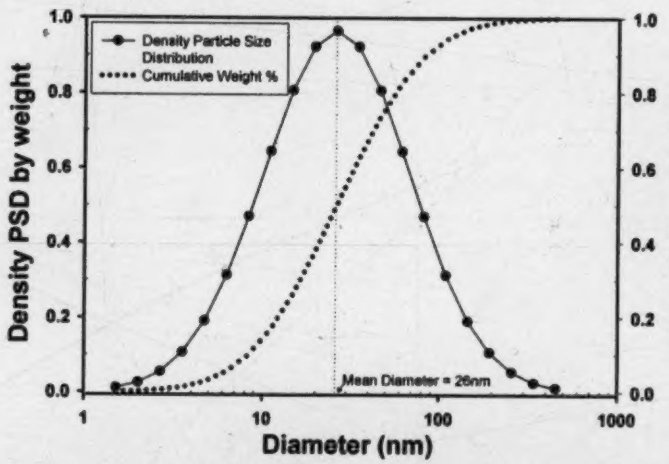

Figure 5.1: Density particle size distribution, on weight basis, of R974 hydrophobic silica nanoparticles in toluene (1.05 wt%) measured with an acoustic spectrometer device.

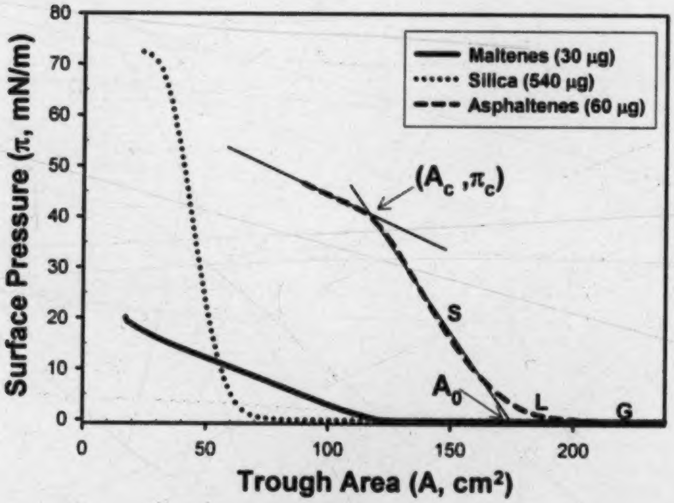

Figure 5.2: Surface pressure-area isotherms of silica nanoparticles, maltenes and asphaltenes.

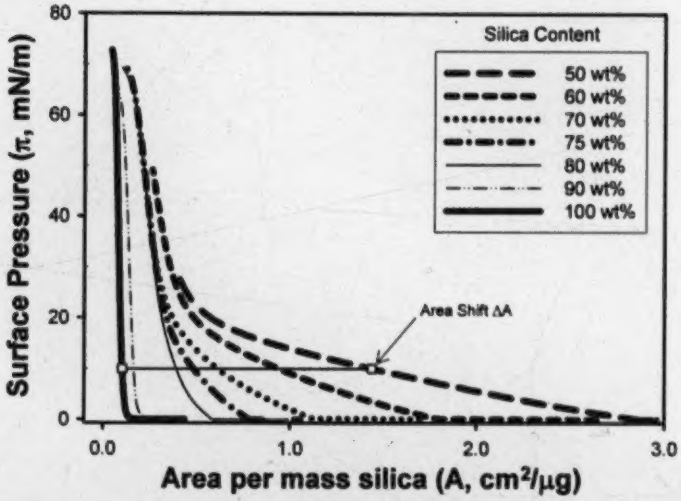

Figure 5.3: Surface pressure-area isotherms of films from maltene and silica mixtures of varying ratios of maltenes:silica. Isotherms are normalized by the mass of silica at the interface.

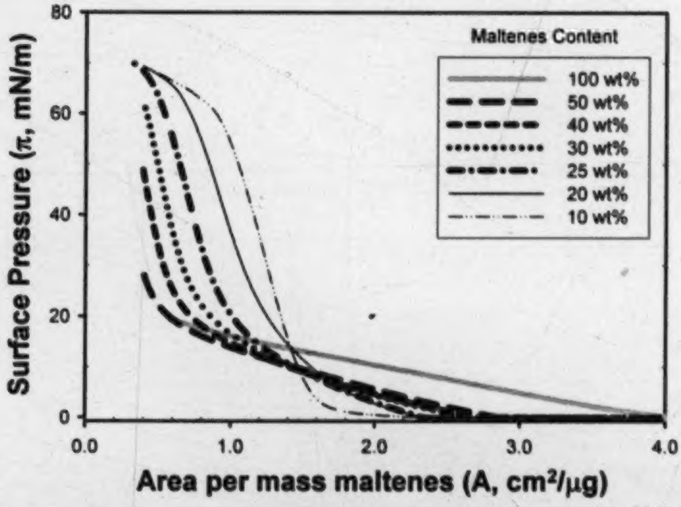

Figure 5.4: Surface pressure-area isotherms of films from maltene and silica mixtures of varying ratios of maltenes:silica. Isotherms are normalized by the mass of maltenes at the interface.

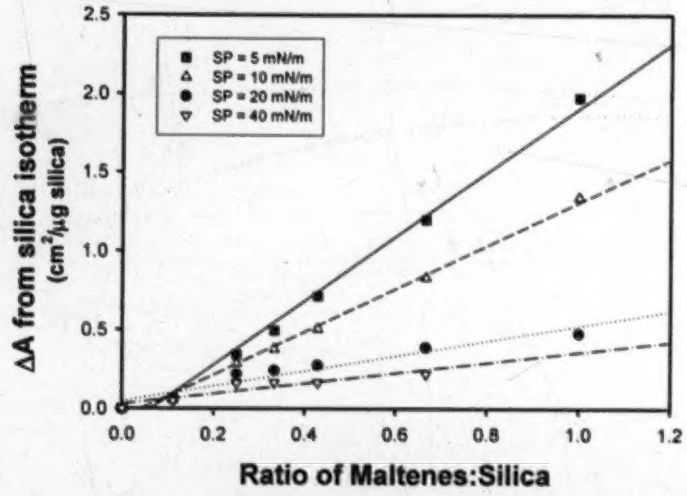

Figure 5.5: Area shift from the isotherm of a silica film for maltene-silica mixtures. At various surface pressures plotted against the ratio of silica:maltenes.

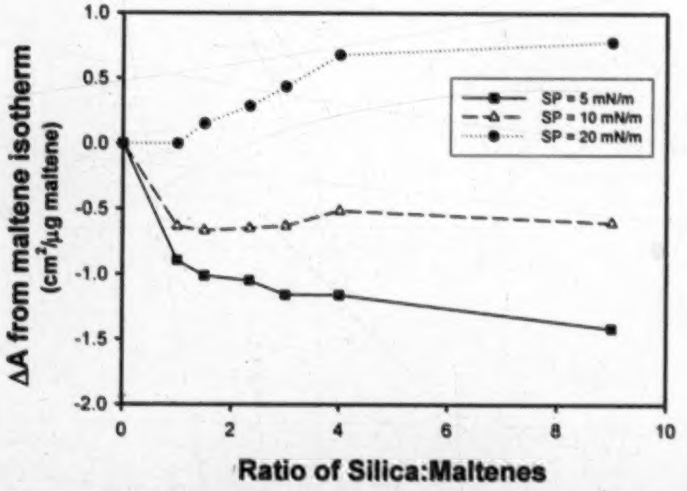

Figure 5.6: Area shift from the isotherm of a maltene film for maltene-silica mixtures. At various surface pressures plotted against the ratio of maltenes:silica.

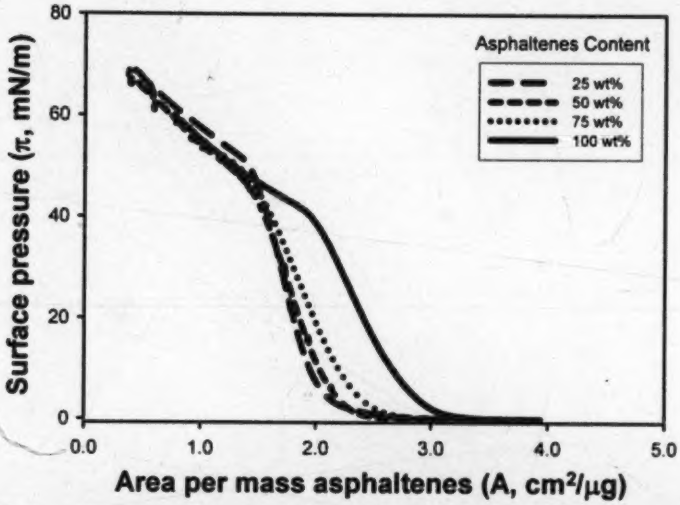

Figure 5.7: Surface pressure-area isotherms of films from asphaltenes and silica mixtures of varying ratios of asphaltenes:silica. Isotherms are normalized by the mass of asphaltenes at the interface.

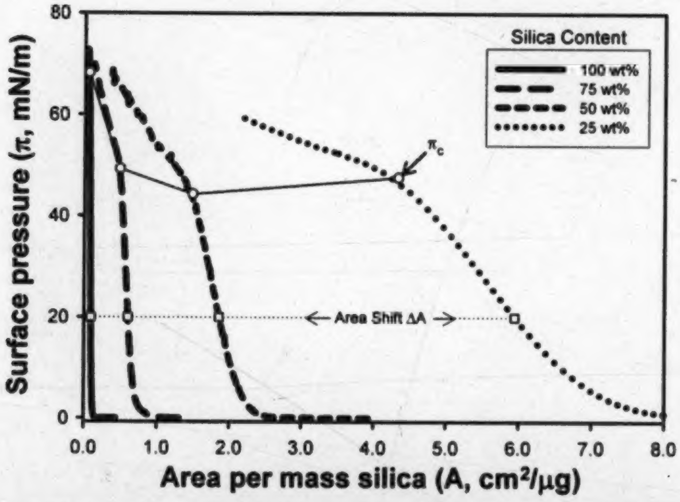

Figure 5.8: Surface pressure-area isotherms of films from asphaltenes and silica mixtures of varying ratios of asphaltenes:silica. Isotherms are normalized by the mass of silica at the interface. Collapse points are enlarged.

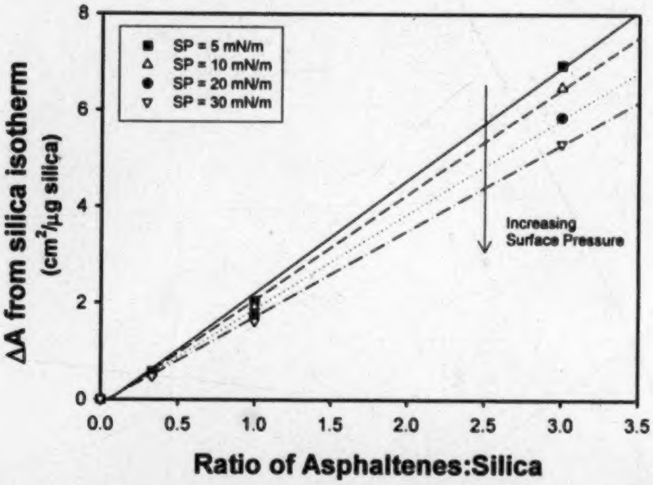

Figure 5.9: Area shift from the isotherm of a silica film for asphaltene and silica mixtures. At various surface pressures plotted against the ratio of asphaltenes:silica.

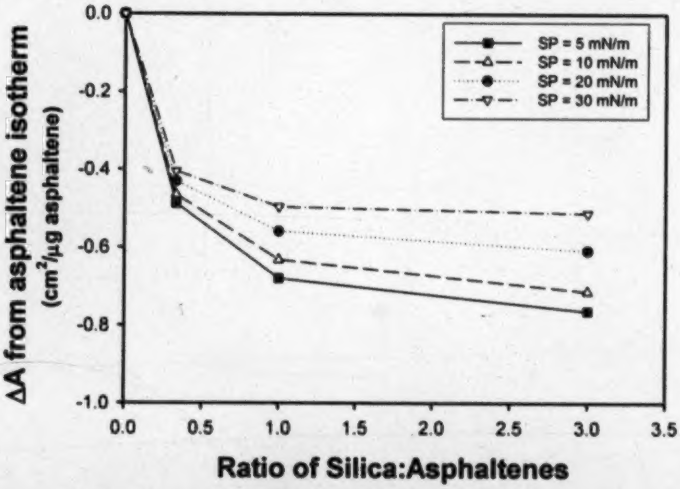

Figure 5.10: Area shift from the isotherm of an asphaltene film for asphaltene and silica mixtures. At various surface pressures plotted against the ratio of silica:asphaltenes.

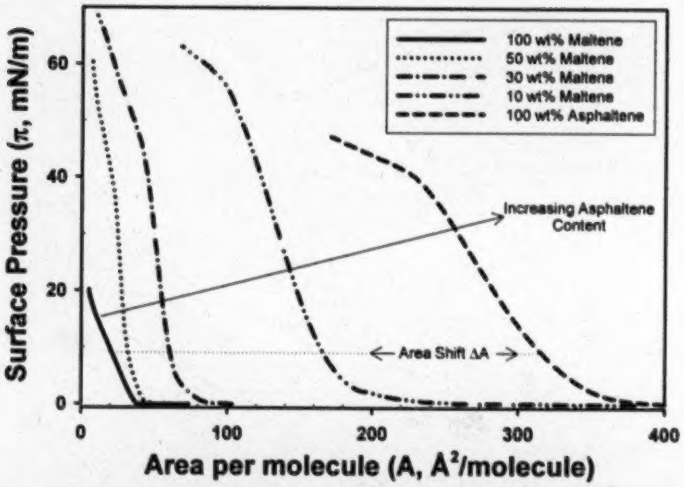

Figure 5.11: Surface pressure-area isotherms of films from asphaltenes and maltenes mixtures of varying ratios of asphaltenes:maltenes. Isotherms are normalized by the number of molecules at the interface.

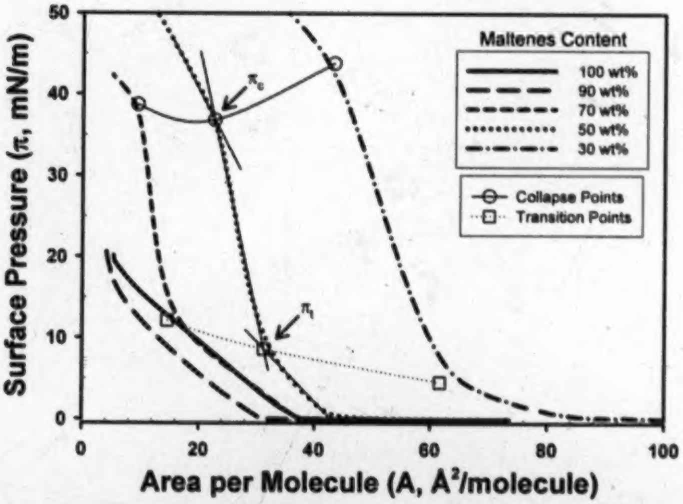

Figure 5.12: Surface pressure-area isotherms of films from asphaltenes and maltenes mixtures at lower area per molecule range than Figure 5.11. Estimated transition and collapse points are highlighted.

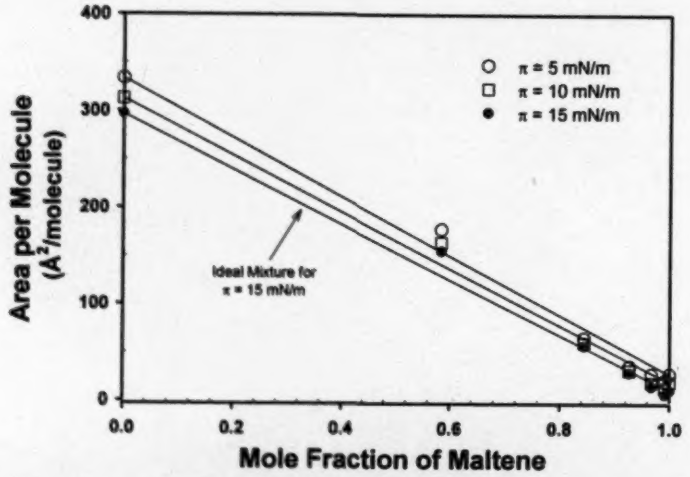

Figure 5.13: Area per molecule of maltene-asphaltene mixtures at 5, 10 and 15 mN/m surface pressures plotted as a function of mole fraction of maltene.

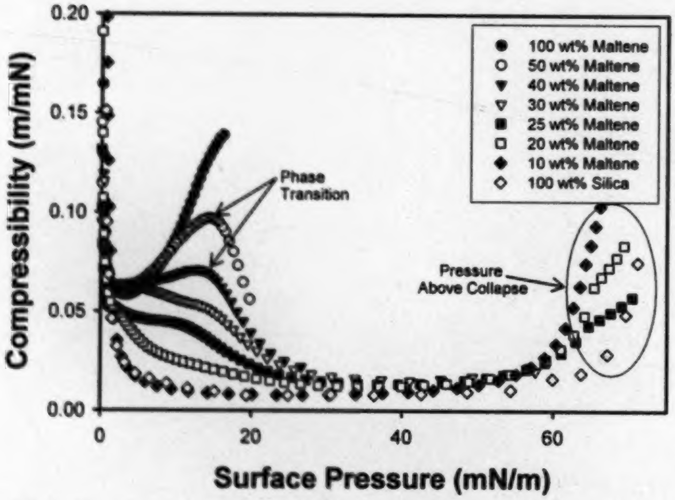

Figure 5.14: Compressibility of films formed from maltene-silica mixtures.

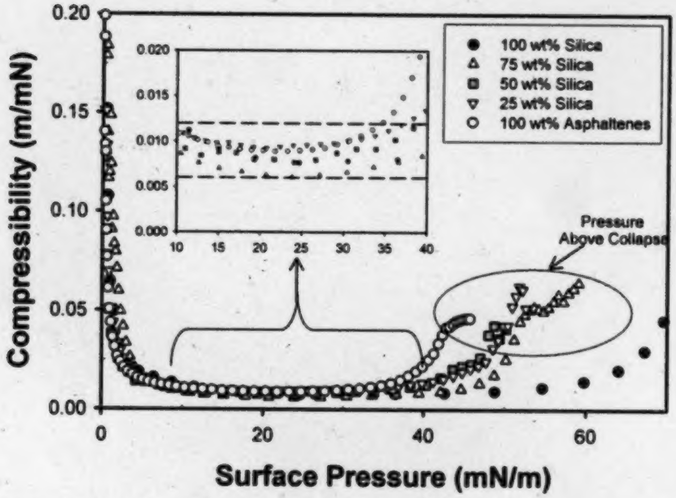

Figure 5.15: Compressibility of films formed from asphaltene-silica mixtures.

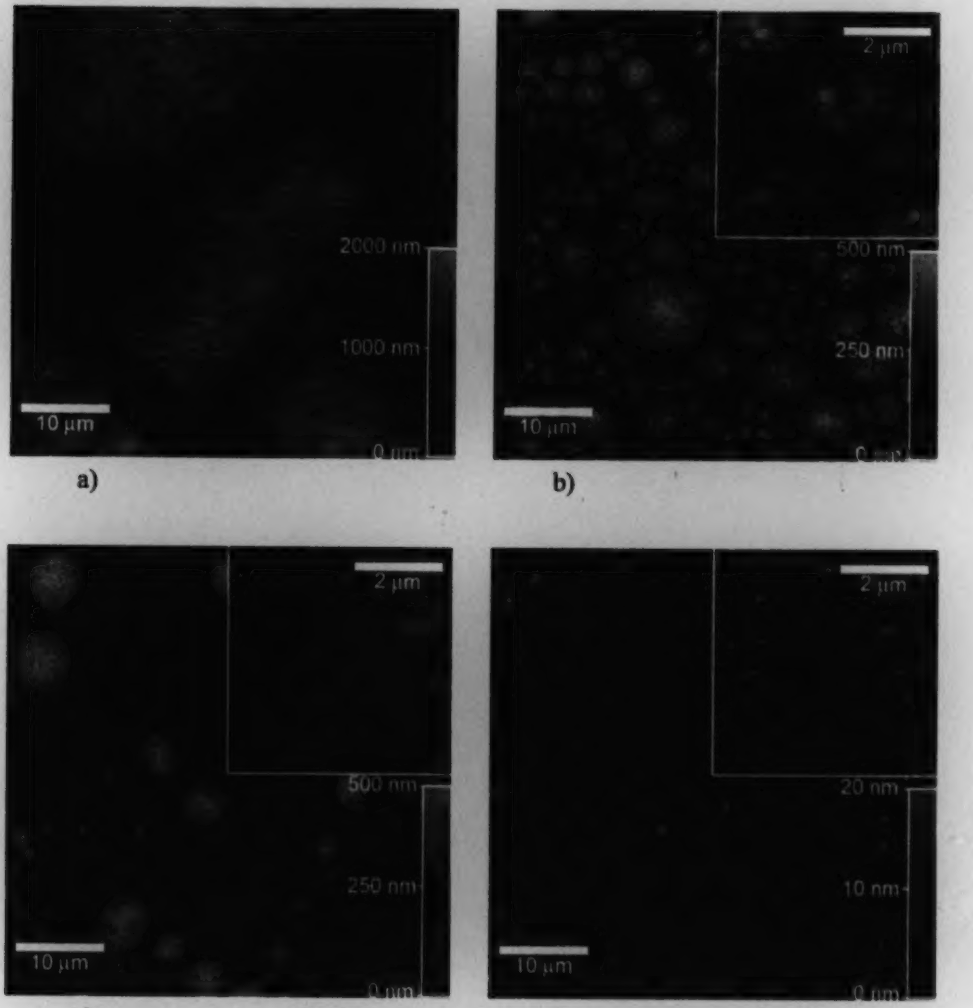

a) b) c) d)

Figure 5.16: AFM images of single layer LB films deposited on to silicon wafers from air-water interface. Surface pressure at deposit, $\pi_{deposit}$ = 10 mN/m. a) Silica only TR=0.51, b) 50 wt % maltene – 50 wt% silica mixture TR = 1.39 c) 50 wt % asphaltene – 50 wt% silica mixture TR = 2.46 d) Asphaltene only TR =0.57

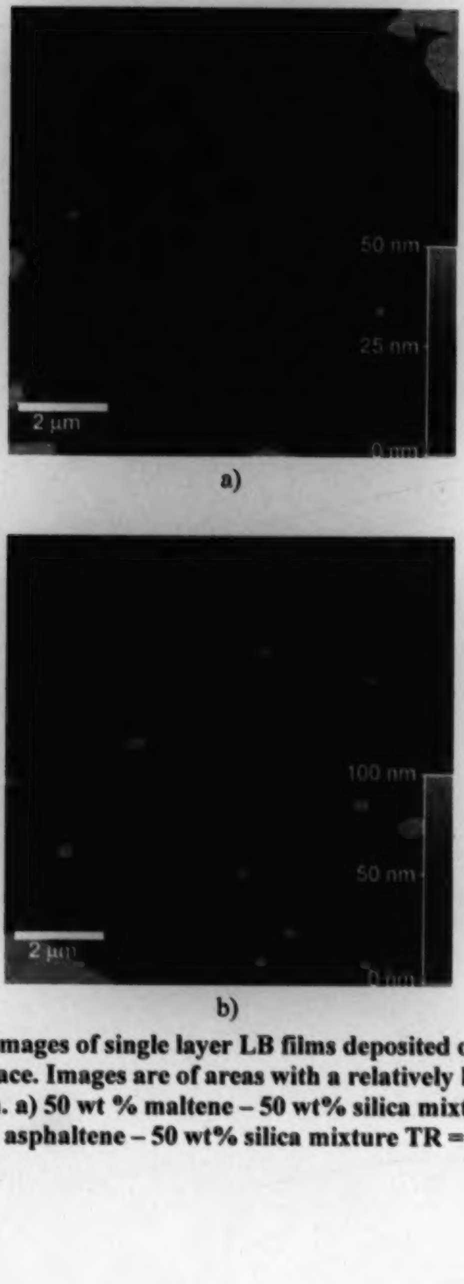

Figure 5.17: AFM images of single layer LB films deposited on to silicon wafers from air-water interface. Images are of areas with a relatively low height compared to the rest of the film. a) 50 wt % maltene – 50 wt% silica mixture TR = 1.39 b) 50 wt % asphaltene – 50 wt% silica mixture TR = 2.46

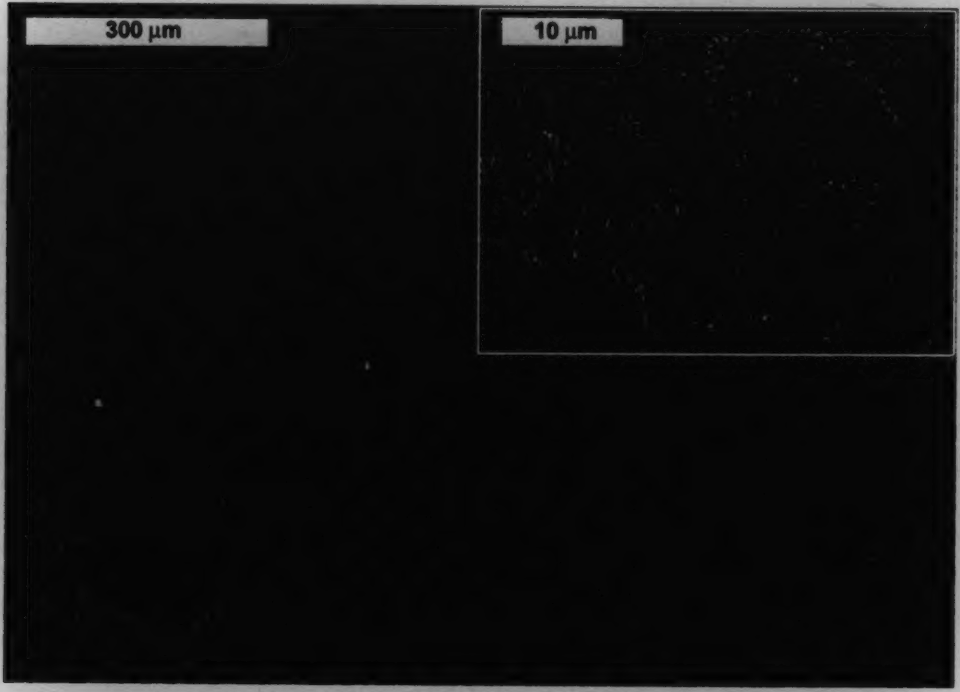

Figure 5.18: SEM images of single layer LB film of silica deposited onto silicon wafers from air-water interface. Inset image shows same film at higher magnification. Surface pressure at deposit, $\pi_{deposit}$ = 10 mN/m. Film was coated with carbon to enable SEM imaging.

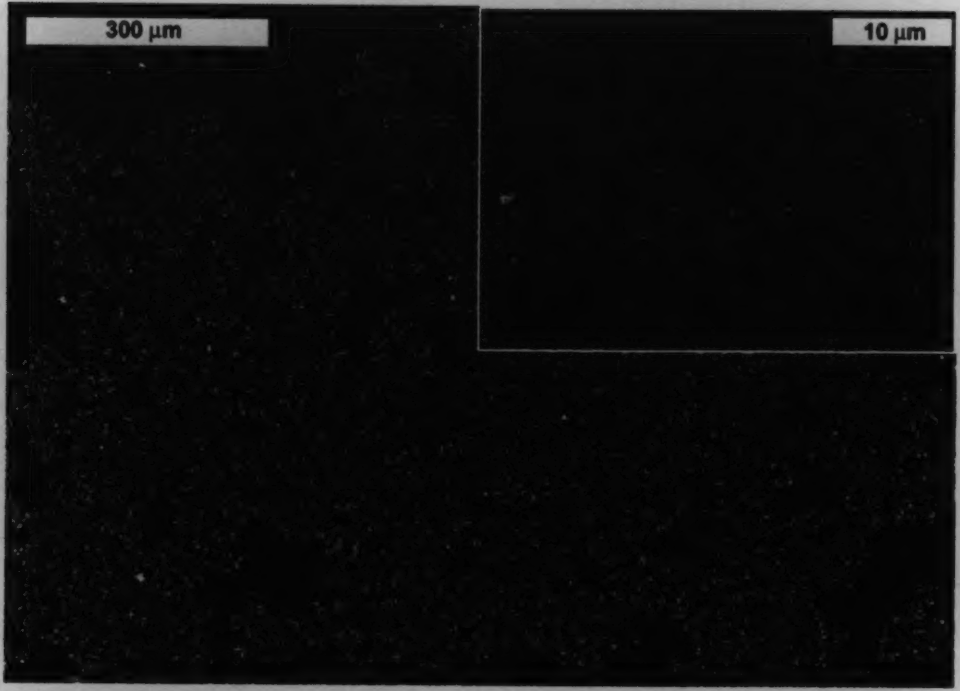

Figure 5.19: SEM images of single layer LB film of 50 wt% silica –50 wt% maltene deposited onto silicon wafers from air-water interface. Inset image shows same film at higher magnification. Surface pressure at deposit, $\pi_{deposit}$ = 10 mN/m. Film was coated with carbon to enable SEM imaging.

Figure 5.20: SEM images of single layer LB film of 50 wt% silica –50 wt% asphaltene deposited onto silicon wafers from air-water interface. Inset image shows same film at higher magnification. Surface pressure at deposit, $\pi_{deposit}$ = 10 mN/m. Film was coated with carbon to enable SEM imaging.

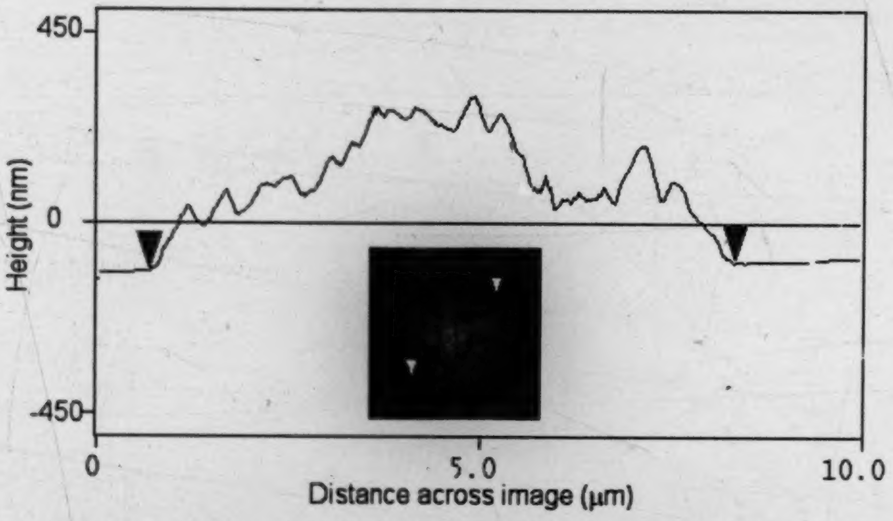

Figure 5.21: Height along cross section of an AFM image for a silica cluster. Inset AFM image from LB film of 50 wt% silica –50 wt% asphaltene mixture.

"Of course there's a lot of knowledge in universities: the freshmen bring a little in; the seniors don't take much away, so knowledge sort of accumulate..."
-A. Lawrence Lowell

6

Nanoparticles, Deasphalted Bitumen, Asphaltenes and Their Mixtures at Toluene-Water Interface

6.1 Introduction

Traditionally, only films formed at an air-water interface were considered as Langmuir films. However, for many applications, including emulsions research, investigating films at a liquid-liquid interface is more beneficial. Recent developments in Langmuir trough design have allowed for the study of films at oil-water interfaces. As described in Chapter 4, the KSV interfacial trough used for experiments in this thesis is equipped with an interfacial trough. This chapter presents results for Langmuir trough and deposition experiments that were conducted at a toluene-water interface. Procedures to obtain these results were described in Chapter 3. Discussions in this chapter focus on comparing the results obtained with unmixed maltenes, asphaltenes and silica, and various mixtures of these substances at toluene-water interfaces.

Results discussed in this chapter are more applicable to industrial bitumen processes than those in Chapter 5 because it is asphaltenes, fine particles and other species at oil-water interfaces that stabilize water-in-diluted bitumen emulsions. Thus, studying silica nanoparticles, asphaltenes and deasphalted bitumen at a toluene-water interface is more likely to lead to insights of these substances behaviour in emulsion systems.

6.2 Results

Results are presented in two sections; those obtained from Langmuir films, including interfacial-pressure area isotherms and compressibility, and those obtained from Langmuir-Blodgett films, including Atomic Force Microscope (AFM) and Scanning Electron Microscope (SEM) images. Results were obtained with the procedures described in Chapter 3. Experiments were conducted at a temperature of 20 °C and water of pH=5.8 was used. Mixtures used were the same as those used for experiments at an air-water interface. Concentrations and composition of the mixtures are outlined in Table 3.4. Fewer mixtures were used at the toluene-water interface. The typical mass of maltenes, asphaltenes and silica at the interface, for the single component films and those mixed films studied, are given in Tables 3.5 and 3.6.

6.2.1 Pressure-area Isotherms and Compressibility

Single Component films

Hydrophobic silica nanoparticles (AEROSIL® R974 fumed silica), asphaltenes and maltenes were studied individually with the Langmuir trough. Shown in Figure 6.1 are the interfacial pressure-area (π-a) isotherms for films of each substance. The isotherms have been normalized by the mass of material at the interface in order to aid comparison of the isotherms. As for the air-water interface, the isotherm for silica is at the lowest area per mass and asphaltenes are at the highest area per mass. At a toluene-water interface the films of asphaltenes can be compressed to relatively high interfacial pressures of approximately 30 mN/m without collapse. This finding indicates that the interfacial tension of the toluene-water interface has been decreased to values close to zero, since the interfacial tension of a pure water-toluene interface is 36.1 mN/m at 25 °C (Washburn, 2003). In contrast, the measured isotherm for the maltene film shows that the maltene film could not be compressed to pressures above 7 mN/m on the equipment available. Comparison of isotherm slopes shows that the silica and asphaltene films have a steeper slope and are thus less compressible than the maltene films. Compressibility was calculated using the method discussed in Appendix B, and comparisons of compressibility are made for mixtures later.

Collapse was only observed for the silica film. It is evident in the isotherm by a sharp change in slope at an interfacial pressure of approximately 23 mN/m, a pressure determined from fitting straight lines to the different sections in the isotherm as shown in Figure 6.2. In addition, the white creases in the film were visually observed through the toluene supraphase. Asphaltene and maltene films could not be compressed to a small enough area to induce film collapse on the KSV minitrough. After the first increase in interfacial pressure, the maltene film is compressed to where the reduction in area is 85% but the film does not collapse. In contrast, the silica film collapses after compression to only 64% of the area where the interfacial pressure first increases.

Maltene silica mixtures

To investigate the film behaviour of maltene-silica mixtures two different mixtures were used on the Langmuir trough in compression experiments. The interfacial pressure-area isotherms for the mixtures are presented in Figures 6.2 and 6.4, in comparison with the isotherms of single component silica and maltene films, respectively.

In Figure 6.2 the isotherms are plotted in terms of interfacial pressure vs. the mass of silica present at the interface. These isotherms show the effect of maltene addition on the properties of a silica film. The isotherms obtained for maltene-silica mixtures are to the right of the isotherm of silica alone. The shapes of the three isotherms are nearly identical except that the appearance of a new region in the isotherms of the mixed films is noticeable. Between areas of 1cm^2/μg to 0.4 cm^2/μg there is a gradual increase in interfacial pressure before the pressure increases almost vertically as for a silica film. A similar change was observed in the isotherm of fine particles when a sodium dodecyl sulphate (SDS) surfactant was added to the water subphase (Aveyard et al., 1994). Aveyard et al. (1994) used the term "tail" to describe this isotherm characteristic. The mixture composed of 50 wt% maltenes and 50 wt% silica did not collapse, and the mixture containing 75 wt% silica collapsed at a pressure of 29 mN/m. As with the single component silica film, the collapse was visually observed with the appearance of creases in the film.

The change in isotherm position due to the addition of various amounts of maltene is further explored in Figure 6.3. The area shift (ΔA) of each mixture from the isotherm of a single component silica film was calculated at several interfacial pressures. The calculation of area shift for the 25 wt% maltenes mixture at a surface pressure of 10 mN/m is shown schematically in Figure 6.2. The results of the area shift vs. the maltenes:silica ratio are shown in Figure 6.3. Because the area has been normalized by the mass of silica, the ratio of maltenes:silica also represents the amount of maltenes added to a given amount of silica. The area shift from an isotherm of a silica film does not increase linearly with increasing maltenes:silica ratio. For a given maltenes:silica ratio, magnitudes of ΔA decrease with increasing interfacial pressure.

In Figure 6.4 the area measurements made for the π-a isotherms have been divided by the mass of maltenes at the interface. In this way, a comparison between the mixtures is made on the basis of the amount of maltenes. As shown in Figure 6.4, the maltene isotherm has a much less steep slope compared to the two mixtures. Isotherms of the two mixtures are of similar shape as the isotherm of single component silica. A position change is observed in the isotherms of maltene-silica mixtures as the amount of silica is increased. The initial increase in interfacial pressure occurs at a greater area for the isotherm of the 75 wt% silica mixture.

In Figure 6.5 the area shift (on the basis of area per mass maltenes) from the isotehrm of maltene alone is plotted against the maltenes:silica ratio in each of the mixtures. Area shifts were calculated at interfacial pressures of 1 and 5 mN/m. The figure shows that an increase of silica content in the mixture initially causes a negative area shift (i.e. the isotherms shift to the left). As the ratio of silica:maltenes increases further, the area shift becomes less negative (i.e. the isotherms shift to the right).

Figure 6.6 shows a comparison of the calculated compressibility curves for maltene, silica and maltene-silica films. The film of maltene alone has a higher compressibility than films of the mixtures and silica alone. For the most part the compressibilities of maltene-silica mixtures are similar to that for a single component silica film. A slight increase in compressibility occurs at lower surface pressures towards the "tail" in the π-a isotherms for the maltene-silica films.

Asphaltene silica mixtures

Three mixtures of varying composition were made with asphaltenes and silica nanoparticles. For the three mixtures, the weight percent of asphaltenes was 25%, 50% and 75%. Interfacial pressure–area isotherms were measured for each of the films in order to compare the isotherms with that of silica and asphaltenes alone. Figure 6.7 shows the π-a isotherms measured for each mixture and single component asphaltenes with the trough area divided by the mass of asphaltenes spread at the interface. Such comparison emphasizes the effect of adding silica to a film of asphaltenes. The isotherm of the asphaltene film is the farthest right on the graph. Isotherms for the asphaltene-silica mixtures are at a lower area per mass than the asphaltene film. The area shift from the isotherm of the asphaltene film is shown in Figure 6.8. For all the silica:asphaltene ratios there is a negative area shift from the asphaltene isotherm. When the mixture contains 25 wt% silica, the shape of the isotherm is almost identical to that of a film of 100 wt% asphaltene. As the amount of silica is increased to 50 wt% and 75 wt%, the isotherm becomes steeper, but only a marginal change in the isotherm position occurs. This result shows that mixed films with a higher mass fraction of silica are less compressible (more rigid) than mixed films with lower mass fraction of silica. To further refine this comparison, compressibility of the mixed films was calculated, and plotted against the interfacial pressure in Figure 6.11. Silica shows the least compressibility. The film containing 75 wt% asphaltene is more compressible than the film of asphaltenes. Other mixtures are less compressible than the asphaltene film. Overall, there is no real trend in compressibility.

When the mass ratio of asphaltenes:silica was greater than one, no collapse was observed within the pressure investigated, but it is possible that the films would collapse at higher interfacial pressures if the films were compressed to smaller areas. The asphaltene film had the highest attainable interfacial pressure of 31 mN/m. Mixed films with silica content greater than 50wt% were observed to collapse, at interfacial pressures near the highest attained by an asphaltene film. A film of 50wt% silica collapsed at 31mN/m and a film of 75wt% silica collapsed at 30mN/m. These collapse pressures are greater than the collapse pressure of the single component silica film (π_c=23mN/m).

Figure 6.9 shows the same π-a isotherms measured for the asphaltene-silica mixtures but the abscissa is the area per mass of silica at the interface. These curves represent the isotherms of asphaltene-silica mixtures with a fixed amount of silica. As the amount of asphaltenes present in the film increases (wt% asphaltenes increases) the isotherms shift to the right, indicating that the film occupies more area at a given pressure. This is to be expected as the film contains more material. However, the shift in area caused by the addition of asphaltenes is more pronounced at lower interfacial pressures. Area shifts (schematic shown in Figure 6.9) from the isotherms of the silica film were calculated for each of the mixtures. Area shifts (in area per mass asphaltenes) are plotted against the ratio of silica:asphaltenes in Figure 6.10. Isotherms in Figure 6.9 also show the same change in slope as observed in Figure 6.7. As the amount of asphaltenes in the film increases the slope of the isotherms decreases.

Maltene-Asphaltene mixtures

Interfacial films of maltene-asphaltene mixtures were prepared from three mixtures with maltene contents of 30 wt%, 50 wt% and 70 wt%, respectively. The pressure-area isotherms obtained from compression of these interfacial films are compared with the isotherm from an asphaltene film in Figure 6.12. In this figure, the measured area has been normalized by the mass of asphaltenes present at the interface. The figure shows that the isotherms obtained from the mixed films are nearly the same as the isotherm of the asphaltene film. The maltene-asphaltene mixtures appear to produce a "tail" in the isotherm similar to that in the maltene-silica mixtures. However, the variation from the isotherm of asphaltene alone is not significant. Furthermore, there is even less variation amongst the isotherms of the three maltene-asphaltene mixtures. This is likely because maltene molecules have moved from the interface to the bulk toluene and the amount left at the interface is not large enough to influence the film behaviour. No further analysis of the mixed isotherms is shown here. Normalizing the isotherms by the mass of maltenes at the interface and determining the area shift from single component isotherms did not reveal any significant results for discussion. Because the presence of maltenes at the interface did not significantly change the isotherms, analysis of the maltene-asphaltene monolayer is equivalent to analysing a mixture of asphaltenes and a non-existent film. For example, the additive rule $A_{12} = (X_1A_1+X_2A_2)$ will always be satisfied when A_2 equals zero.

6.2.2 SEM and AFM images of LB films:

Single layer depositions of the Langmuir films were made onto hydrophilic silicon wafers. The LB films were then imaged using atomic force microscopy (AFM) and scanning electron microscopy (SEM). In order to aid SEM imaging, the deposited films were carbon coated to make the film surface conductive. Coating also produced better AFM images because the lateral force of the AFM cantilever tip easily displaced the silica particles in uncoated films. Significant displacement did not occur with the coated films. All Langmuir-Blodgett depositions were performed at 10 mN/m except for the maltene film, which could not be compressed to an interfacial pressure greater than 5 mN/m. The deposition of the maltene film was performed at 3 mN/m. Transfer ratios of all films were greater than one except for the silica film, which had a much lower transfer ratio of 0.21.

SEM images of the films containing silica are shown in Figures 6.13, 6.14 and 6.15. Each figure contains two images; larger arrangements of the particles in the film can be seen in the main image of each figure and a higher magnification of the silica particles gives some depth of field to the images. Horizontal scale bars are given for each image. SEM images of films without silica did not show any distinguishable characteristics because the topography of asphaltene and maltene units is smaller than the resolution of the electron microscope. The SEM image of the silica film shows some cracks in an otherwise continuous film, which may also be present in the interfacial Langmuir film. However, it is more likely that the cracks occurred during deposition. Some cracks were large enough to be noticeable with the naked eye immediately after deposition and so they are not likely the result of film drying or carbon coating. The SEM image of the 50 wt% maltene-50 wt% silica mixture looks very similar to the image of the silica film except that there are no large cracks. In addition, the maltene-silica mixture appears to be smoother than the silica film. The SEM image of the asphaltene-silica mixture looks markedly different. In this case, silica particles have aggregated into clusters, and the clusters appear evenly dispersed throughout the film.

AFM images obtained from a film of (a) silica, (b) maltene-silica mixture, (c) asphaltene-silica mixture, and (d) asphaltenes are shown in Figure 6.16. Scales are given as horizontal bars and the vertical bars on each image show the height of the features. Each subfigure (a, b, c, d) contains a 50 μm x 50 μm image and a smaller (higher magnification) 5 μm x 5 μm image. The higher magnification images in Figures 6.16a), 6.16b) and 6.16d) are representative of most areas of the film and do not focus on any specific feature. The higher magnification image in Figure 6.16c) focuses on a silica cluster. Figure 6.17 shows another magnified image of a film containing 50 wt % asphaltene-50 wt% silica. The figure is different from the magnified image shown in Figure 6.16c) because Figure 6.17 focuses on a film area between the silica clusters. The areas between the silica clusters are flatter than the silica clusters; the height scale bar in Figure 6.17 ranges from 0-10 nm compared to 0-1000 nm for Figure 6.16c). No AFM images are reported for maltene films because images produced by AFM scanning in contact mode showed flat, featureless films.

6.3 Discussion

6.3.1 Single Component films

Asphaltenes and maltenes are soluble in toluene. In fact, a part of the asphaltene extraction process is to dissolve bitumen in toluene. However, π-a isotherms were obtainable for both asphaltenes and maltenes at a toluene-water interface. Some material in the maltene fraction is interfacially active and is not soluble once it has been contacted with water. After evaporation of the toluene used as spreading solvent, part of the maltene fraction becomes toluene insoluble and remains at the interface. These maltene molecules then produce a π-a isotherm upon compression. Although some of the maltene fraction remains at the interface most of the fraction is dissolved from the interface into the bulk toluene supraphase. Comparison of the toluene-water isotherms with the air-water isotherms (see Appendix F) shows that the area per mass occupied by the maltenes is less at the toluene-water interface suggesting that fewer maltenes are at the interface. In addition, the lack of variation between maltene-asphaltene mixture isotherms at the toluene-water interface demonstrates that few maltenes have become toluene-insoluble and remain at the toluene-water interface.

A comparison of the single component isotherms from a toluene-water interface, to the isotherms from an air-water interface shows that the films are more compressible at a toluene-water interface. At a toluene-water interface silica and asphaltene films are less compressible than maltene films as shown by the slopes of the respective isotherms and calculations of the film compressibility. The greater compressibility of maltenes results from weaker interactions among maltene molecules as compared to the interactions among asphaltene molecules and asphaltene aggregates. Also, it is likely that maltene molecules are prone to be displaced from the interface during compression, resulting in a greater compressibility. The film of silica nanoparticles is rigid; upon compression the film exists in a solid phase. Images of deposited silica films show that the film is fairly continuous across the interface; there are many particle-particle contacts. For this reason, compressibility is most likely due to reorganization of silica particles.

6.3.2 Maltene-Silica films

The isotherm obtained for a maltene film shows that the presence of the maltenes at a toluene-water interface is virtually non-existent. Not surprisingly, the isotherms of maltene-silica mixtures are dominated by the presence of silica. The effect of maltenes on the isotherm is limited to the creation of the "tail" in the isotherm and shifting the position of the mixed films from single component silica films and single component maltene films. The maltene introduces an extended liquid phase in the isotherm, i.e. the "tail". During this region of the isotherm the film is more compressible because maltene molecules are occupying some of the interfacial area and are being squeezed out of the interfaces. At higher interfacial pressures the film is in a solid phase, like a silica film. At the toluene-water interface, behaviour of the maltene-silica mixtures differs from the air-water interface. Although there is a "tail", the toluene-water isotherm lacks the liquid phase (dominated by maltenes) and accompanying phase transition present in isotherms from an air-water interface. Refer to Appendix F for further discussion on the differences between the interfaces.

Occupation of interfacial area by maltene molecules also explains the positive area shift at low pressures in Figure 6.3. Additional maltenes at the interface increases the area per mass of silica occupied by the film. However, the relationship between the amount of maltenes added (maltenes:silica ratio) and the area shift is not linear for the two mixtures investigated. In addition to occupying interfacial area, maltenes appear to increase the area that the silica particles occupy at the interface. By comparing SEM images of the silica films with SEM images of the maltene-silica mixtures, it appears that the silica is more evenly spread out when maltenes are present in the film. AFM images of the films show that a higher topography (white coloured areas) exists in the silica film. At higher interfacial pressures, all the maltenes may be squeezed out of the interface and the positive area shift is due to the change in the silica particle behaviour. This explains the decrease in area shift as the interfacial pressure increases.

The maltenes may cause the change in silica behaviour by adsorption onto particle surfaces. When this occurs the interfacial area occupied by a given mass of maltenes is reduced because less maltene molecules will be at the interface. This accounts for the negative area shift (area per mass of maltenes) from an isotherm of maltene films. Adsorption of maltenes onto the silica particle surfaces may reduce hydrophobic forces between the particles, decreasing the strength of aggregation between particles. In this way the maltenes may act as a lubricant allowing the silica particles to form a more coherent closely-packed structure upon compression.

The rigidity (compressibility) of an interfacial film of solid particles is unchanged by the presence of maltene molecules. Because of this it is not expected that maltenes would increase the ability of an interfacial film of solids to improve emulsion stability. However, since the maltenes do seem to change the coherency of the interfacial film as shown in images of the LB films, the presence of the maltenes at the interface could have an effect on emulsion stability. Yan, Elliott and Masliyah (1999) have shown that deasphalted bitumen decreases the emulsion stability of water-in-diluted bitumen emulsions. The deasphalted bitumen lessens the effectiveness of asphaltenes and solids from bitumen as emulsion stabilizers. Although the maltenes do influence the interfacial film behaviour of silica particles, the extent of the contribution is minor. In addition, the influence of maltenes on the interfacial behaviour of asphaltenes could not be distinguished with the current experiments. Therefore it seems that the change in emulsion stability caused by deasphalted bitumen is not due to the change in the interfacial behaviour of asphaltenes or solids, but by altering other mechanisms, such as asphaltene adsorption at the interface.

6.3.3 Asphaltene-Silica films

In the asphaltene-silica mixtures the silica nanoparticles aggregate into clusters (as shown in Figures 6.15 and 6.16c) and are embedded into the film of asphaltene aggregates. The areas in between the silica clusters, shown in Figure 6.17 appear to be asphaltene aggregates. The aggregates are similar to the asphaltenes in the maltene-asphaltene mixture and in asphaltene films studied previously by Zhang et al. (2005). The asphaltenes and maltenes are thus partially mixable. The asphaltenes are distributed among the silica nanoparticles. Some of the silica particles are aggregated into clusters. (In Appendix D a comparison of the asphaltene-silica mixtures to an ideal mixture shows that the components behave as if they were miscible and there is some attraction between components). It is likely that silica clusters form because asphaltenes reduce interparticle forces and increase the hydrodynamic resistance to aggregation, which prevents the formation of a continuous silica film. But there are insufficient asphaltene molecules to completely disperse the silica nanoparticles and as a result some clusters are present.

The structure of the mixed film shown by the images can be used to explain the results obtained from π-a isotherms and the area shift. The presence of silica decreases the compressibility of the asphaltene film shown by the steeper isotherm slopes and compressibility curves. This is due to the rigid silica particles embedded and evenly dispersed in the asphaltene films, making the entire film more rigid. Isotherms from the mixtures are shifted to the right of the isotherm of silica films (positive area shift) because asphaltenes cause the silica film to become more expanded and asphaltenes occupy the interfacial area between silica clusters. Conversely the area shift for the mixtures is negative when compared to an asphaltene film. This could be due to asphaltene adsorption onto particle clusters, causing asphaltenes to occupy less interfacial area per mass. The adsorption of asphaltenes onto the silica particles could also provide a reduction in the hydrophobic forces between particles, reducing aggregation.

Another attribute of the asphaltene-silica films is that the collapse pressure is higher than that of a silica film. Higher asphaltene content in the mixed film translates into a higher collapse pressure. Collapse in these films is likely to occur when the silica particles are forced out of the interface, evidenced by the appearance of white creases. Asphaltene molecules may hold them to the interface resulting in an increased collapse pressure.

The results obtained with asphaltene-silica mixtures suggest that a film formed from a mixture of asphaltenes and silica nanoparticles should be more effective for emulsion stabilization since the asphaltenes seem to cover the silica clusters and the silica is spread out in the film. The interfacial structure of emulsion droplets stabilized by particles can vary (Lopetinsky et al., in press). Studies have shown that emulsion droplets can be completely covered by the particles (Binks and Kirkland, 2002), but randomly distributed clusters of particles have also been observed to stabilize emulsion droplets (Vignati, Piazza, and Lockhart, 2003). In the asphaltene-silica films the interfacial mobility of the silica clusters would be limited by the surrounding asphaltenes. Thus the asphaltene-surrounded silica in an asphaltene-silica film should provide an effective steric stabilization. The film stabilization properties may be enhanced over a film of asphaltenes because the particle clusters are extended farther away from the interface, increasing the range of the steric hindrance, and the asphaltene-silica films are more rigid. The asphaltenes also hold the silica particles to the interface strongly, which could increase their effectiveness in steric stabilization.

6.4 Summary and Conclusions

Solid nanoparticles, along with maltenes and asphaltenes extracted from bitumen have been studied at a toluene-water interface using a Langmuir trough. For the maltene fraction of bitumen presently studied, most of the material leaves the toluene-water interface and is dissolved into the bulk toluene, and the remainder forms a very compressible film. Asphaltenes and silica form relatively rigid films (i.e. less compressible films). Results from maltene-silica and maltene-asphaltene mixtures show that the maltene molecules do not substantially change the interfacial behaviour of silica or asphaltenes. Direct qualitative evidence has been obtained to show that asphaltenes change the behaviour of solid particles at a solvent-water interface. In mixed films of asphaltenes and silica, the silica nanoparticles form aggregated clusters that are evenly dispersed amongst asphaltenes.

The interfacial behaviours observed for maltenes, either alone or in a mixture, do not coincide with behaviours that promote emulsion stability. The asphaltenes and silica nanoparticles both form rigid and continuous films at the toluene-water interface. The interfacial behaviour of these substances is likely to aid in emulsion stability. In addition, a mixture of asphaltenes and silica has shown a combined behaviour that could make a mixed film of asphaltenes and silica an even more effective emulsion stabilizer.

6.5 References

Aveyard, R., Binks, B.P., Fletcher, P. D. I., Rutherford, C. E., *Measurement of contact angles of spherical monodisperse particles with surfactant solutions*, Colloids and Surfaces A: Physicochemical and Engineering Aspects, 83(1):89-98, 1994.

Binks, B.P., and Kirkland, M., (2002). *Interfacial structure of solid-stabilised emulsions studied by scanning electron microscopy*. Physical Chemistry Chemical Physics, 4(15), 3727-3733.

Lopetinsky, R., Masliyah, J.H., Xu, Z., *Solids-Stabilized emulsions: A review* in B.P. Binks and T.S. Horozov (Ed.), Colloidal Particles at Liquid Interfaces, Cambridge University Press, In press.

Washburn, E.W, (Ed.), International critical tables of numerical data, physics, chemistry, and technology, 1st electronic edition, New York., Knovel, 2003.
Retrieved March 28, 2005 from
http://www.knovel.com/knovel2/Toc.jsp?SpaceID=10093&BookID=735

Vignati, E., Piazza, R., Lockhart, T.P,, *Pickering emulsions: Interfacial tension, colloidal layer morphology, and trapped-particle motion*, Langmuir, 19(17):6650-6656, 2003.

Y Yan, Z.L., Elliott, J.A.W., Masliyah, J.H., *Roles of various bitumen components in the stability of water-in-diluted-bitumen emulsions*, Journal of Colloid and Interface Science, 220(2):329-337, 1999.

Zhang, L.Y., Lopetinsky, R., Xu, Z., Masliyah, J.H., *Asphaltene monolayers at a toluene-water interface*, Energy and Fuels, To Be Published, 2005.

6.6 Figures

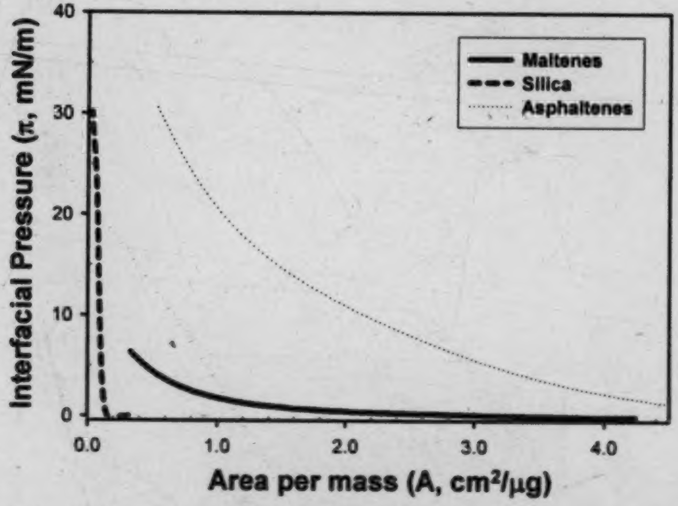

Figure 6.1: Interfacial pressure-area isotherms of silica nanoparticles, maltenes and asphaltenes.

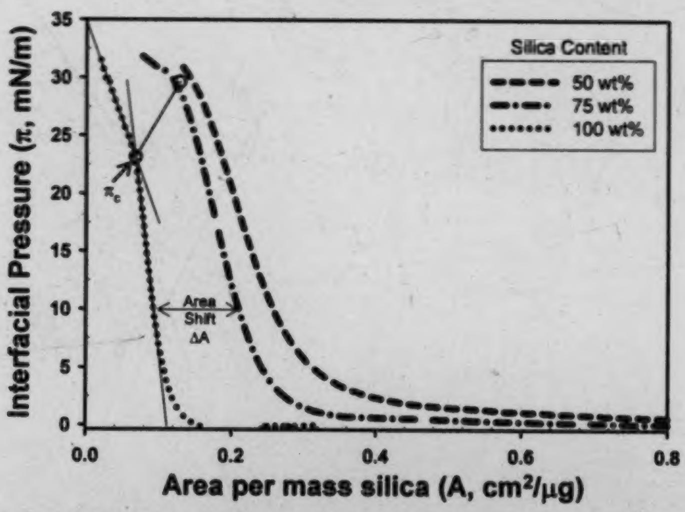

Figure 6.2: Interfacial pressure-area isotherms of films from maltene and silica mixtures of varying maltenes:silica ratios. Isotherms are normalized by the mass of silica at the interface.

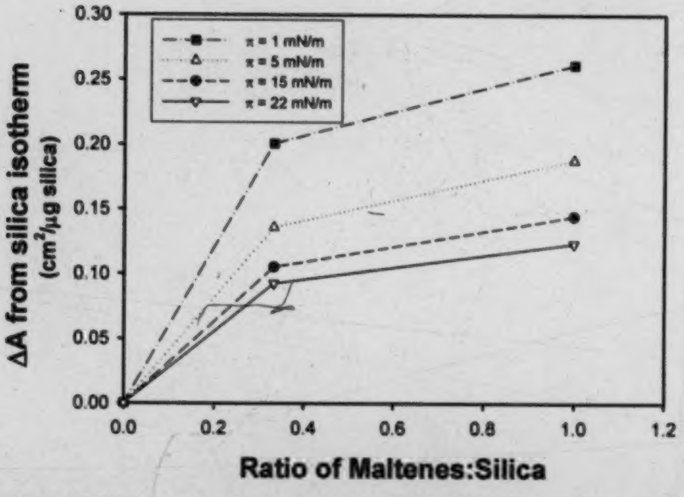

Figure 6.3: Area shift from the isotherm of a silica film for maltene-silica mixtures. At various interfacial pressures plotted against the ratio of maltenes:silica.

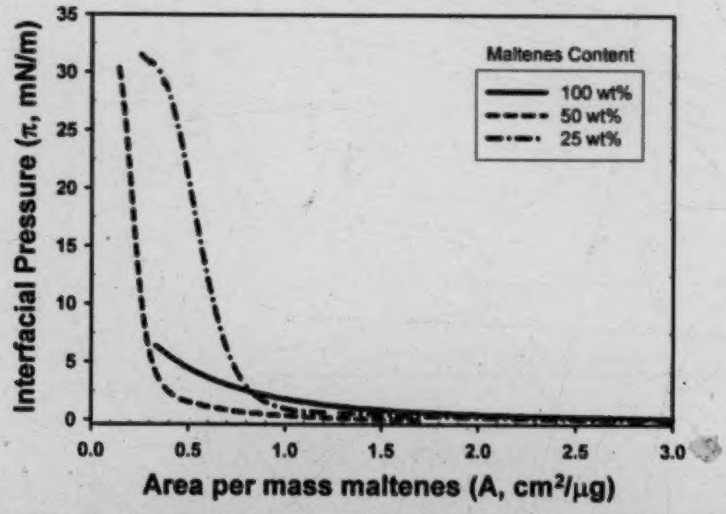

Figure 6.4: Interfacial pressure-area isotherms of films from maltene and silica mixtures of varying maltenes:silica ratios. Isotherms are normalized by the mass of maltenes at the interface.

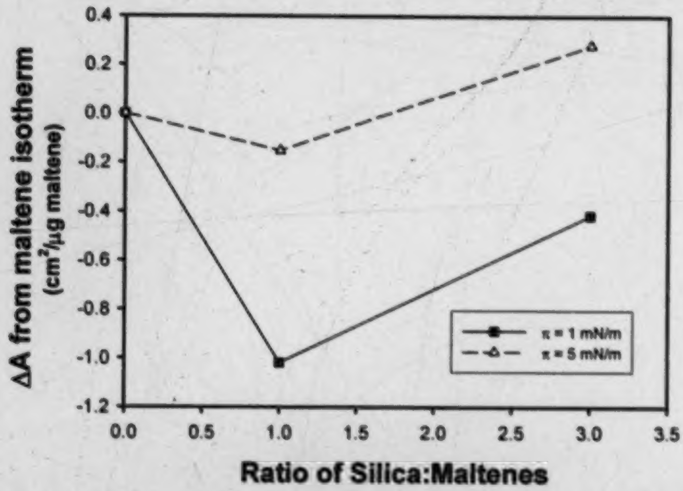

Figure 6.5: Area shift from the isotherm of a maltene film for maltene-silica mixtures. At various interfacial pressures plotted against the ratio of silica:maltenes.

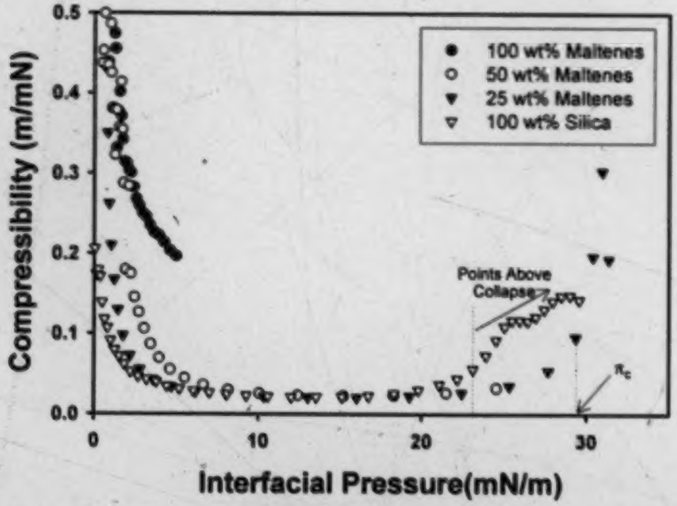

Figure 6.6: Compressibility of films formed from maltene-silica mixtures at toluene-water interface.

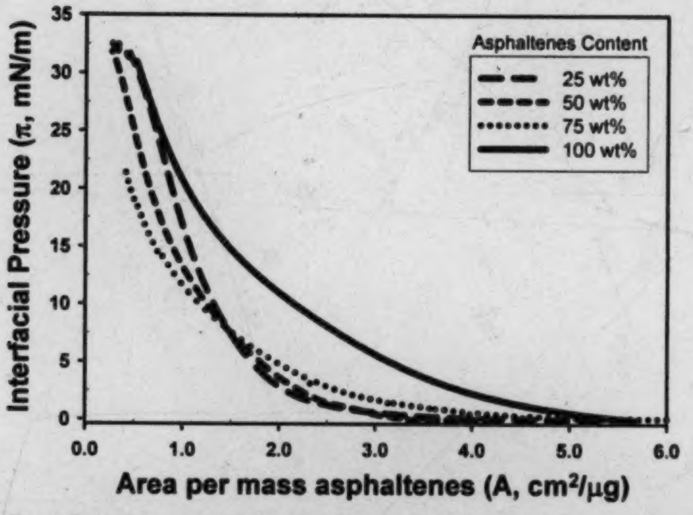

Figure 6.7: Interfacial pressure-area isotherms of films from asphaltenes and silica mixtures of varying ratios of asphaltenes:silica. Isotherms are normalized by the mass of asphaltenes at the interface.

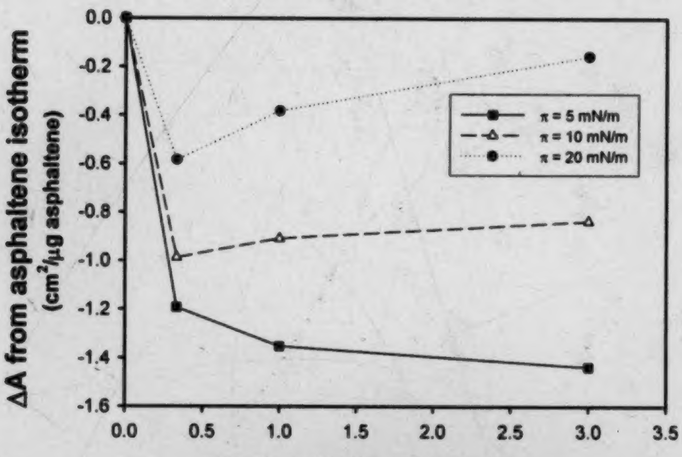

Figure 6.8: Area shift from the isotherm of an asphaltene film for asphaltene-silica mixtures. At various interfacial pressures plotted against the ratio of silica:asphaltenes.

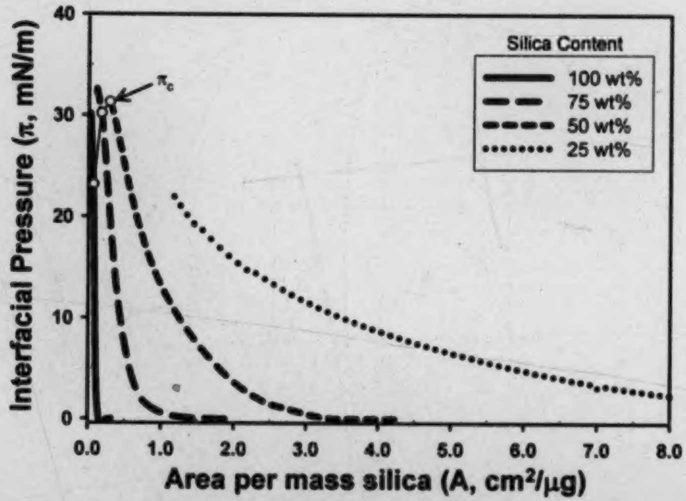

Figure 6.9: Interfacial pressure-area isotherms of films from asphaltenes and silica mixtures of varying ratios of asphaltenes:silica. Isotherms are normalized by the mass of silica at the interface.

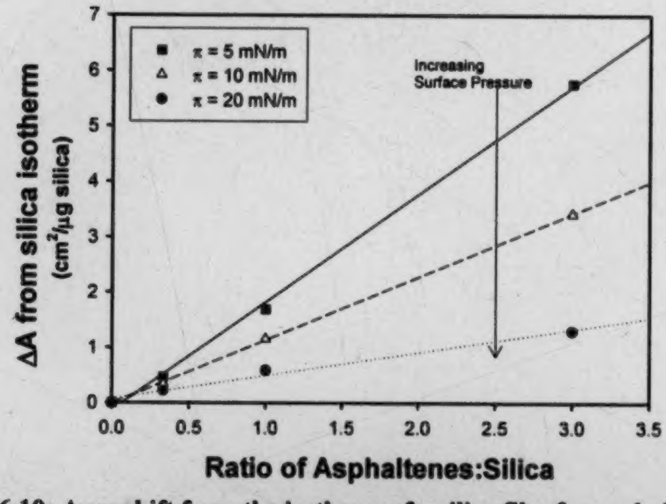

Figure 6.10: Area shift from the isotherm of a silica film for asphaltene -silica mixtures. At various interfacial pressures plotted against the ratio of asphaltenes:silica.

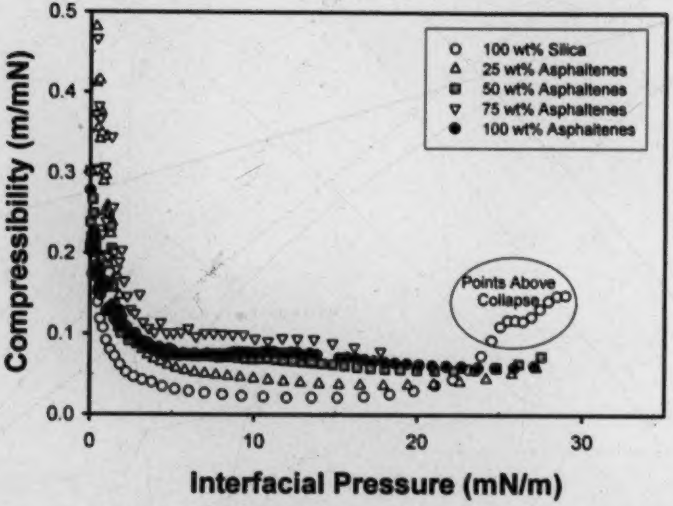

Figure 6.11: Compressibility of films formed from asphaltene-silica mixtures at toluene-water interface.

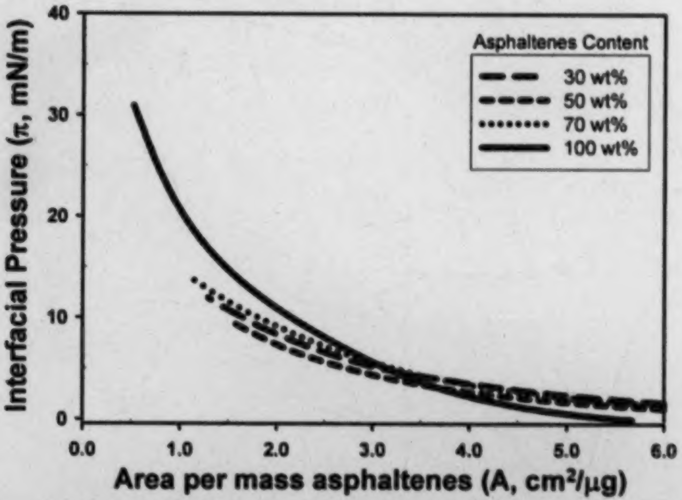

Figure 6.12: Interfacial pressure-area isotherms of films from asphaltenes and maltenes mixtures of varying ratios of asphaltenes:maltenes. Isotherms are normalized by the mass of asphaltenes at the interface.

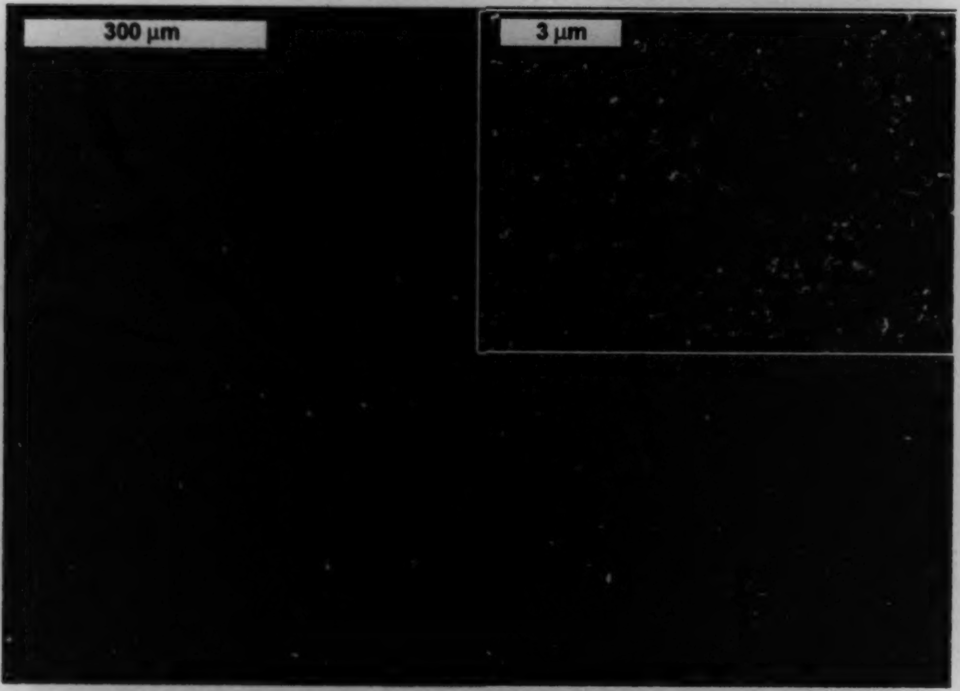

Figure 6.13: SEM images of single layer LB film of silica deposited onto silicon wafers from toluene-water interface. Inset image shows same film at higher magnification. Interfacial pressure at deposit, $\pi_{deposit} = 10$ mN/m. Film coated with carbon to enable SEM imaging.

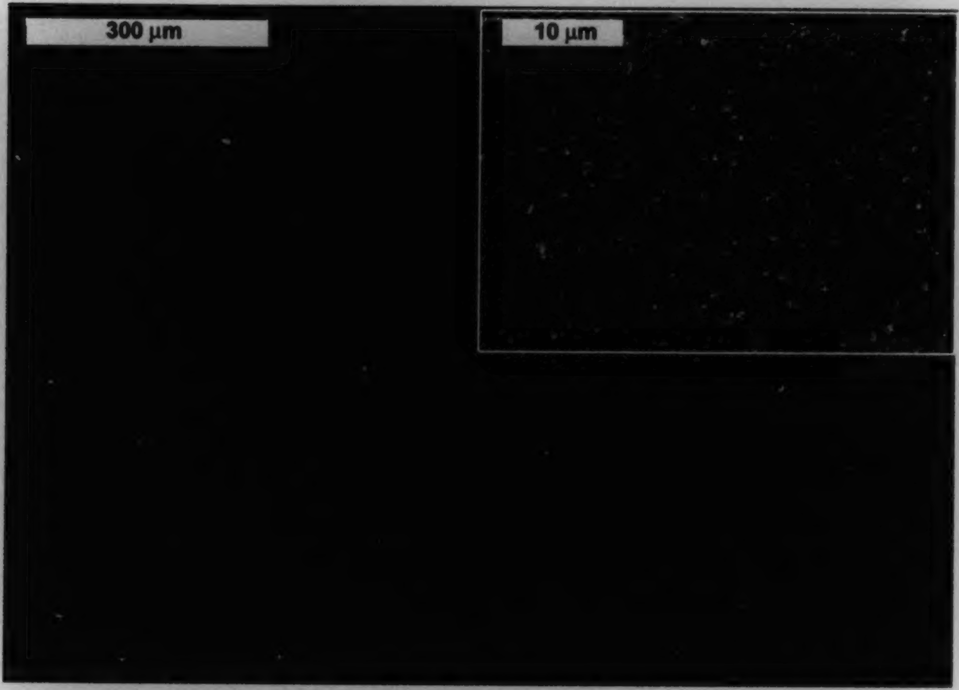

Figure 6.14: SEM images of single layer LB film of 50wt% silica –50 wt% maltene deposited onto silicon wafers from toluene-water interface. Inset image shows same film at higher magnification. Interfacial pressure at deposit, $\pi_{deposit}$ = 10 mN/m. Film coated with carbon to enable SEM imaging.

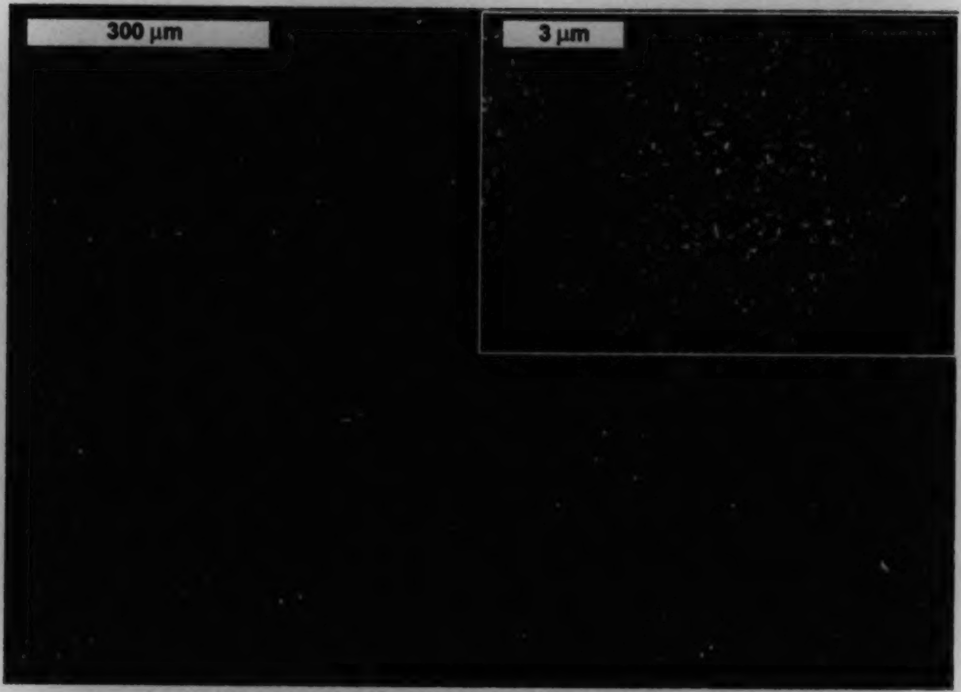

Figure 6.15: SEM images of single layer LB film of 50wt% silica –50 wt% asphaltene deposited onto silicon wafers from toluene-water interface. Inset image shows same film at higher magnification. Interfacial pressure at deposit, $\pi_{deposit}$ = 10 mN/m. Film coated with carbon to enable SEM imaging.

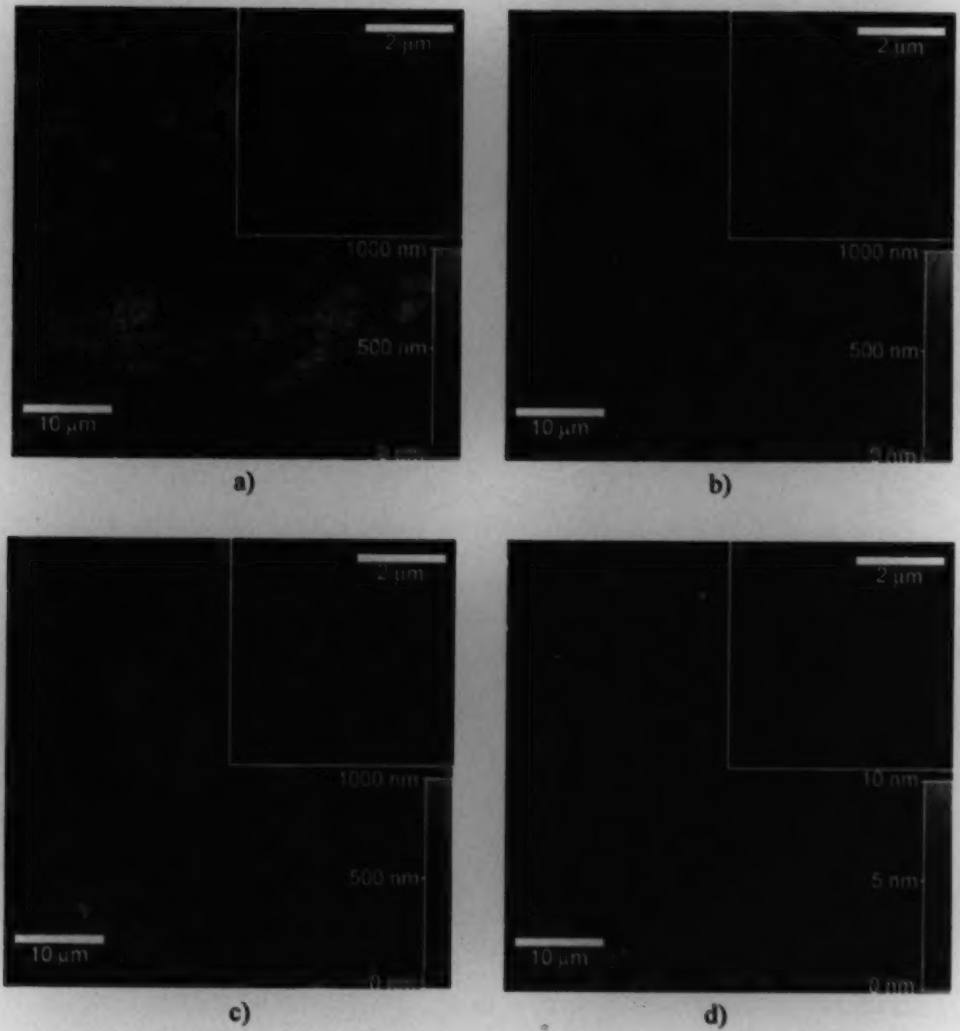

a) **b)**

c) **d)**

Figure 6.16: AFM height images of single layer LB films deposited on to silicon wafers from toluene-water interface. Interfacial pressure at deposit, $\pi_{deposit}$ = 10 mN/m. a) Silica only TR=0.21, b) 50 wt % maltene – 50 wt% silica mixture TR = 0.90 c) 50 wt % asphaltene – 50 wt% silica mixture TR = 1.89 d) 50 wt % maltene – 50 wt% asphaltene TR =1.70

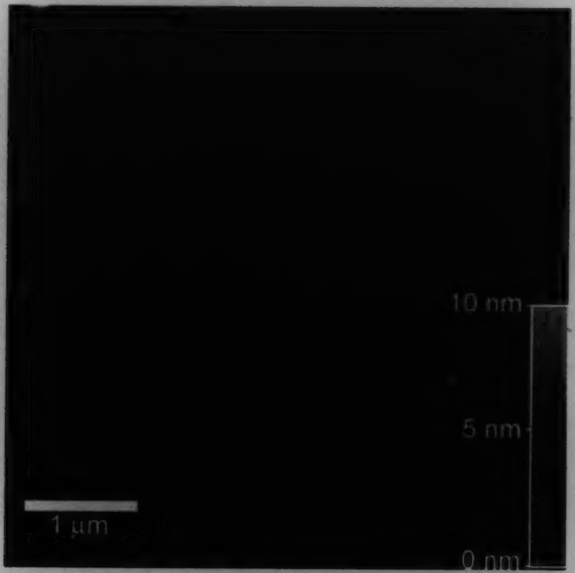

Figure 6.17: AFM height image of single layer LB films deposited on to silicon wafers from toluene-water interface. Image is of areas with a relatively low profile compared to the rest of the film. 50 wt % asphaltene – 50 wt% silica mixture TR =1.89

"Now this is not the end. It is not even the beginning of the end. But it is, perhaps, the end of the beginning."
-Sir Winston Churchill

7

Conclusions and Recommendations

7.1 Summary and Conclusions

Water-in-diluted bitumen emulsions present in bitumen froth offer a continual challenge to the oil sands industry. It is commonly believed that fine solids and surface-active components (such as asphaltenes) in bitumen makeup the interfacial films responsible for stabilization of water-in-diluted bitumen emulsions.

Langmuir and Langmuir-Blodgett films were used to study the interfacial behaviour of asphaltenes, maltenes and hydrophobic silica nanoparticles. Preliminary experiments were conducted to determine the effect of variables such as compression rate and evaporation time in order to establish controlled conditions in other Langmuir trough experiments. In addition, an acoustic spectrometer was used to determine the particle size of the fumed silica nanoparticles dispersed in toluene. Experimental results include surface or interfacial pressure-area isotherms, scanning electron microscope images and atomic force microscope images. Subsequent analysis of pressure-area isotherms produced compressibility curves and area-shift plots for the Langmuir films.

Based on the various experimental results obtained from air-water and toluene-water interfaces the following conclusions can be drawn:

- Maltenes produce interfacial films that are more compressible than the films of asphaltenes and silica nanoparticles. Maltenes have a minor influence on the isotherm shape of silica nanoparticles and asphaltenes at the toluene-water interface. Thus it appears that the role of Maltenes in emulsions stability does not stem from changing the interfacial behaviour of asphaltenes or solids.
- The silica nanoparticles aggregate into clusters at the air-water interface, likely due to attractive hydrophobic forces. Maltenes and asphaltenes alter the interparticle forces causing a reduction in the particle cluster size at the air-water interface. Asphaltenes also change the behaviour of solid particles at the toluene-water interface causing them to form particle clusters that are dispersed across the interface. At a toluene-water interface silica nanoparticles form a continuous film without clusters
- Similarities in the behaviour at the air-water interface of the films containing asphaltenes and films containing fumed silica nanoparticles were observed, including low compressibility and similar phase transitions when mixed with maltenes.
- When combined with silica or asphaltenes, maltenes do not substantially change the characteristics of the mixed film at a toluene-water interface.
- The behaviour of asphaltenes and silica at a toluene-water interface is indicative of characteristics that are likely to aid in emulsion stability. A mixture of asphaltenes and silica has shown a combined behaviour that could make a mixed film of asphaltenes and silica an even more effective emulsion stabilizer. The film stabilization properties may be enhanced over a film of asphaltenes because the particle clusters extend away from the interface, increasing the range of the steric hindrance, and the asphaltene-silica films are more rigid.

7.2 Recommendations for Future Work

The following research activities are recommended in future studies. This work should extend the concepts uncovered in the thesis and give a more complete view of the interfacial behaviour of the components studied.

- Deposit Langmuir films onto transmission electron microscope (TEM) grids. The additional resolving power of a transmission electron microscope may reveal more details about the silica structures observed with AFM and SEM in this thesis.
- Investigate solids extracted from the coker feed bitumen, the same solids responsible for emulsion stability in the industrial process. Mixed films similar to those presently studied could be produced with extracted solids and bitumen components.
- Clarification into particle aggregation and particle interactions may be gained by using monodisperse silica particles in Langmuir trough experiments. This is possible by creating silica using the Stober process or by treatment of commercial colloidal silica that has a narrow size distribution.
- To further link the Langmuir trough studies to emulsion stability, it would be beneficial to prepare emulsions using combinations of the fumed silica and bitumen components presently studied. Experiments could be performed with toluene, water and specific ratios of silica, asphaltenes and maltenes. This work may further elucidate the role of maltenes in emulsion stability in relation to its interactions with nanoparticles and asphaltenes.
- Few published studies have investigated the effects of particle shape on solids-stabilized emulsions. Colloidal silica with elongated particle shapes is commercial available. Investigations using the Langmuir trough and preparation of emulsions with elongated silica particles could aid in the study of particle shape.

A

Appendix A: Additional Trough Experiments

In addition to the pressure-area isotherms obtained for the main study, some additional experiments were conducted to investigate some other areas of interest. Two of these additional studies are the investigation of different containment methods for silica dispersions and the investigation of spreading technique.

A.1 Silica Dispersions in Different Containers

In all of the Langmuir trough experiments conducted in the main thesis, solutions were stored in glass containers. It was noticed that some silica from silica-in-toluene dispersions stuck to the walls of the glass containers. The same phenomenon was not apparent for mixtures of maltenes and silica or asphaltenes and silica. In order to determine if storing silica-in-toluene dispersions in glass containers changed the reported isotherms, a series of surface pressure-area isotherms were obtained for different dispersions. A total of four dispersions were prepared at two different concentrations. For each concentration, one dispersion was made in a Teflon container. Concentrations were measured by weighing the mass of dry silica and toluene added to the container.

The container was sonicated for 60 minutes and half of the dispersion was poured into a glass container of similar size. The size of the containers was as close to the same as was available in the laboratory (A 120 ml glass bottle and 110 ml Teflon bottle were used). Using similar sized containers ensured that the dispersion was exposed to a similar surface area for each container. Surface pressure-area isotherms were obtained for the dispersions using the procedures outlined in Chapter 3. The spreading volume for the high concentration dispersions (9.92 mg/ml) was 55 μl, which corresponds to 546 μg of silica spread at the interface. Due to the small syringe volume, only 200 μl of the low concentration dispersions (2.24 mg/ml) was spread, equalling 448 μg of silica. The measured surface-pressure isotherms for each dispersion are shown in Figure A1, with the trough area normalized by the calculated amount of silica spread at the interface. The isotherms in Figure A1 do not lie in the same position showing that the amount of silica at the interface is different for each test. The isotherms from the glass container are left of the isotherms from the Teflon container, especially at higher concentrations. The shift of silica isotherms is likely due to the deposition of silica particles onto the container surface. At lower concentrations the amount of material sticking to the sides of the container is enough to significantly alter the bulk concentration of the solution. At high concentrations the shift in isotherm caused by using glass containers is at an acceptable level for other experiments. In addition, all isotherms reported in previous chapters are obtained from mixtures that were stored in glass containers, thus when comparing different mixtures the difference in isotherm position should be diminished.

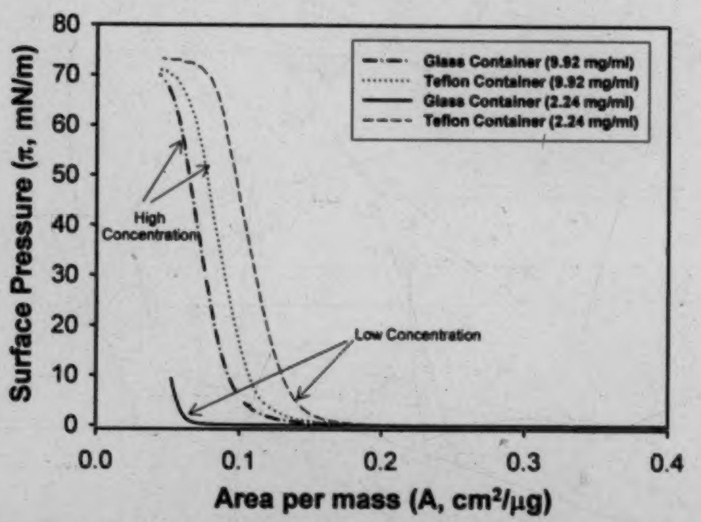

Figure A.1: Surface pressure-area isotherms of hydrophobic silica (118°) where silica in toluene dispersion was stored in different container materials.

A.2 Sequential Spreading

There are two techniques of spreading mixed monolayers on the Langmuir trough. In all of the experimental work presented in previous chapters, the classic spreading technique was used. The classic spreading technique involves combining the substances in a single mixture prior to spreading material at an interface. Sequential spreading, the other technique, involves spreading each of the substances in the mixture from its own solution. The sequential spreading technique can save preparation time because Langmuir films of many different concentrations can be formed from the same two stock solutions. However, the spreading technique can alter the isotherm obtained from the mixed film. Surface pressure-area isotherms were obtained for mixed films of maltenes and hydrophobic silica (AEROSIL® R972) using both classical and sequential spreading techniques. The mass fraction of maltenes and silica was the same for both spreading techniques (6 wt% maltenes, 94 wt% silica). Figure A2 shows the isotherms obtained from unmixed maltenes, unmixed silica and the two spreading techniques. The mass spread at the interface is shown for each isotherm.

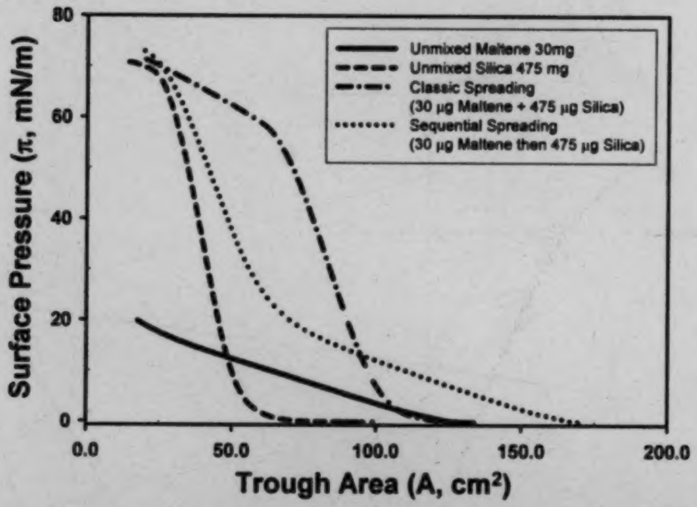

Figure A.2: Surface pressure-area isotherms of mixtures of hydrophobic silica (118°) and maltenes. Isotherms shown include silica only, maltene only, mixture formed with classic spreading technique and mixture formed with sequential spreading.

Results in Figure A.2 show the difference between the two spreading techniques. The isotherm for the sequential spreading technique has two distinct phases and a transition point between the phases. The isotherm appears to be a combination of the isotherms of unmixed maltenes and silica. In contrast, the isotherm from the classical spreading technique does not clearly have two distinct phases. There is no initial slope change and the contribution of the maltenes to the isotherm is not as apparent as for the sequential spreading isotherm. These results clearly show that the spreading technique will have an affect on the isotherm measured for mixed Langmuir films. In previous chapters only the classical spreading technique was used because combining the fine particles and the bitumen components prior to formation of the film, rather than sequential film formation, more accurately represents what occurs in diluted bitumen emulsion systems.

B

Appendix B: Procedure to Construct Compressibility Curves

B.1 Introduction

The theory of monolayer compressibility and the relation of Langmuir film compressibility to emulsion stability are discussed in Chapter 2. As defined previously, monolayer compressibility is analogous to bulk compressibility and is defined by Equation B.1 below (Gaines, 1966),

$$C_s = -\frac{1}{A_t}\frac{dA_t}{d\pi} \qquad \text{[B.1]}$$

where C_s is the film compressibility, A_t is the trough area and π is the surface pressure. Compressibility of a Langmuir film can not be directly measured by the Langmuir trough and Wilhelmy plate system used in this thesis. Values of film compressibility were calculated from pressure-area measurements using equation B.2. Analytical calculations of the derivative $dA/d\pi$ were not possible because curve-fitting expressions to incongruously shaped pressure-area isotherms was not possible. Thus, numerical methods were used to calculate compressibility. The following procedure was used to construct the compressibility curves presented in previous chapters (e.g. Figure 5.14).

B.2 Procedure

First, measured area values are normalized by the total mass spread at the interface. Using area per mass instead of area does not make a difference in the calculation of the compressibility because the distributive property of differentiation causes the mass term to be cancelled out.

Second, measured area and surface pressure values are "smoothed" using a pre-programmed algorithm from the SigmaPlot 2002 software. This removes much of the data and avoids problems with estimating the derivative caused by fluctuations in the surface pressure readings. Several options exist for the smoothing procedure. For the most part a "Negative Exponential" smoothing was used. This method is described in a menu in SigmaPlot; "[a] Local smoothing technique using polynomial regression and weights computed from the Gaussian density function". The Gaussian density function is given in equation B.2

$$e^{-u^2} \quad \text{...} [B.2]$$

Occasionally, a method called "Inverse Square" was used to smooth the measured data. The description provided is: "The weighted average of the values at neighbouring points is computed using the Cauchy density function" The Cauchy density function is given in equation B.3

$$\frac{1}{1+u^2} \quad \text{...} [B.3]$$

No matter what settings were specified in SigmaPlot, the smoothing was visually compared to the actual data to ensure the smoothed data was representative of the original data. Figure B.1 compares an isotherm from asphaltenes at a toluene water-interface before and after the data has been smoothed. The isotherm did not change shape or position. Inset in Figure B.1 is a magnified section of the two isotherms, which shows the effectiveness of data smoothing in removing fluctuations in the pressure readings.

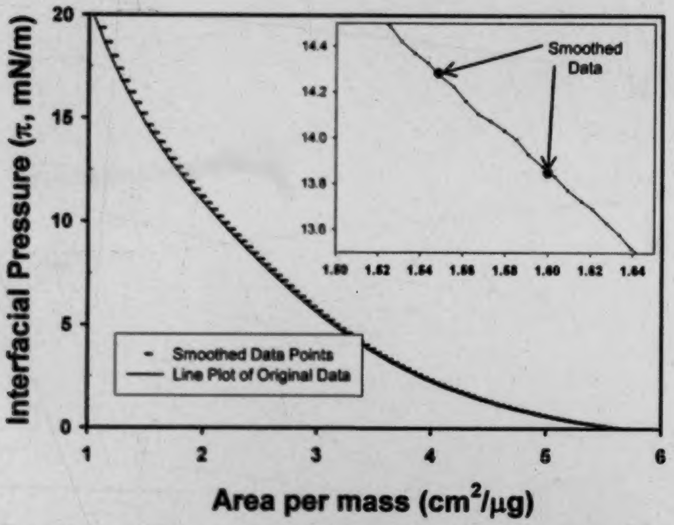

Figure B.1: Comparison of smooth data with measured data for asphaltene isotherm.

Third, the derivative of area with respect to surface pressure was calculated and then compressibility was calculated. The derivative was calculated with a built-in macro from SigmaPlot (Compute 1st Derivative). The results were compared to a simple forward difference calculation made in Excel and there was little difference between the two. Shown in Figure B.2 is a comparison of the two compressibility calculations. Data measurements are for an asphaltene film from a toluene-water interface.

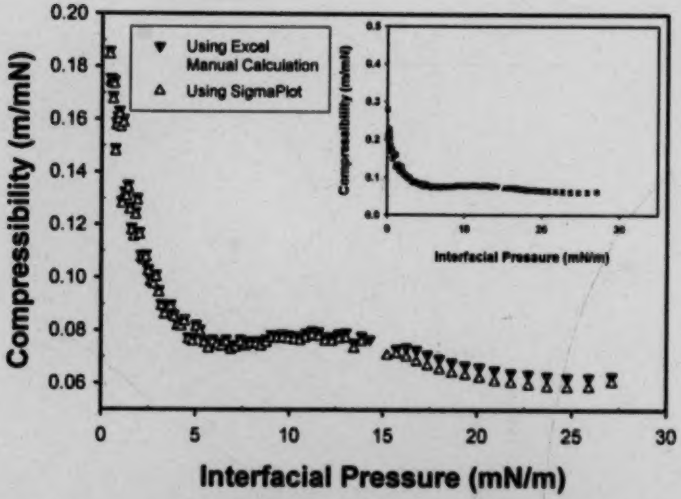

Figure B.2: Comparison of compressibility calculations using a forward difference method (Excel) and a macro from SigmaPlot.

B.3 References

Gaines, G. L., *Insoluble monolayers at liquid-gas interfaces,* New York, Interscience Publishers 1966.

SigmaPlot 2002 for Windows Version 8.0 [Computer Software], Chicago, SPSS Inc., 2001.

Microsoft Excel 2000 [Computer Software], Seattle, Microsoft Corporation, 1999.

C

Appendix C: Isotherm Averaging Technique

C.1 Introduction

For experiments presented in Chapters 5 and 6, pressure-area isotherms were measured at least three times for each film. For some films variation occurred in the different isotherm measurements, usually the position of the curve (i.e. area) varied. Experimental errors due to spreading volumes, water meniscus levels, and Wilhelmy paper tilt can all cause measured isotherms to shift position. In order to determine which isotherm should be presented, an averaging procedure was utilized. Averaged isotherms and measured isotherms that closely match the averaged isotherms are presented in previous chapters.

C.2 Procedure

An Excel macro was written in the Visual Basic programming language to automatically calculate the average isotherm from a set of measured isotherms. In general, the macro completes the following steps. Several steps are accompanied by figures to help illustrate the procedure

1. The maximum and minimum area values amongst all of the area measurements are determined.

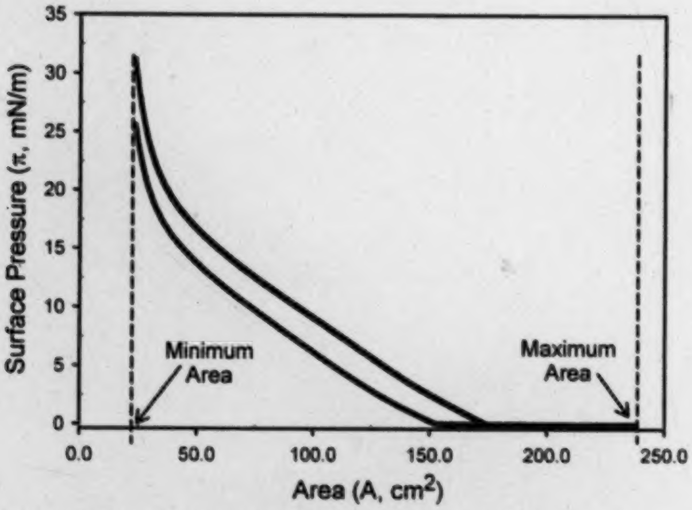

Figure C.1: Maximum and minimum determined

2. An array of standard area values that spans values between the maximum and minimum is automatically calculated. This array contains at least 800 evenly distributed values.

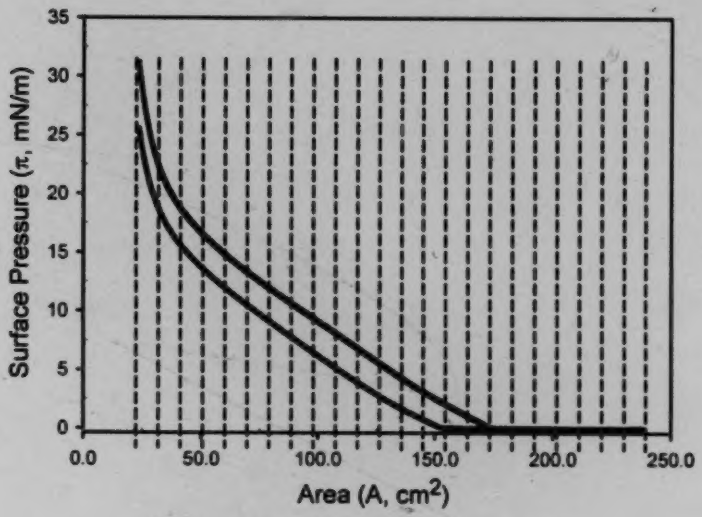

Figure C.2: Standard areas applied

3. For each isotherm, linear interpolation is used to estimate the surface pressure at every area value. This ensures that surface pressure values are obtained for every area value, and that the area values match for each isotherm.

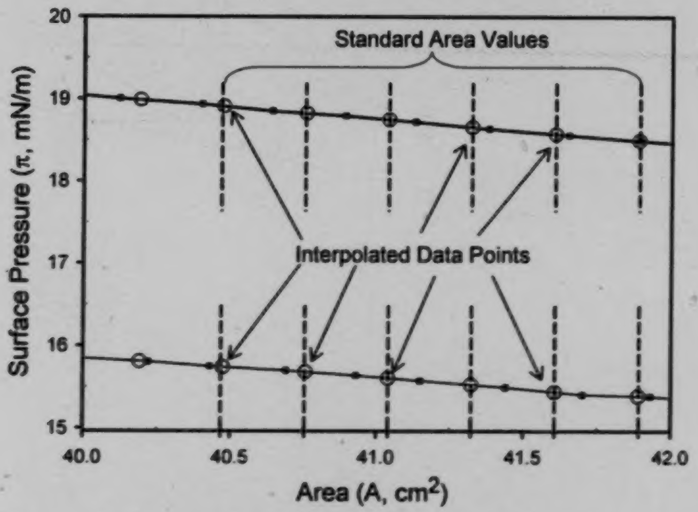

Figure C.3: Interpolation of pressures at standard area values

4. The surface pressure values from each of the isotherms are averaged using a simple average calculations (no weighting applied). Thus, for each area value there exists an average surface pressure.

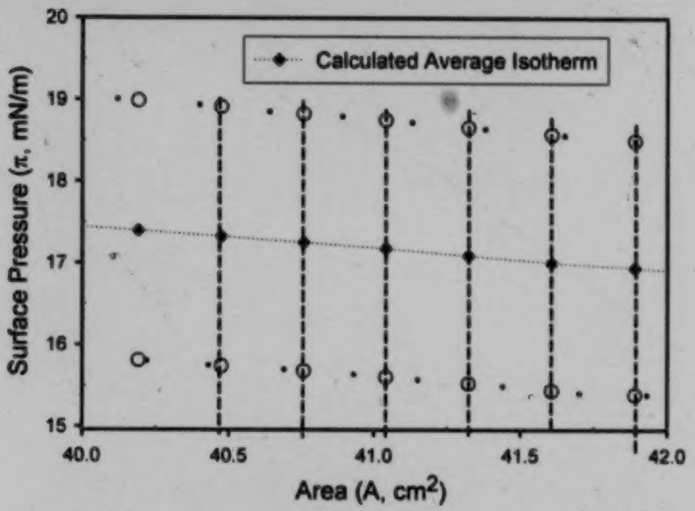

Figure C.4: Average surface pressure values are calculated

5. The resulting array of surface pressure and area values are used to plot the average isotherm.
6. The average isotherm is plotted with the measured isotherms. Visual inspection of the curves reveals any artefacts created by the averaging procedure.
7. If a measured isotherm lies on the average isotherm then the data of that measured isotherm is used for thesis figures because it contains a larger amount of data

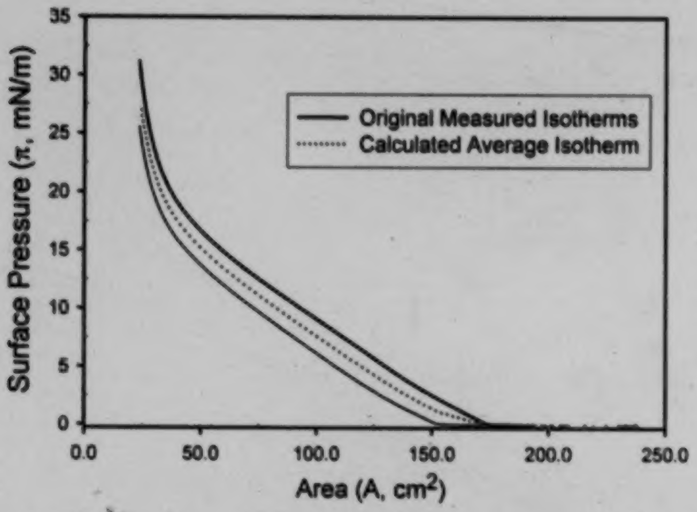

Figure C.5: Comparison of average isotherm to two measured isotherms

C.3 References

Microsoft Excel 2000 [Computer Software], Seattle, Microsoft Corporation, 1999.

D

Appendix D: Mixed Langmuir Films and the Additive Rule

D.1 Introduction

When studying mixed monolayers of two components using a Langmuir trough, analysis of the pressure-area isotherms of mixtures can be used to determine whether the mixture is ideal and to help determine the nature of interactions between the components. When the components in the mixed monolayer are ideally mixed or completely immiscible trough areas will obey the additive rule as given by Gaines (1966):

$$A_{12} = X_1 A_1 + X_2 A_2 \quad \text{[D.2]}$$

where X_1 and X_2 represent the molar fractions of components 1 and 2, A_1 and A_2 are the area per molecule of each unmixed component, and A_{12} is the area per molecule of the mixed monolayer. When the mixture is not ideal and some level of miscibility occurs the area of the mixed monolayer deviates from the above equation. Deviation in mixtures is characterized by determining the excess area ΔA_{xs} that occurs in measured isotherms.

$$\Delta A_{xs} = A_{12} - (X_1 A_1 + X_2 A_2) \quad \text{[D.2]}$$

Alternatively, plotting the measured area against molar fraction can be used to graphically show the deviation from an ideal mixture. A straight line from the areas of pure components occurs when the excess area is zero (i.e. ideal mixture). Points above the line have a positive excess area indicating repulsive behaviour between the components, points beneath the line have a negative excess area indicating attraction between the components.

Equations D.1 and D.2 are commonly used for mixtures where the molecular weights are known. However, by performing some algebra it can be shown that the formula for the area for an ideal mixed monolayer is true on both area per molecule and area per mass basis. Consider the terms A_1, A_2 and A_{12}. They are calculated by measuring the trough area and dividing by the number of molecules at the interface. The equation for A_1 is thus given by:

$$A_1 = \frac{Area}{m_1 Na} M_1 \quad \text{[D.3]}$$

where m_1 is the mass of component 1 at the interface, M_1 is the molecular weight of component 1 and Na is Avogadro's number. The area per mass, A_1', can be defined by:

$$A_1' = \frac{Area}{m_1} \quad \text{[D.4]}$$

Substituting equation D.4 into D.3 gives:

$$A_1 = A_1' \frac{M_1}{Na} \quad \text{[D.5]}$$

This gives the area per molecule in terms of area per mass. Using equation D.5, and equivalent expressions for A_2, and A_{12}, in equation D.1 gives:

$$\frac{A_{12}' M_{12}}{Na} = \frac{X_1 A_1' M_1}{Na} + \frac{X_2 A_2' M_2}{Na} \quad \text{[D.6]}$$

Multiplying by Na gives:

$$A_{12}' M_{12} = X_1 A_1' M_1 + X_2 A_2' M_2 \quad \text{[D.7]}$$

The molecular weight of the mixture, M_{12}, is determined by the expression

$$M_{12} = X_1 M_1 + X_2 M_2 \quad \text{[D.8]}$$

Using equation D.8 in D.7 and rearranging gives:

$$A'_{12} = \frac{X_1 A'_1 M_1 + X_2 A'_2 M_2}{X_1 M_1 + X_2 M_2} \tag*{[D.9]}$$

The molar fraction of each component is the number of moles of each component (n_i) divided by the total number of moles in the mixture (n_t), i.e.:

$$X_1 = \frac{n_1}{n_t} \tag*{[D.10]}$$

Using equation D.10, and the equivalent expression for X_2 in equation D.9, and after simplification gives:

$$A'_{12} = \frac{A'_1 n_1 M_1 + A'_2 n_2 M_2}{n_1 M_1 + n_2 M_2} \tag*{[D.11]}$$

But the mass of each component m is equal to nM so that D.11 is equivalent to:

$$A'_{12} = \frac{A'_1 m_1}{m_1 + m_2} + \frac{A'_2 m_2}{m_1 + m_2} \tag*{[D.12]}$$

Finally, the mass fraction (f) of each component is defined as:

$$f_1 = \frac{m_1}{m_1 + m_2} \tag*{[D.13]}$$

Therefore, the additive rule can be written in a per mass basis:

$$A'_{12} = f_1 A'_1 + f_2 A'_2 \tag*{[D.14]}$$

where f_1 and f_2 represent the molar fractions of components 1 and 2, A'_1 and A'_2 are the area per mass of each unmixed component, and A'_{12} is the area per mass of the mixed monolayer.

Since the silica nanoparticles are not monodisperse and aggregate into clusters, the number of silica molecules at the interface cannot be established. However, determining if maltene-silica and asphaltene-silica mixtures behave as ideal mixtures is possible using equation D.14. The area per mass of mixtures A'_{12} at a given surface pressure is determined for the isotherm of each different mixture. The mixture area is then plotted against the mass fraction of silica in the mixture. The resulting graphs are shown below.

D.2 Maltene-Silica Mixtures

Figures D.1 and D.2 are results for maltene-silica mixtures from air-water and toluene-water interfaces respectively. At both interfaces the mixtures deviate from an ideal mixture. This shows that they are at least partially mixed and behave as if they were miscible. Silica is a solid and in bulk not miscible with asphaltenes or maltenes. However, 2D mixing occurs because the silica particles aggregate to form clusters at the interface and the clusters are smaller in the mixed films (see AFM images in Chapter 5). There is a definite trend at the air-water interface showing negative deviation. The negative deviation occurs because the maltene molecules fill in the area between silica clusters and possibly adsorb onto the silica particles. As shown in Figure D.3, the area of the mixed film is less than the combined areas of unmixed silica and unmixed maltenes. At the toluene-water interface the mixtures do not appear to be ideal but no definite trend is observed.

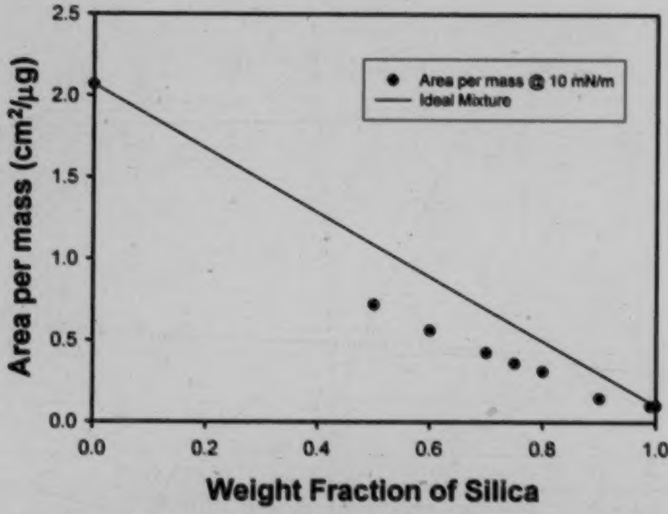

Figure D.1: Area occupied by a mixture of maltenes and silica at an air-water interface. Area per mass plotted as a function of weight fraction of silica.

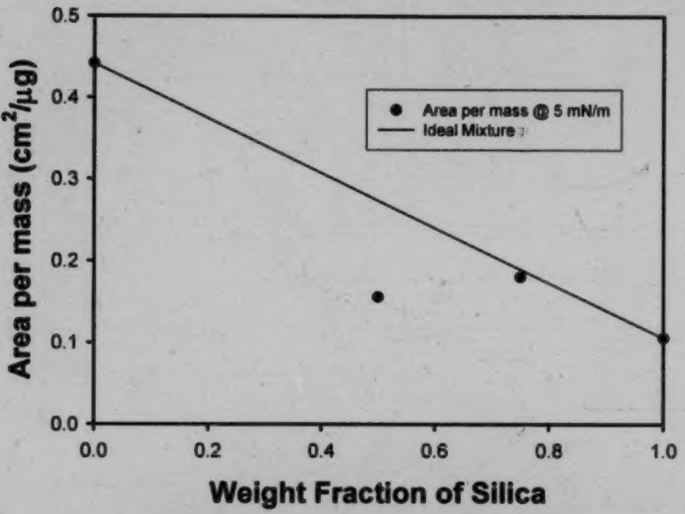

Figure D.2: Area occupied by a mixture of maltenes and silica at a toluene-water interface. Area per mass plotted as a function of weight fraction of silica.

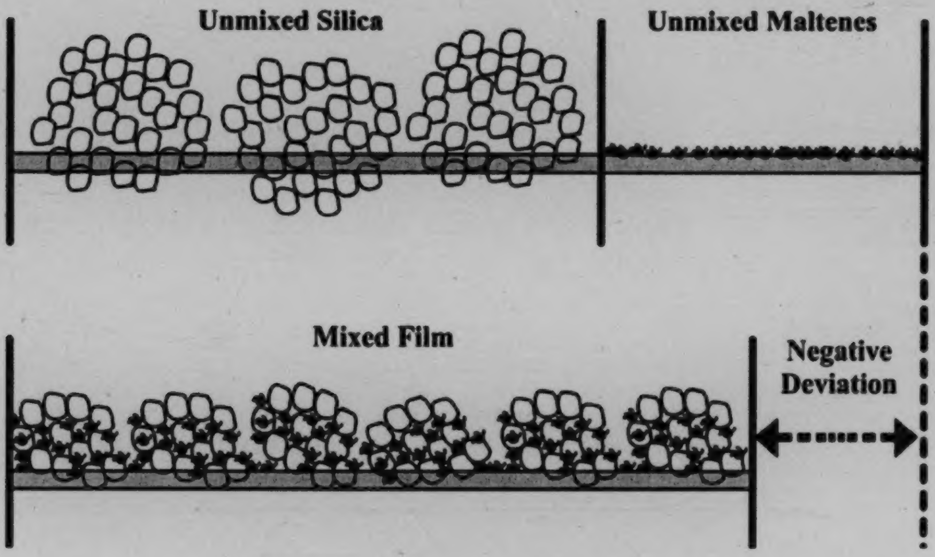

Figure D.3: Schematic showing a possible cause of the negative excess areas reported by mixed films.

D.3 Asphaltene-Silica Mixtures

For asphaltene-silica mixtures the area per mass at specified interfacial pressures are plotted against the weight fraction silica in Figure D.1 (air-water interface) and Figure D.2 (toluene-water interface). As with the maltene-silica mixtures the two components are mixed but do not behave as an ideal mixture. At both interfaces the mixtures have a negative excess area corresponding to attractive interactions between the components. As with the maltene-silica mixture the negative deviation can be explained in terms of asphaltene molecule adsorption onto the silica particles and asphaltene molecules filling in areas between silica particles.

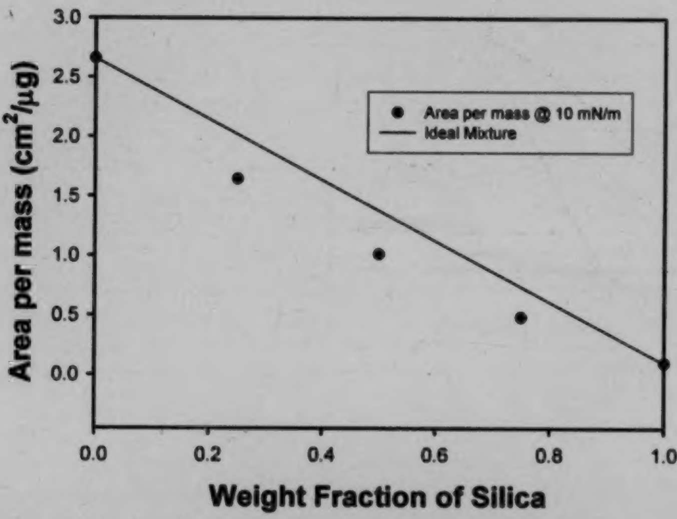

Figure D.4: Area occupied by a mixture of asphaltenes and silica at an air-water interface. Area per mass plotted as a function of weight fraction of silica.

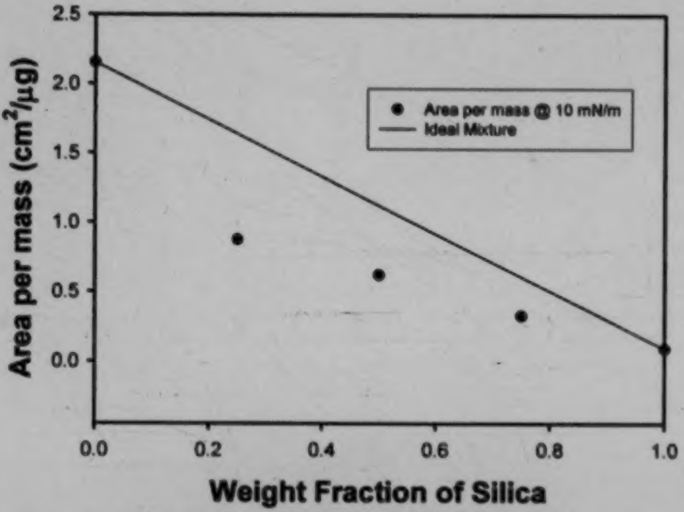

Figure D.5: Area occupied by a mixture of asphaltenes and silica at a toluene-water interface. Area per mass plotted as a function of weight fraction of silica.

D.4 References

Gaines, G. L., *Insoluble monolayers at liquid-gas interfaces*, New York, Interscience Publishers 1966.

E

Appendix E: Area per Mass Isotherms of Maltene-Asphaltene Mixtures

E.1 Introduction

Surface pressure-area isotherms of five different mixtures of maltenes and asphaltenes are presented and discussed in Chapter 5 (section 5.3.3). The molecular weights of the maltene and asphaltene fractions were available from VPO measurements, so isotherms obtained from their mixtures can be plotted using area per molecule on the abscissa. This is unlike the mixtures containing silica, for which isotherms are presented as surface pressure versus area normalized by the mass of material at the interface. In Chapter 5 the area shift from single component isotherms was determined for each of the maltene-silica and asphaltene-silica mixtures. For the sake of comparison, isotherms obtained for maltene-asphaltene mixtures at the air-water interface have been plotted with the abscissa as area per mass. Area shift values were then calculated for the maltene-asphaltene mixtures.

In Chapter 5 some comparisons were made to show that asphaltenes and silica have similar behaviour. In this chapter, the area shift curves for maltene-asphaltene mixtures are discussed in comparison to the curves from maltene-silica mixtures.

E.2 Results

Surface pressure-area isotherms were measured using the experimental procedure described in Chapter 3. Trough area is normalized by the mass of maltenes at the interface for isotherms shown in Figure E.1. Presenting isotherms in this way illustrates the change in the isotherm of a maltene film associated with the addition of asphaltenes to the film. A schematic depiction of the area shift for the 10 wt% maltenes mixture at a surface pressure of 10 mN/m is shown in Figure E.1. For each of the maltene-asphaltene mixtures the area shift from a maltene isotherm at different surface pressures is plotted in Figure E.2.

In Figure E.3 the isotherms are plotted in terms of surface pressure vs. the mass of asphaltenes spread at the interface. These isotherms show the effect of maltene addition on the properties of an asphaltene film. A plot of the area shift vs. the asphaltenes: maltenes ratio is shown in Figure 5.5

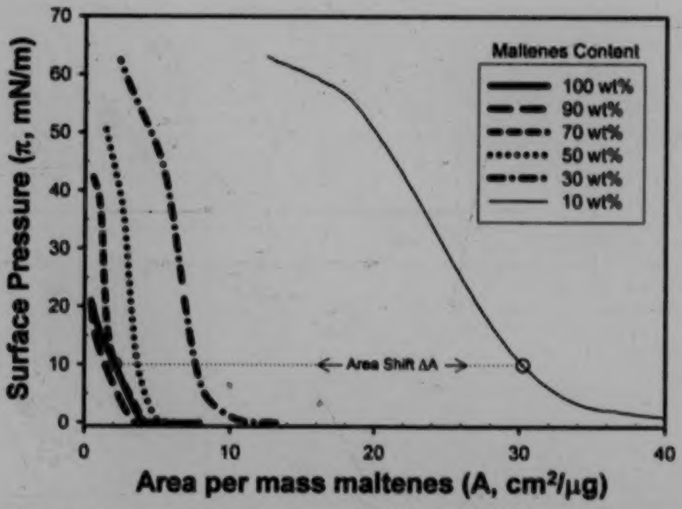

Figure E.1: Surface pressure-area isotherms of films from maltene-asphaltene mixtures. Isotherms are normalized by the mass of maltenes at the interface.

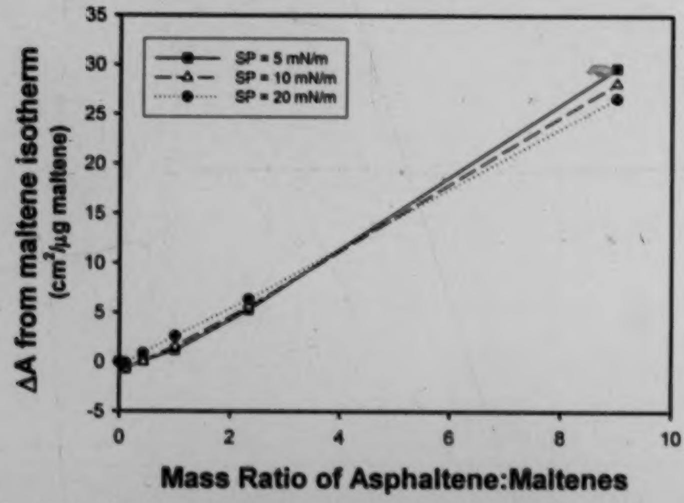

Figure E.2: Area shift from the isotherm of a maltene film for maltene-asphaltene mixtures. At various interfacial pressures plotted against the ratio of asphaltenes:maltenes.

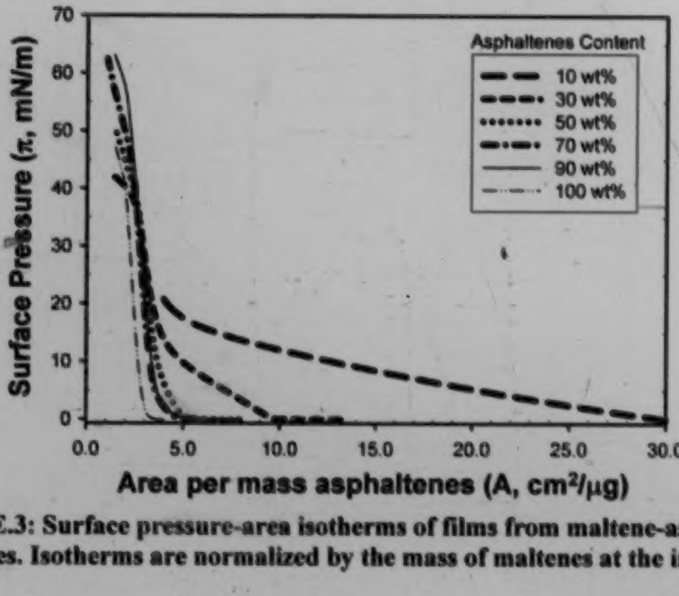

Figure E.3: Surface pressure-area isotherms of films from maltene-asphaltene mixtures. Isotherms are normalized by the mass of maltenes at the interface.

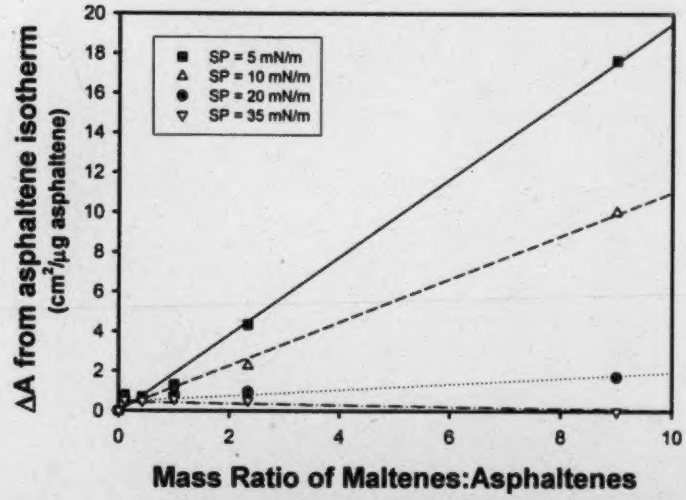

Figure E.4: Area shift from the isotherm of an asphaltene film for maltene-asphaltene mixtures. At various interfacial pressures plotted against the ratio of maltenes:asphaltenes.

E.3 Discussion

In Figure E.1 the isotherms are normalized by the mass of maltenes spread, showing the effect of adding asphaltenes to a maltene film. As the amount of asphaltenes in the film is increased the isotherm changes position to a higher area per mass, i.e. there is a positive area shift. Calculated area shift values in Figure E.2 show that there is a positive area shift from the isotherm of the maltene film for all mixtures except the one containing 10 wt% asphaltenes (asphaltenes:maltenes = 0.11) which has a relatively small negative area shift (shift to smaller area per mass maltenes). The area shift increases linearly with an increasing asphaltenes:maltenes ratio at all three surface pressures shown.

The area shift caused by increasing the silica content added to a maltene film (see Figure 5.4, and 5.6) is much smaller (in some cases negative) compared to the area shift caused by increasing the mass of asphaltenes to a maltene film. The difference is likely due to the comparatively large are per mass that asphaltenes occupy at the interface. For example, see Figure 5.2, where an isotherm from 30μg of asphaltenes is at a greater area than the isotherm of 540 μg of silica. Thus, the addition of a given mass of asphaltenes causes the same area shift of a much larger mass of silica.

Figure E.3 shows that addition of maltenes to an asphaltene film produces a similar "tail" to the isotherm as was shown in maltene-silica mixtures. The maltenes create a liquid phase at lower surface pressures. When the mixtures exist in a solid phase the isotherms overlap and there is no position change in the isotherm for different mixtures. A linear relation between the area shift and the amount of maltenes added to the film at lower surface pressures is shown in Figure E.4. As the surface pressure increases the area shift decreases for a given maltenes:asphaltenes ratio. At a surface pressure of 35 mN/m the area shift is close to zero for all mixtures.

Addition of maltenes does not cause a positive area shift from asphaltene isotherm at higher pressures like the area shift shown from the silica isotherm. This is because the silica clusters are large compared to the asphaltene aggregates and the clusters also extend away from the interface. The maltenes may still cause a reduction in the asphaltene aggregate size as they did for the silica clusters. However any reduction in aggregate size would not cause much of increase in the area occupied by the asphaltenes. This is because the asphaltene aggregates are smaller than silica clusters and do not appear to extend away from the interface (see Figure 5.16). The height scale on AFM images of silica clusters is an order of magnitude larger than the scale on an image of an asphaltene film.

In Chapter 5 the maltene-asphaltene mixtures were shown to behave ideally because they obeyed the additive rule for mixed monolayers. The area-shift figures support the idea that the maltenes and asphaltenes form an ideal mixture because the area shift increases linearly with increases in asphaltene:maltene ratio and increases in maltene:asphaltene ratio. This shows that the asphaltenes and maltenes obey the additive rule on a mass basis. Further discussion on the additive rule is given in Appendix D.

E.4 Conclusion

Isotherms with area normalized by mass and area shift diagrams show that there are some similarities and some differences between the maltene-silica mixtures and maltene-asphaltenes mixtures at the air-water interface. There is a similar liquid to solid phase transition in the isotherms and the area shift in relation to an asphaltene isotherm is similar to that from a silica isotherm. The much larger area per mass that the asphaltenes occupy cause the differences in the mixture behaviour.

F

Comparison of Toluene-Water Interface to Air-Water Interface

F.1 Introduction

Chapters 5 and 6 focused on results obtained from a single interface. Results from an air-water interface were presented separately from the results from a toluene-water interface. Further information can be obtained from these results by making a comparison of the results from each interface. Isotherms from different interfaces are plotted in the same figure for unmixed silica, maltenes and asphaltenes and several mixtures. Also, images of deposited films from both interfaces are shown side by side to aid in comparison. Procedures to obtain isotherm data, and deposited film images are the same as previously discussed in Chapter 3. Experiments were conducted at 20 °C with water of pH=5.8. Concentrations of the components in the mixtures are given in Table 3.4. Typical masses spread at the interface are given in Table 3.5 and Table 3.6. Some general comments about the different interfaces are made here.

F.2 Unmixed Films

F.2.1 Silica

Figure F.1 shows the pressure-area isotherms of an unmixed silica film from air-water and toluene-water interfaces. The isotherms show that the film at a toluene-water interface is more compressible and weaker because of the lower collapse pressure.

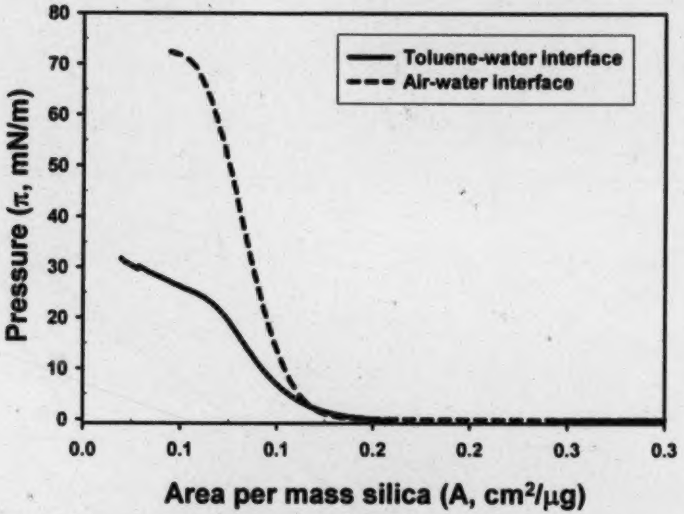

Figure F.1: Pressure-area isotherms of R974 hydrophobic silica nanoparticles at air-water and toluene-water interfaces.

Another method of comparing the measured isotherms is to normalize the measured pressures by the interfacial (surface) tension of the pure interface. The normalized surface pressure is thus $(\gamma_{pure}-\gamma_{film})/\gamma_{pure}$. If the normalized pressure is multiplied by 100%, the result is the percent change in interfacial tension. The normalized pressures obtained for a silica film at the two interfaces are plotted against the area per mass silica in Figure F.2. Figure F.2 shows that the film at toluene-water interface gives a less steep slope and is more compressible than the film at air-water interface. Also it shows that the collapse pressure as a fraction of the interfacial tension is lower at the toluene-water interface. Because of the increased compressibility and lower collapse pressure the silica film is weaker at a toluene-water interface.

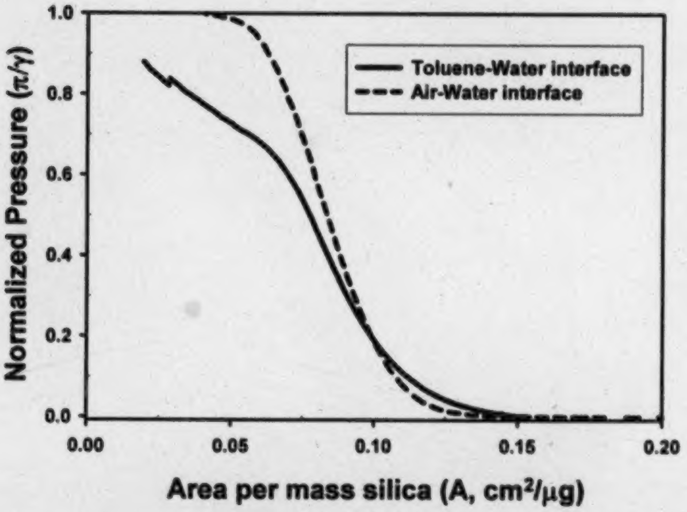

Figure F.2: Pressure-area isotherms from silica films with pressure normalized by the interfacial tension (γ_{tw}=36 mN/m, γ_{aw}=72.8 mN/m)

A comparison of SEM images of a silica film from the two-interfaces is shown in Figure F.3. The silica film is continuous at the toluene-water interface but mesostructures (clusters) form at the air-water interface. It may be expected that the film from an air-water interface would be more expanded because of the vacant areas between clusters. Isotherms do not reveal this to be so because the A_o of the two isotherms is approximately the same with the air-water interface being slightly lower. This shows that neither film is more condensed or expanded than the other, in terms of the isotherms.

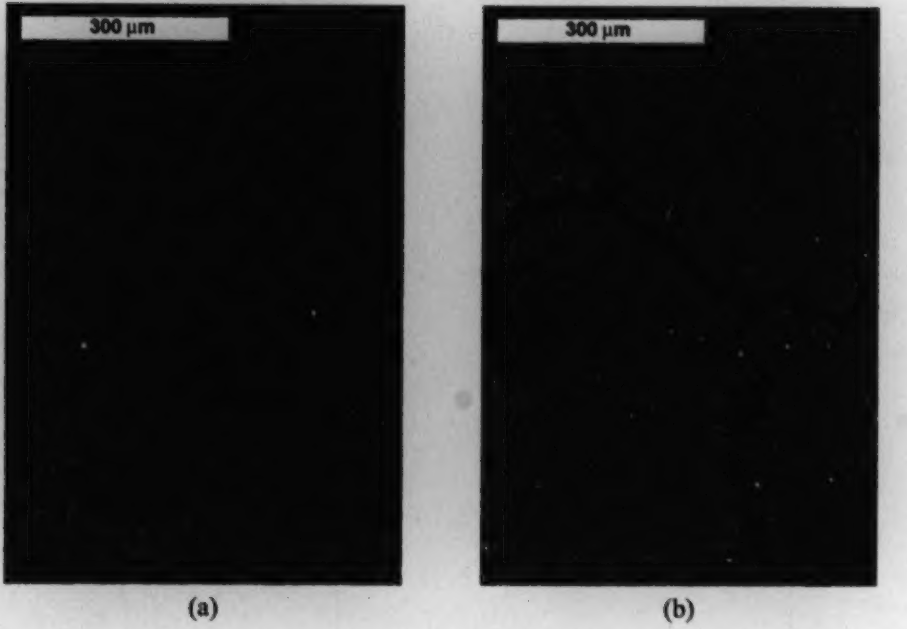

(a) (b)

Figure F.3: SEM images of silica films from (a) air-water interface and (b) toluene-water interface

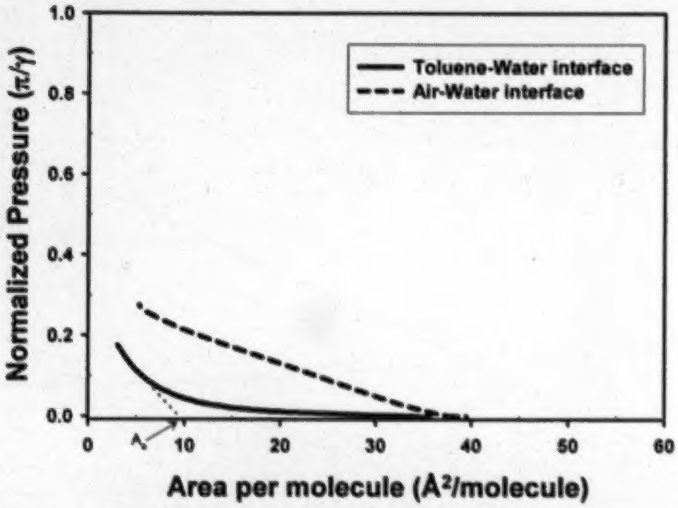

Figure F.4: Comparison of normalized pressure-area isotherms of maltene films from air-water and toluene-water interfaces.

F.2.2 Maltenes

Compared to films of unmixed silica the behaviour of asphaltene and maltene films changes substantially amongst the different interfaces. To aid comparison between the interfaces, maltene isotherms are plotted separately from asphaltene isotherms and the pressures are normalized by the interfacial tension of a pure interface. Figure F.4 shows that the isotherm shape of maltene films from each interface is different. For the majority of the isotherm the compressibility of the film has been increased at the toluene-water interface. However, at low area per molecule (~5 $Å^2$/molecule) the slope of the toluene-water isotherm increases, thus there is a decrease in compressibility. The most significant difference is that at a toluene-water interface the isotherm reports a very small increase in interfacial pressure. The small increase in interfacial pressure is evidence that there is little interfacially active material in the maltene fraction. The limiting area (A_o) of the maltenes at the air-water interface is approximately 36 $Å^2$/molecule. In contrast, the A_o at the toluene-water interface is substantially smaller. Although difficult to determine because of the isotherm shape, the A_o is approximately 10 $Å^2$/molecule as shown in Figure F.5. Thus, the A_o of maltenes is reduced by 72% at the toluene-water interface. As discussed in Chapter 6 a majority of the maltenes are removed from the toluene-water interface, dissolved into the bulk toluene supraphase. The reduction in A_o is most likely because there are fewer molecules at the interface, not because the size of the molecules has changed.

F.2.3 Asphaltenes

There is a substantial change in the isotherm shape of asphaltene films at the two different interfaces. As shown in Figure F.5, the air-water isotherm has a small gas phase and has more of a solid phase with lower compressibility. At the toluene-water interface the isotherm shows a lack of definite gas and solid phases and appears to remain in a liquid phase throughout compression. The air-water isotherm shows a collapse pressure at approx 55% of surface tension of water. At a toluene-water interface the pressure has reached 80% of the interfacial tension without any collapse. The asphaltene film is more compressible at the toluene-water interface and can be compressed to a relatively higher pressure. Conversely to the maltene films, the area per molecule has increased for the toluene-water film. The A_o at the air-water interface is approximately 370 Å^2/molecule. Without a distinct solid phase the A_o cannot be calculated for the toluene-water interface, but the interfacial pressure starts to increase when the area per molecule is 600 Å^2/molecule. The increase in A_o may stem from increased interaction between hydrocarbon chains of the asphaltenes, or a reduction in asphaltene aggregate size.

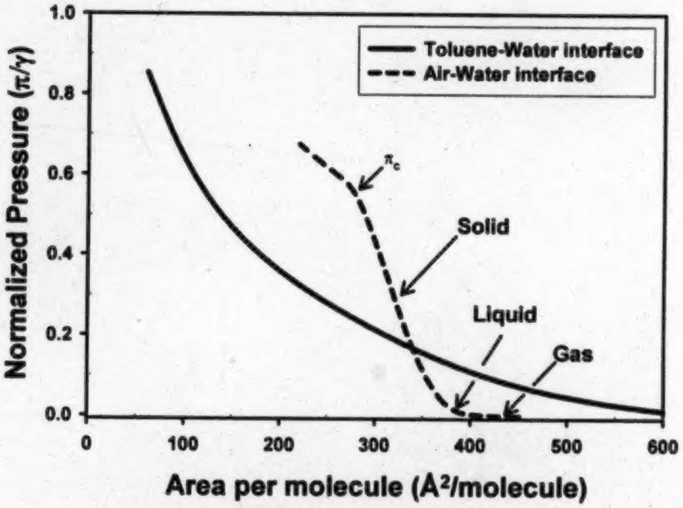

Figure F.5: Comparison of normalized pressure-area isotherms of asphaltene films from air-water and toluene-water interfaces.

Figure F.6 shows the pressure-area isotherms of asphaltene and maltene films at air-water and toluene-water interfaces. In this figure the pressure measurements have not been normalized by interfacial tension. The interfacial pressure obtained from compression of the films at a toluene-water interface is lower than the surface pressure obtained from compression at an air-water interface due to the difference between the surface tension of water and the interfacial tension of a toluene-water interface.

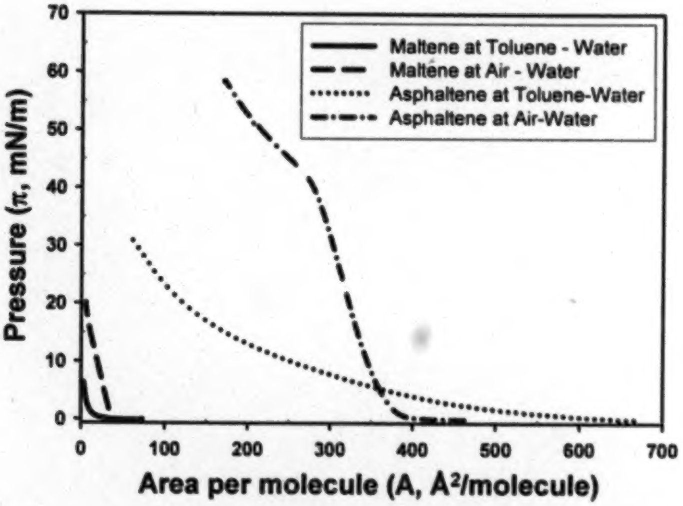

Figure F.6: Pressure-area isotherms of maltene and asphaltene films at air-water and toluene-water interfaces.

F.3 Mixtures

Mixtures containing 75 wt% silica and 25 wt% maltenes were picked for comparison because at an air-water interface they most clearly show the transition between a liquid phase (dominated by maltenes) and a solid phase (dominated by silica). Mixtures with 75 wt% silica and 25 wt% asphaltenes were also then used for comparison. Figure F.7 shows the pressure-area isotherms of the mixed films from air-water and toluene-water interfaces. Collapse was observed for all films. The isotherm of the 75 wt% silica mixture is the farthest right, showing this film occupies more area per mass than other films. In general, the toluene-water films are more compressible (isotherms have less steep slopes) and do not have a distinct phase transition because the liquid phase dominated by maltenes is missing.

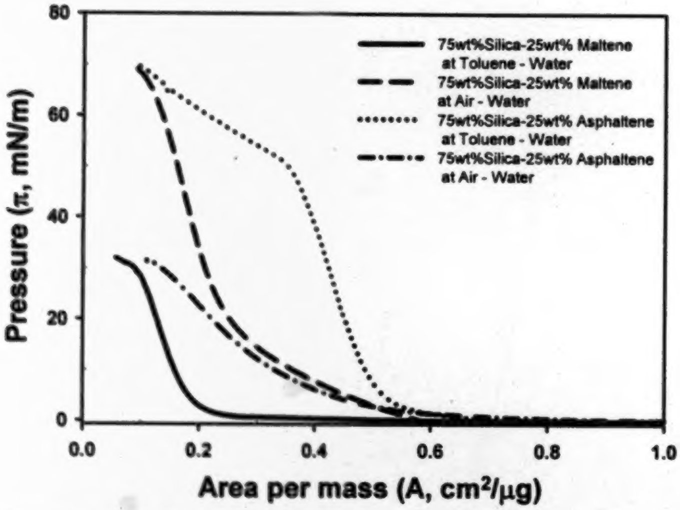

Figure F.7: Pressure-area isotherms of maltene-silica mixtures and asphaltene-silica mixtures at air-water and toluene-water interfaces.

A more meaningful comparison can be made between films of the same composition from normalized pressure figures. Figures F.8 and F.9 show isotherms obtained from films of the maltene-silica mixture and Figures F.11 and F.12 show isotherms from films of the asphaltene-silica mixtures.

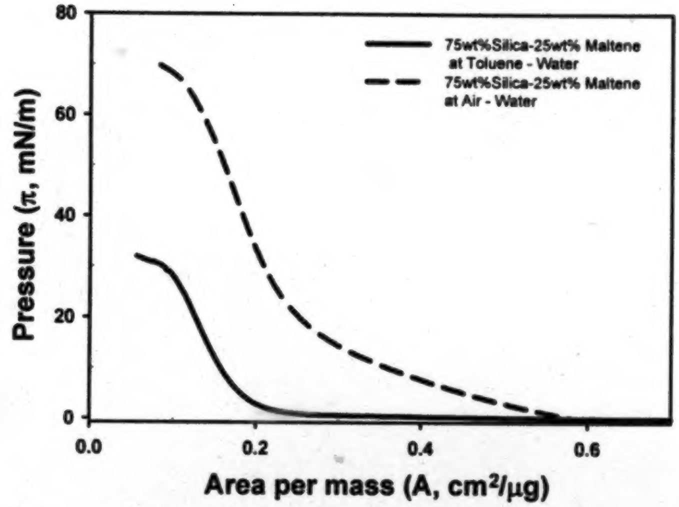

Figure F.8 Pressure-area isotherms of 25 wt% maltene – 75 wt % silica mixture from films at air-water and toluene-water interfaces.

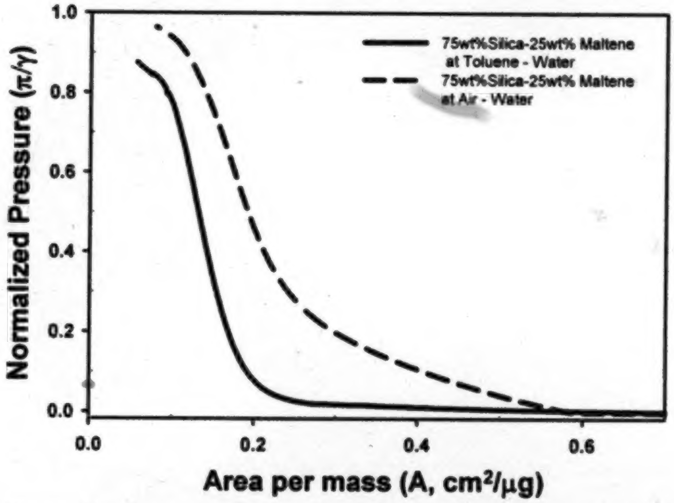

Figure F.9: Normalized pressure-area isotherms of 25 wt% maltene – 75 wt % silica mixture from films at air-water and toluene-water interfaces.

For the maltene-silica mixtures transition between a liquid and solid phase is diminished at the toluene-water interface due to the dissolving of maltenes from the interface. The solid phases have close to the same slope, showing that the silica is just as compressible at a toluene -water interface as at an air-water interface. The same is shown for unmixed silica films. Both films reach a pressure of above 80% the interfacial tension before collapse.

Further evidence that maltene molecules are removed from the toluene-water interface is shown in Figure F.10, where SEM images of deposited LB films of maltene-silica films (50 wt% maltenes) from the two interfaces are compared. At the air-water interface the silica particles have formed clusters that are dispersed across the interface, most likely separated by maltenes. In contrast, the film from a toluene-water interface is a continuous film similar to the case of unmixed silica.

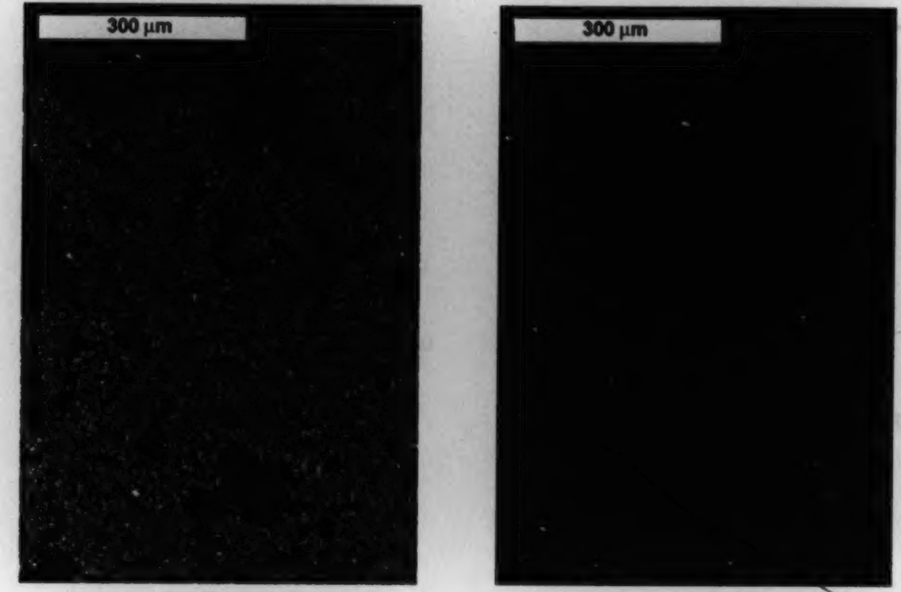

(a) (b)

Figure F.10: SEM images of 50 wt% maltenes – 50 wt% silica films from (a) air-water interface and (b) toluene-water interface

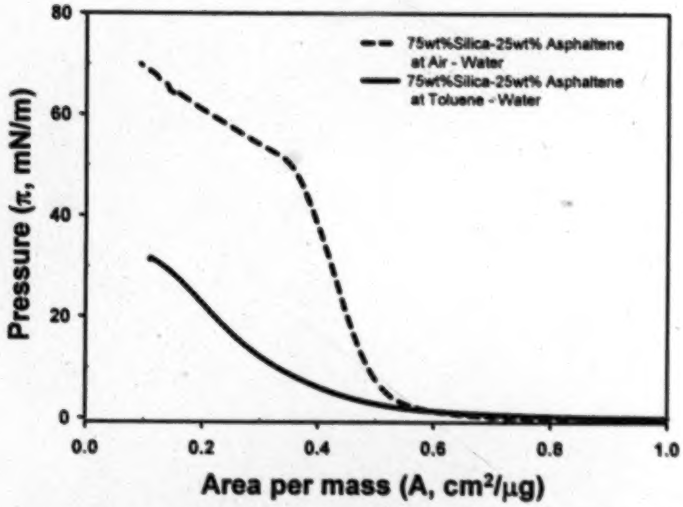

Figure F.11: Pressure-area isotherms of 25 wt% asphaltene – 75 wt % silica mixture from films at air-water and toluene-water interfaces.

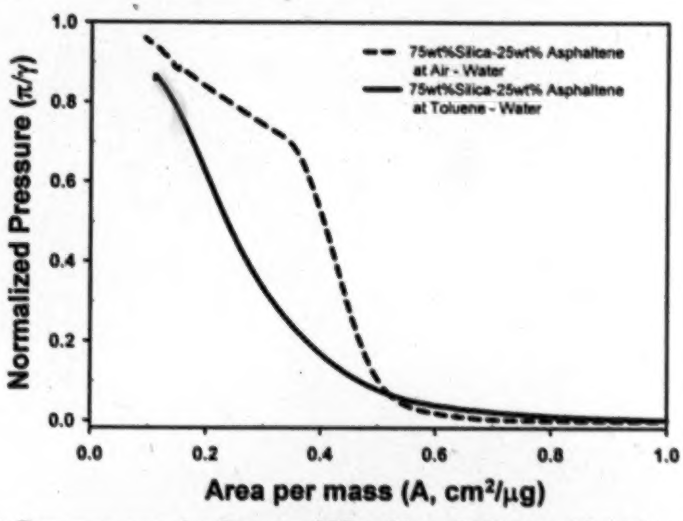

Figure F.12: Pressure-area isotherms of 25 wt% asphaltene – 75 wt % silica mixture from films at air-water and toluene-water interfaces.

Expansion of the asphaltene film and a change in asphaltene behaviour at toluene-water has influenced the isotherm from mixed asphaltene-silica films. In contrast to unmixed silica films, which gave isotherms with similar shapes at both interfaces, the asphaltene-silica mixed films have different shapes at the two interfaces. At the air-water interface the isotherm shows three phases (gas, liquid, and solid) similar to an unmixed asphaltene film. At the toluene-water interface there is a drawn out transition from gas to solid phase. Also, the solid phase has a less steep slope at the toluene-water interface. As with an unmixed asphaltene film the film has a higher relative collapse pressure at the toluene-water interface showing that the asphaltene molecules influence film collapse.

SEM images of deposited films from each interface are shown in Figure F.13. At both interfaces the silica particles are arranged in clusters, separated by a film of asphaltenes. AFM images in previous chapters show that areas between the silica clusters are occupied by asphaltenes. At both interfaces the silica particle-particle interactions have been altered by the presence of asphaltenes. As discussed previously, the asphaltenes likely diminish the attractive hydrophobic forces and also cause resistance to particle movement at the interface.

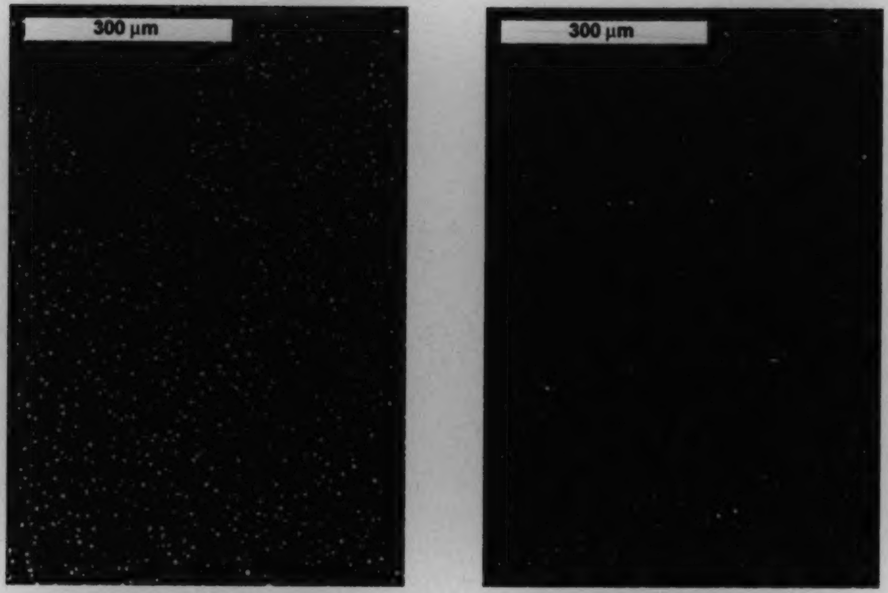

(a) (b)

Figure F.13: SEM images of 50 wt% asphaltenes – 50 wt% silica films from (a) air-water interface and (b) toluene-water interface

F.4 Conclusion

Comparisons between isotherms form the air-water and toluene-water interfaces have shown differences in the interfacial behaviour of the three substances studied. For the mixed films the different isotherms and differences in LB films are caused by changes in the maltene and asphaltene behaviour. The differences in mixed film isotherms are not influenced as much by the silica nanoparticles. Comparisons of air-water and toluene-water isotherms of films containing maltenes further supports the idea discussed in Chapter 6 that little of the maltene fraction of bitumen remains at the toluene-water interface.

Toluene-water results are more applicable to emulsion-studies because oil-water interfaces are present in the emulsions. Some links between the Langmuir trough and emulsion studies have been outlined in Chapter 6.